Altered MD-PFC thalamocortical network dynamics in an NMDAR antagonist animal model of cognitive control deficits in Schizophrenia

A DISSERTATION

SUBMITTED TO THE FACULTY OF

UNIVERSITY OF MINNESOTA

BY

Adele Lucia DeNicola

IN PARTIAL FULLFILLMENT OF THE REQUIREMENTS FOR THE

DEGREE OF DOCTOR OF PHILOSOPHY

Advisor: Dr. Matthew Valentine Chafee

August 2019

ACKNOWLEDGEMENTS

I would like to start by thanking my advisor, Dr. Matt Chafee. Your passion and drive for the scientific endeavor is unrivaled. Your enthusiasm and positivity, particularly in the face of never-ending recording and analysis crises, is inspiring. Thank you for taking a chance on my project to reach deeper in the brain than either of us had gone and to explore an unknown aspect of schizophrenia. Your guidance through any and all issues I brought to you throughout these years has helped me immensely. I am grateful for all that you have done to help me pursue my scientific questions, professional development, and to develop a line of research that could carry me forward in my career.

Dean Evans, thank you for supporting my animals and me throughout my experiments. Your knowledge, insight, advice, support, and so much more were integral to my success. I have said it before, and I will continue to say it again and again, my project would not have happened without you.

I thank Min-Yoon Park for your help in setting up a brand-new recording, troubleshooting issues late into the night, coming in early in the morning to get a recording session in before noon, listening to me explain my data after running new analyses, and helping me talk through the implications of my findings. My dissertation would not be what it is without you. And I can't forget to thank you for always being there to listen to me complain about the struggles of graduate school. Not only were you a wonderful lab-mate, you are a wonderful friend.

I thank the other past and present Chafee lab members, Dr. David Crowe, Dr. Rachael Blackman, Dr. Jenny Zick, and Dale Boeff for being an ear to listen to the ups and downs of graduate school. Dave, thank you for your guidance and insight with data analysis technique, helping to teach me to code, discussing my results and their implications, and providing me with teaching mentorship. Rachael, thank you for developing the animal model that I was able to use. Your graduate school work paved the way for my project to be possible. Jenny, thank you for supporting and believing in me. You were always there to build me up and help me see the importance of my research. Dale, thank you for all the troubleshooting help through long recording days and getting the spike sorting system to run efficiently. I would still be sorting spikes if it wasn't for you.

I am thankful for my committee members, Dr. Tim Ebner, Dr. Matt Johnson, and Dr. Angus MacDonald III. Thank you for guiding my project, discussing the implications of my work, and helping my progression throughout my time in graduate school. Thank you to Tim for serving as my chair and keeping me focused on reaching milestones in my project. Thank you to Matt for teaching me to use Cicerone and guidance targeting a deep subcortical structure. Thank you to Angus for serving as my co-sponsor on my NRSA and for our on-going collaboration that allowed me to use a task you helped develop.

I would also like to thank all the student members of the GPN. I couldn't have imagined a better community to be a part of throughout graduate school. I am thankful to the class of 2012, Kellie Gross, Nathalia Torres-Jimenez, Martha Streng, Kelsey Moore, Anna

Ingebretsen, Katie Tonn Eisinger, and Vadim Petruk, for their emotional and professional support and guidance. I am extremely grateful for my friend Jen Cook who has become my confidante and rock throughout graduate school. I don't think I could've made it through graduate school without you.

To my parents, thank you for your unwavering support, without which I would not be the person I am today. To my Mom, Susan Stiles, I could never thank you enough for all that you have done for me. You have always been my most vocal and supportive cheerleader no matter what endeavor I chose and allowing me to be independent, curious, and opinionated. To my Dad, Michael DeNicola, thank you for you love and support throughout all of my major life decisions. You always trusted that I would make the right decision for myself and I am so grateful that you believed in my abilities. To my Step-Dad, Jeffrey Robbins, thank you for supporting and believing in me.

Lastly, but most certainly not least, I would like to thank my husband William Pappas. You have been a light in my life during some of the darkest times in graduate school. I could not have completed this dissertation without your support. Your love, encouragement, and understanding have been vital to my success. Thank you for choosing me as your partner throughout this wild life. I will continue to work to be worthy of your unending love.

DEDICATION

This dissertation is dedicated to the unsung heroes of this research, without whom none of it would’ve been possible.

ABSTRACT

Schizophrenia (SZ) is debilitating neuropsychiatric disorder and afflicted patients exhibit an array of symptoms including hallucinations, delusions, flat affect, and deficits in cognitive functioning. Even though the functional outcome of patients with SZ is correlated with the severity of cognitive deficits, current therapeutics do not effectively improve cognitive deficits. However, there is still not a clear understanding of the pathophysiology underlying cognitive deficits, making it difficult to develop therapeutics target at the improvement of cognition in patients. The mediodorsal nucleus of the thalamus (MD) has been thought to play a role in cognitive control behaviors alongside the prefrontal cortex (PFC). This is largely due to the reciprocal connections between the MD and PFC, reports of MD neurons exhibiting similar task-related activity patterns during cognitive behaviors, and that lesions in the MD produce deficits in cognition similar to PFC lesions. Also, in patients with SZ the MD and PFC exhibit correlated reduced activation during cognitive control performance and are function disconnected from each other. In order to further our understanding of the pathophysiology in the MD-PFC thalamocortical network, I trained monkeys to perform a cognitive control task that exposes cognitive control deficits in patients with SZ. First, I relate thalamocortical distributed processing and functional coupling to cognitive control by recording in the MD and PFC simultaneously in the healthy state. Then, I characterize the effects of NMDA receptor (NMDAR) blockade on thalamocortical distributed processing and functional coupling underlying cognitive deficits. I found that MD neurons represent cognitive control state similarly to PFC neurons, but that PFC state neurons contain more information early in the trial, while MD state neurons contain more information late in the trial, MD neurons are more involved in response selection than PFC neurons and

neurons in the MD and PFC transmit state and response information reciprocally during cognitive control performance. Following NMDAR blockade, there were less MD and PFC neurons recruited to encode state and response information and the neurons that did encode task information were delayed in their recruitment. Additionally, representation of task state was decreased at the single neuron and population levels in both the MD and PFC, but to a stronger degree in the PFC than the MD, and these changes in state representation predicted task failure on a trial-by-trial basis more strongly in the MD than the PFC. Lastly, NMDAR blockade strongly attenuated transmission of information in local circuits in and between the MD and PFC. Overall, I am the first to characterize MD-PFC cellular level network dynamics underlying cognitive control and the effect of NMDAR blockade on this thalamocortical network that results in pathophysiology and SZ-like cognitive deficits.

TABLE OF CONTENTS

LIST OF TABLES

LIST OF FIGURES

CHAPTER 1:

Introduction

Schizophrenia (SZ) is a neuropsychiatric disorder that is related to dysfunction across many neural systems, resulting in wide-ranging symptoms in afflicted patients. Clinically, SZ presents as a mixture of positive symptoms (e.g. hallucinations and delusions), negative symptoms (e.g. loss of motivation and anhedonia), and cognitive symptoms (e.g. impairments in executive function, working memory, and attention) in multiple combinations and levels of severity (American Psychiatric Association, 2013). Due to this extensive and heterogeneous expression of symptoms across patients, SZ is particularly difficult to treat. Current therapeutics, anti-psychotics (typical and atypical), mainly treat the positive symptoms, while leaving the other symptom categories relatively unimproved (Mortimer, 1997; Stip et al., 2005; Tandon, 2011; Schulz et al., 2016). Improving cognitive symptoms, in particular, should be a main goal of treatments because inferior functional outcomes of patients are correlated with the severity of cognitive deficits (Green et al., 2000; Green, 2006; Ventura et al., 2009). Additionally, treatments that are targeted towards improving cognitive symptoms also improve negative symptoms, and vice versa (Censits et al., 1997; Schuepbach et al., 2002). However, as a community we are lacking an understanding of the nature of the failure of neural networks that produces cognitive deficits.

Human functional neuroimaging studies have identified brain regions that exhibit lower activation in patients during cognitive control performance compared to healthy controls. For example, the prefrontal cortex (PFC) and the mediodorsal nucleus of the

thalamus (MD) exhibit reduced functional activation in patients with schizophrenia to a degree that is correlated across individuals across a range of cognitive control tasks (Minzenberg et al., 2009), as well as reduced functional connectivity at rest (Welsh et al., 2010; Anticevic et al., 2014b; Anticevic et al., 2014a). In addition, the integrity of white matter tracts linking MD to PFC (imaged with diffusion tensor imaging) is reduced in patients with schizophrenia relative to controls and the severity of white matter and working memory deficits is correlated over patients (Giraldo-Chica et al., 2018). Patients with schizophrenia exhibit reduced spine density in prefrontal cortex in cortical layers that receive thalamocortical afferents (Kolluri et al., 2005; Lewis and González-Burgos, 2008; Glausier and Lewis, 2013; Dorph-Petersen and Lewis, 2017). This data indicates that the MD-PFC thalamocortical network may be a key target for treating cognitive control deficits in SZ. However, little is known about the role of the MD at the cellular level in cognitive control or the nature of information carried between the MD and the PFC in the healthy or disordered state.

Studies focusing on synaptic mechanisms underlying cognitive deficits in SZ provide convergent evidence in animal models, control subjects, and patients that a defect in NMDA (*n-Methyl-d-aspartate*) receptor (NMDAR) mediated synaptic transmission may be a causal factor in clinical symptoms and cognitive deficits in SZ (Luby et al., 1959; Nuechterlein and Dawson, 1984; Krystal et al., 1994; Humphries et al., 1996; Sokolov, 1998; Olney et al., 1999; Tsukada et al., 2005; Javitt, 2007; Stone et al., 2007; Lisman et al., 2008; Funk et al., 2009; Jones et al., 2011; Blackman et al., 2013; Schizophrenia Working Group of the Psychiatric Genomics Consortium, 2014; Howes et al., 2015; Xu et al., 2015; Balu, 2016; Cheng et al., 2018). However, how NMDAR synaptic impairment negatively impacts MD-PFC thalamocortical information

processing is not known. Answering this question is one of the main goals of this dissertation. I characterize healthy state neurophysiology in the MD and PFC and relate pathophysiology in the MD and PFC to cognitive deficits following NMDAR blockade.

Cognitive control processing in the prefrontal cortex

Cognitive control, and a related construct, executive control, have been variously defined (Baddeley and Della Sala, 1996; Perner and Lang, 1999; Smith and Jonides, 1999; Pineda, 2000), based on several characteristics (Funahashi and Andreau, 2013). First, cognitive control enables attention to switch toward sources of information that are contextually relevant. Second, cognitive control organizes behavior temporally by planning the series of tasks required to reach the intended goal. Third, cognitive control requires accessing and manipulating stored information. Fourth, cognitive control monitors and integrates information about internal and external states concurrently to select future goals. Altogether, cognitive control can be defined as the ability to select contextually relevant information to make and monitor flexible goal-oriented decisions (Miller and Cohen, 2001). By its nature, cognitive control requires the engagement of multiple brain regions and coordination between them, perhaps by a single structure (usually referred to as the central executive).

The PFC has long been identified as likely to function as the central executive due to its ability to interact with, modulate, and recruit other brain regions during cognitive control performance. The pervasive theory of the PFC is that it plays a primary role in the integration of incoming information and provides top-down control on sensory and motor processing to flexibly map stimuli to responses and therefore coordinate behavior(Miller, 2000; Miller and Cohen, 2001). In support of this, imaging studies have

shown that the PFC is activated during information maintenance (D'Esposito et al., 1999; D'Esposito et al., 2000) and response selection (Rowe et al., 2000; Rowe and Passingham, 2001), is functionally correlated with other brain structures such as the ACC to a degree that reflects response conflict (Dove et al., 2000; MacDonald et al., 2000; Menon et al., 2001; Dreher and Berman, 2002; Braver et al., 2003; Egner and Hirsch, 2005; Kerns et al., 2005; Liston et al., 2006; Boschin et al., 2017), and parietal cortex associated with shifting attention and stimulus-response learning (Sohn et al., 2000; Bunge et al., 2002). Additionally, damage to the human PFC causes deficits in context maintenance and response inhibition (Shallice and Burgess, 1991; Miller, 2000; Thompson-Schill et al., 2002; Gläscher et al., 2012).

Neurophysiological recording of the non-human primate PFC (Principal sulcus, Brodmann's Area 46, analogous to the dorsolateral PFC in humans) has found that single prefrontal neurons exhibit patterns of activity that reflect cognitive control. For example, neurons in the PFC encode abstract rules (Wallis et al., 2001a), categories (Freedman et al., 2001; Goodwin et al., 2012), and numbers (Bongard and Nieder, 2010; Moskaleva and Nieder, 2014), indicating that PFC neurons encode abstract state variables that can provide control signals needed to flexibly adjust responses to stimuli as a function of context. Neural signals reflecting cognitive control are typically found not only in prefrontal cortex but the cortical association areas to which prefrontal cortex projects. For example, the object category of a visual stimulus is encoded by prefrontal and inferotemporal neurons in parallel (Freedman et al., 2003) and the rule-dependent spatial category of a visual stimulus is jointly encoded by the activity of prefrontal and posterior parietal neurons (Crowe et al., 2010). Likewise, the number of items in a visual display is encoded by patterns of activity distributed between prefrontal and posterior

parietal neurons (Nieder and Miller, 2004; Vallentin et al., 2012). Finally, abstract rules are encoded by prefrontal, inferotemporal and striatal neurons concurrently (Muhammad et al., 2006). These data indicate that the abstract representations on which cognitive control is based exist as neural representations that are distributed across prefrontal cortical networks. Moreover, under conditions that rules change and the mapping from stimuli to categories must rapidly adapt, prefrontal neurons transmit information to posterior parietal neurons (Crowe et al., 2013a), reflecting the influence of prefrontal cortex on distributed processing in large-scale brain networks.

In addition to cognitive control, PFC has a well-established role in working memory. PFC neurons exhibit persistently elevated activity during the working memory period of delayed response tasks as a function of the item stored in working memory (Fuster, 1990; Funahashi et al., 1993b; Funahashi et al., 1993a; Chafee and Goldman-Rakic, 1998; Goldman-Rakic, 1999). Although often discussed as separate functions, working memory is necessary to maintain rules while the brain combines and evaluates new information with internal states to select the correct rule-dependent response (D'Esposito et al., 1999; D'Esposito et al., 2000; Braver et al., 2003; Bunge et al., 2003; Thompson-Schill et al., 2005). This process becomes particularly salient when confronted with conflicting behavioral options. Therefore, working memory and cognitive control are related constructs. The literature regarding the role of the PFC in cognitive control is extensive and supports the theory that PFC implements cognitive control by modulating operations across multiple brain areas in distributed networks.

MD as a higher order thalamic nucleus modulating cognitive function

Interactions between PFC and target structures that receive PFC input is not limited to corticocortical interactions. The involvement of the thalamus in cortical processing of information, particularly during cognition, has been a topic of a long-standing theory for thalamocortical projections. In this theory, the thalamus is split into two distinct classes of nuclei based on the information they carry, their cortical targets, and their cortical inputs (Sherman and Guillery, 1996, 2002; Guillery and Sherman, 2011; Sherman and Guillery, 2011; Mitchell et al., 2014). First order thalamic nuclei (like the lateral geniculate nucleus) relay sensory information from the periphery to primary sensory cortical targets, whereas higher order thalamic nuclei (like the MD) are extensively interconnected via reciprocal projections with association cortex. In this theory, 'driver' and 'modulator' projections are distinguished. 'Driver' inputs convey the sensory, motor, or cognitive information relayed through the thalamus. 'Modulator' inputs influence this transmission. Higher order thalamic nuclei receive their driver inputs from layer V of association cortical areas, and their modulator inputs from layer VI (Sherman and Guillery, 1996, 2002; Rovó et al., 2012). Modulator inputs predominate over drivers in higher order thalamic nuclei (Wang et al., 2002). Higher order thalamic nuclei send driver inputs to layer IV and modulatory inputs to layer III of association cortex (Sherman, 2012). By projecting to areas other than those providing their input, higher order thalamic nuclei can serve to relay information from one cortical association area to another (Sherman and Guillery, 2011).

Recently, the MD has been identified as a likely higher-order thalamic nucleus because it is reciprocally connected with the PFC, MD lesions result in PFC-like cognitive deficits, and MD neurons exhibit activity patterns that reflect cognitive functions like their prefrontal counterparts (Watanabe and Funahashi, 2012; Mitchell and

Chakraborty, 2013; Mitchell et al., 2014; Mitchell, 2015; Parnaudeau et al., 2018). Functional imaging studies in humans indicate that MD is activated during the delay period of working memory tasks and at the times that subjects receive negative feedback in Wisconsin Card Sorting Task, which is used to adjust cognitive strategies (Elliott and Dolan, 1999; de Zubicaray et al., 2001; Monchi et al., 2001). Therefore, the MD appears to be functionally recruited along with the PFC to mediate cognitive control. However, there is still much to be explored as to the nature of the involvement of the MD in cognitive control particularly at the cellular level.

Anatomy and Structure of the MD

The MD is considered to be the most developed in primates and its increase in size across species is comparable to that of the prefrontal cortex (Jones, 1998; Mitchell and Chakraborty, 2013). The primate MD contains four distinct divisions: the magnocellular (MDmc) division located antero-medially, the parvocellular (MDpc) division that is located centrally throughout the rostro-caudal extent, and the pars multiform (MDmf) and the densocellular (MDdc) divisions located laterally, rostrally and caudally, respectively (Bachevalier et al., 1997; Jones, 1998). Each division of the MD is reciprocally connected to specific regions in the PFC. The MD receives inputs from layers V and VI (Giguere and Goldman-Rakic, 1988; Yeterian and Pandya, 1994; Xiao et al., 2009). MD neurons that receive input from layer VI project back to layer IV, while the neurons that receive inputs from layer V project to layer III (Jones, 1998; Xiao et al., 2009). Layer V pyramidal inputs are thought to recruit higher order thalamic nuclei, like the MD, which then influence cortico-cortical communication and cognition (Sherman and Guillery, 1996, 2011).

MD divisions send and receive projections to distinct PFC regions. The MDmc is reciprocally connected to the orbitofrontal cortex and the ventromedial PFC and receives inputs from the ventrolateral PFC and dorsal anterior cingulate cortex (Preuss and Goldman-Rakic, 1987; Russchen et al., 1987; Barbas et al., 1991; Bachevalier et al., 1997; Haber and McFarland, 2001; McFarland and Haber, 2002). The MDpc is reciprocally connected to the dorsolateral PFC and area 10 and receives inputs from the orbitofrontal cortex, ventrolateral PFC, and the dorsal anterior cingulate cortex (Preuss and Goldman-Rakic, 1987; Russchen et al., 1987; Barbas et al., 1991; Bachevalier et al., 1997; Haber and McFarland, 2001; McFarland and Haber, 2002; Erickson and Lewis, 2004). MDdc and the MDmf project diffusely to the PFC, dorsal anterior cingulate cortex, the frontal eye fields, and the basal ganglia (Preuss and Goldman-Rakic, 1987; Russchen et al., 1987; Barbas et al., 1991; Bachevalier et al., 1997; Haber and McFarland, 2001; McFarland and Haber, 2002; Erickson and Lewis, 2004; Erickson et al., 2004).

The MDpc, which is reciprocally connected to the dorsolateral PFC, also receives input from the basal ganglia, specifically from the globus pallidus interna (GPi) and the substantia nigra reticulata (SNr) (Haber and McFarland, 2001; Haber and Calzavara, 2009). These structures are associated with the direct pathway in the basal ganglia, the activation of which is associated with the production of movement. Inputs from the basal ganglia suggest that the MD plays a role in relaying motor information to prefrontal cortex (Alexander et al., 1986; Haber and McFarland, 2001; Yin and Knowlton, 2006; Haber and Calzavara, 2009).

Lesions of the mediodorsal nucleus of the thalamus

In humans, lesions restricted to the MD produce deficits on classical measures of prefrontal cognitive function including the WCST and Stroop task (Van der Werf et al., 2000; Van der Werf et al., 2003). A finer grained analysis of MD lesions provided evidence that lesions restricted to the lateral portion (the MDpc) which projects to the dorsolateral PFC, produce stronger deficits in working memory than lesions of the medial portion (Zoppelt et al., 2003). Still, these experiments are sparse and inconclusive as to the full scope of executive function deficits following MD lesions, or the extent to which cognitive deficits derive solely from damage to MD, as infarcts restricted to MD are rare in human patients.

In rats, MD lesions produce deficits in spatial working memory (Harrison and Mair, 1996; Hunt and Aggleton, 1998a, b; Floresco et al., 1999; Mitchell and Dalrymple-Alford, 2005; Block et al., 2007; Ouhaz et al., 2015). In non-human primates, MD lesions produce deficits in a variety of long term and working memory tasks, including deficits in recognition memory, novel object in place discrimination, object reward association, spatial delayed alternation and spatial delayed response (Isseroff et al., 1982; Aggleton and Mishkin, 1983a, b; Zola-Morgan and Squire, 1985; Gaffan and Murray, 1990; Gaffan and Watkins, 1991; Parker et al., 1997; Mitchell et al., 2007a; Mitchell et al., 2007b; Mitchell and Gaffan, 2008). Even though many of the behavioral effects of MD lesions also occur following PFC lesions, the level of deficit is attenuated following MD lesions compared to PFC lesions (Fuster, 2008; Chudasama, 2011). This suggests that MD influences but cannot replace cognitive functions mediated by the PFC.

Neurophysiology of the primate MD and MD-PFC network in relation to PFC cognitive functions

Neurophysiological exploration of the MD has repeatedly found neurons that encode information about items stored in working memory during the delay period of delayed response tasks, similar to their PFC counterparts. The first reports of MD neurons exhibiting task selective activity during the delay period was provided by Fuster and Alexander (Fuster and Alexander, 1971, 1973). In these experiments, the authors recorded from MD neurons while monkeys performed a delayed response task and found that a majority of the recorded neurons exhibited significant delay period activity. Cooling the PFC diminished delay period activity in the MD, indicating that PFC input was necessary for the expression of delay period activity in MD neurons (Alexander and Fuster, 1973). Since these initial experiments, spatially-selective delay period activity in MD neurons has been reported during the performance of the oculomotor delayed response task (ODR) in which monkeys direct saccades to the locations of remembered visual targets (Tanibuchi and Goldman-Rakic, 2003; Funahashi et al., 2004; Watanabe and Funahashi, 2004a, 2018). Significantly more MD than PFC neurons encoded the direction of the saccadic response in the ODR task during the response period (Funahashi et al., 2004; Watanabe and Funahashi, 2004a). Also, in a version of the ODR task requiring that monkeys make a saccade in a direction rotated relative to the visual target (R-ODR), the neuronal population vector (vector sum of preferred directions of active neurons weighted by their firing rate) computed from MD neural activity rotated before the population vector in PFC (Watanabe et al., 2009). By comparing the activity of neurons between the ODR and R-ODR tasks, it was possible to determine whether delay period activity encoded the location of the prior visual cue or the future saccadic

response. These authors found that delay neurons encoding the future saccade direction comprised a larger fraction of active neurons in MD than PFC (Watanabe and Funahashi, 2004a, 2018). Taken together, these data suggest that the MD may play a stronger role in selection and execution of the motor response in comparison to the PFC.

In alignment with the idea that MD plays a direct role in PFC network computations related to response selection, Wurtz and colleagues have provided evidence that MD neurons relay saccadic corollary discharge signals from the superior colliculus (SC) to the frontal eye fields (FEF) (Sommer and Wurtz, 2004b, a). In this experiment, the authors utilized electrical stimulation to trace anatomical pathways linking the SC to the PFC through the MD. They identified single MD neurons that both received SC input (as indicated by orthodromic responses to SC stimulation) and also projected to the FEF (as indicated by antidromic responses to FEF stimulation). Then, while monkeys performed a delay-saccade task they characterized the information encoded by this subpopulation of MD relay neurons. They found that MD relay neurons most effectively conveyed signals from the SC to the FEF that occurred at the time of the saccadic response and reflected its direction. Additionally, when the authors inactivated the MD using muscimol (a GABA agonist), the monkeys could still perform saccades to visual targets accurately. However, when two saccades needed to be made to two visual targets flashed in series, the direction of the second saccade did not take the first saccade into account – that is, the second saccade was made in the direction originating from the initial fixation position to the second peripheral target. This reflects a failure to update the saccade plan by the shift in eye position produced by the first saccade. The observations that MD relay neurons primarily conveyed saccade related information and that inactivation of the MD caused a failure to update saccade plans based on prior

movements together support the theory that copies of saccade commands ('corollary discharge') are conveyed from the SC to the FEF through the MD. This is one of the most well worked out frameworks for the functional significance of MD-PFC interactions, and the results are consistent with a strong role in response processing in this thalamocortical network.

MD neurons also participate in nonspatial working memory. Tanibuchi and colleagues recorded MD neural activity during the performance of a delayed color match-to-sample, go/no go task (Tanibuchi et al., 2009b, a). They presented a stimulus (S1), either red or green, followed by a delay and second stimulus (S2), either red or green. The response was determined by the combination of the two stimuli: If S1 and S2 were the same color, the monkey lifted a lever ('Go' response), if they were different colors, the monkey did nothing ('NoGo'). The authors utilized electrical stimulation to identify MD neurons that received input from the SNr (substantia nigra reticulata) and that also projected to the principal sulcus. They report that activity in MD relay neurons encoded the color of S1 during the delay, as well as the color of S2 and the Go/NoGo response during the response period.

Neurophysiology of the rodent MD-PFC network in cognitive control

A number of studies have investigated the MD-mPFC network during task performance in rodents. Bolkan and colleagues (Bolkan et al., 2017) explored thalamocortical reciprocal interactions while mice performed a T-maze delayed nonmatch to sample task. Optogenetic inhibition of mPFC-to-MD and MD-to-mPFC pathways during the delay period impaired behavioral performance, suggesting a role for both reciprocal pathways in the maintenance of spatial information. However, delay

period inactivation of MD inputs to the mPFC had a stronger effect on behavioral performance than delay period inactivation of the mPFC inputs to the MD. Further, delay period inactivation of the MD-to-mPFC pathway weakened delay-period neural activity in the PFC and increasing activation in the MD-to-mPFC pathway during the delay improved working memory performance. In the choice phase, mPFC-to-MD interaction predominated. Specifically, optogenetic inhibition of the mPFC-to-MD pathway during the choice phase impaired performance, but inhibition of the reciprocal pathway did not. This suggested that communication between MD and PFC differed between the delay and choice phases of the task. Consistent with this, these authors also reported that the phase relationship between spikes in mPFC and beta oscillations in MD shifted between these periods, with mPFC spikes lagging MD beta oscillations in the delay period (suggesting MD-to-mPFC drive) and mPFC spikes leading MD beta oscillations in the choice period (suggesting mPFC-to-MD drive). Taken together, this data suggests that working memory maintenance of information relies on MD-PFC reciprocal interactions, with MD to the mPFC drive being particularly important, and further that response selection relies on mPFC input to the MD. Parnaudeau and colleagues (Parnaudeau et al., 2013) also examined the role of the MD in spatial working memory. They reported that pharmacogenetic inhibition of the MD resulted in the emergence of a behavioral impairment during the performance of the DNMS T-maze task and that MD neural activity phase locking to mPFC local field potentials (LFPs) in the beta frequency was strengthened during the choice phase and was preferentially affected when MD was inhibited (leaving phase-locking intact at theta and gamma frequencies). Lastly, Schmitt and colleagues (Schmitt et al., 2017) found that optogenetic inactivation of the MD resulted in a behavioral impairment in a 2- or 4- alternative forced-choice task that

resembled behavioral deficits following PFC optogenetic inactivation. MD inhibition resulted in diminished rule maintenance in PFC neurons during the delay period and PFC suppression resulted in the elimination of MD nonselective delay period activity. Studies of the rodent MD and mPFC network support the reciprocal dependency between the two areas for accurate and sustained maintenance of information during delay and choice periods.

Taken together, these anatomical, lesion, and neurophysiological experiments demonstrate that the MD is crucial for PFC-dependent cognitive function. The involvement of the MD in relation to spatial working memory has been the focus of many of the described lesion and neurophysiological studies; however, it is still relatively unknown how the MD participates in cognitive control behaviors at a cellular level and how MD-PFC network dysfunction relates to cognitive deficits in patients with SZ.

Cognitive deficits in Schizophrenia associated with MD-PFC network dysfunction

Even though cognitive deficits are not part the diagnostic criteria for SZ, it is well documented that patients exhibit a wide-range of cognitive deficits. These include impairments in attention, working memory, processing speed, executive functioning, verbal fluency, verbal memory, and learning (Nuechterlein and Dawson, 1984; Hoff et al., 1992; Saykin et al., 1994; Censits et al., 1997; Mohamed et al., 1999; Riley et al., 2000; Townsend et al., 2001; Kerns et al., 2008; Kravariti et al., 2009; McCleery et al., 2014). Executive function deficits consist of impairments on strategy formation and initiation, inhibition of prepotent responses and cognitive set shifting (Abramczyk et al., 1983; Sullivan et al., 1993; Riley et al., 2000; Kerns et al., 2008; McCleery et al., 2014).

Patients exhibit these deficits often years before the onset and diagnosis of the illness as measured in clinically high risk populations (Jones et al., 1994; Cannon et al., 2000; Niendam et al., 2003; Wood et al., 2003; Hawkins et al., 2004; Bartók et al., 2005; Keefe et al., 2006; Lencz et al., 2006; Niendam et al., 2006; Pukrop et al., 2006; Smith et al., 2006; Eastvold et al., 2007; Niendam et al., 2007; Pukrop et al., 2007; Simon et al., 2007; Lesh et al., 2011), are stable over time (Jones et al., 2010; Albus et al., 2019), occur regardless of medication used (MacDonald et al., 2005b; Jones et al., 2010), and are predictive of functional outcome for patients (Green et al., 2004; Green, 2006; Ventura et al., 2009). Interestingly, first degree relatives of patients exhibit cognitive deficits, although milder in their expression (Franke et al., 1993; Keefe et al., 1994; Faraone et al., 1995; Egan et al., 2001; MacDonald et al., 2003; Kuha et al., 2007). Although cognitive deficits are pervasive across many patients with SZ, they are not reliably improved by either typical or atypical neuroleptics (Mortimer, 1997; Stip et al., 2005).

A key aspect of cognitive deficits in patients is the inability to use contextual information maintained across a delay to flexibly modify responses to subsequent stimuli (Barch et al., 2003; MacDonald, 2008; Lesh et al., 2011; Barch and Ceaser, 2012). Context processing combines many of the deficits described above into one construct (i.e. working memory, selective attention, response inhibition, executive control) (Cohen and Servan-Schreiber, 1992; MacDonald, 2008). This construct of context processing has provided a particularly selective measure of cognitive dysfunction in patients with SZ as deficits are found in patients regardless of medication state (Servan-Schreiber et al., 1996) and in first-degree relatives (MacDonald et al., 2003; Richard et al., 2013). Additionally, context processing impairments are not simply due to working memory

deficits but also to response inhibition and executive control, as deficits in context processing are correlated with deficits in the Stroop task (Cohen et al., 1999; MacDonald, 2008) and patients exhibit deficits in context processing even when the delay is removed from the task (MacDonald et al., 2003). Context processing deficits have been reliably measured in patients with SZ during the performance of the AX-continuous performance task (AX-CPT) (Barch et al., 2003; MacDonald, 2008). Additionally, performance on the AX-CPT appears to reveal more severe and chronic impairments in patients with SZ spectrum disorders compared to patients with non-SZ psychosis, bipolar disorder, or depression (Barch et al., 2003; Barch et al., 2004; Holmes et al., 2005; MacDonald et al., 2005b; Brambilla et al., 2007). In addition to the AX-CPT, a variant of it, the dot-pattern expectancy (DPX) task, has also been used as a measure of context processing deficits in patients with SZ (MacDonald et al., 2005a; Jones et al., 2010; Strauss et al., 2014; Lopez-Garcia et al., 2016; Ray et al., 2017; Chun et al., 2018; Smucny et al., 2019). The AX-CPT and DPX task have also been reported to engage the same neural network including the dorsolateral PFC and dorsal posterior regions, indicating similar recruitment of neural system independent of the stimuli used (Lopez-Garcia et al., 2016). Due to the removal of familiar stimuli (letters) and replacement with unfamiliar stimuli (dot-patterns), the DPX task has been used in a pharmacological monkey model of SZ for translational purposes (Blackman et al., 2013).

Functional neuroimaging and EEG studies have compared physiological activation of PFC and its distributed network in patients with SZ and control subjects to determine the mechanism cognitive control deficits that patients exhibit. PFC activation is consistently reduced in patients with SZ performing cognitive control tasks, including the AX-CPT and DPX tasks, relative to comparison subjects (Berman et al., 1986;

Weinberger et al., 1986; Weinberger et al., 1992; Seidman et al., 1994; Barch et al., 2001; Perlstein et al., 2003; Yoon et al., 2008; Lesh et al., 2013; Poppe et al., 2016) and has been reported in SZ patients at first episode that are not on antipsychotic medication (MacDonald et al., 2005b). Additionally, disconnection across PFC networks has been found to be associated with cognitive control deficits. A recent functional imaging study investigated patterns of functional coupling between areas in PFC cortical networks during DPX task performance and found significant reductions in network connections in patients with SZ (Ray et al., 2017), a pattern that has been observed in multiple task contexts (Fornito et al., 2012).

Additional evidence indicates that reduced functional activation specifically of the MD-PFC network is associated with cognitive control impairments in patients with SZ. A meta-analysis of 41 imaging studies in patients with SZ during performing cognitive control tasks identified which activation differences between patients and control subjects were most commonly associated with poorer cognitive performance in the patient group (Minzenberg et al., 2009). Studies using many different cognitive tasks were selected to probe effects across different cognitive domains, including DMS, N-back, AX-CPT and Stroop tasks. They report reduced activation in the left dorsolateral PFC, rostral/dorsal ACC, and left MD correlated with poorer cognitive control performance in patients and that these regional reductions were significantly correlated across individuals. A recent study determined that a reduction in anatomical connectivity using DTI between MD and PFC correlated with poorer working memory performance on delayed response tasks but did not correlate with poorer performance on the AX-CPT (Giraldo-Chica et al., 2018). Lastly, another recent study reported that improvement in

cognitive behaviors following cognitive behavioral therapy correlated with functional thalamocortical coupling (Ramsay et al., 2017).

In order to better characterize the potential dysfunction in MD-PFC network in SZ, imaging studies have explored thalamocortical functional connectivity at rest. Resting state functional connectivity using MRI has shown that MD-PFC connectivity is reduced in SZ (Welsh et al., 2010; Woodward et al., 2012; Anticevic et al., 2014b; Anticevic et al., 2014a; Tu et al., 2015). This reduction was unique to MD-PFC thalamocortical connections, as functional connectivity between motor and somatosensory cortices and the thalamus were increased in SZ (Woodward et al., 2012; Anticevic et al., 2014a). Moreover, MD-PFC functional disconnection has been demonstrated in patients at both early-stage and chronic stages of illness (Woodward and Heckers, 2016), as well as in clinically high-risk individuals before the onset of SZ symptoms (Anticevic et al., 2015b). This suggests that the thalamocortical disconnection between the MD and PFC occurs, potentially, prior to onset and persists throughout the course of the disorder. Taken together, these studies support functional disconnection between the MD and PFC in patients with SZ that may result in PFC-network failures underlying cognitive deficits.

NMDA receptor hypofunction and the disconnection theory of Schizophrenia

Glutamatergic signaling, particularly via NMDARs, has been implicated via genetic, molecular, and pharmacological studies as altered in SZ (Stone et al., 2007). Post-mortem assays have reported decreased cortical expression of NMDAR mRNA in prefrontal cortex (Sokolov, 1998) and temporal cortex (Humphries et al., 1996), as well as decreased expression of synaptic proteins associated with NMDAR mediated

transmission, including PSD95 (Funk et al., 2009). Additionally, genome-wide association studies have identified a family of single nucleotide polymorphisms (SNPs) that increase risk of SZ and that are located near genes coding for proteins that influence NMDAR dependent synaptic transmission (Schizophrenia Working Group of the Psychiatric Genomics Consortium, 2014). Pharmacological studies have reported that NMDAR antagonists, like phencyclidine (PCP), ketamine, and dizocilpine (MK-801) can reliably reproduce positive, negative and cognitive symptoms of SZ (Luby et al., 1959; Krystal et al., 1994; Javitt, 2007; Anticevic et al., 2015a; Xu et al., 2015; Cheng et al., 2018). Recently, pharmacological treatments targeted at NMDAR modulation via glycine or d-serine have found improvement in positive and negative symptoms (Tsai and Lin, 2010; Umbricht et al., 2014). However, these effects have been hard to replicate reliably (Weiser et al., 2012; Goff, 2014).

A dominant theory of schizophrenia proposes that disconnection of prefrontal networks underlies the essential dysfunctions in neural activity and cognition in patients (Friston, 1998; Stephan et al., 2006). Post-mortem studies in SZ reveal a loss of dendritic spines on pyramidal neurons, particularly in layer 3 of dorsolateral PFC cortex (Glantz and Lewis, 1997, 2000; Kolluri et al., 2005; Glausier and Lewis, 2013). NMDARs are involved in spike timing dependent plasticity (Dan and Poo, 2004; Stephan et al., 2006; Feldman, 2012), and deficits in NMDAR function could contribute to activity-dependent disconnection of PFC local and thalamocortical circuits. It was recently reported that repeated exposure to phencyclidine (PCP, an NMDAR antagonist) in monkeys resulted in a reduction in synchronous (‘0-lag’) spiking in prefrontal neurons along with the chronic disconnection of local PFC circuits (Zick et al., 2018). Therefore, aberrant NMDAR function in SZ could contribute to disconnection of MD-PFC

thalamocortical networks both by disturbing the molecular mechanisms of synaptic plasticity as well as the synchronicity of spiking activity that enhances synaptic connectivity via spike-timing dependent plasticity. It has been hypothesized that loss of thalamic glutamatergic input to layer three of dorsolateral prefrontal cortex may contribute to the reduction in dendritic spines that is found there (Kolluri et al., 2005; Lewis and González-Burgos, 2008; Glausier and Lewis, 2013). Finally, thalamic volume has also been found to be altered, particularly in higher order thalamic nuclei like the MD, in SZ (Smith et al., 2011). Together, this data points to the potential for thalamocortical disconnection to underly cognitive control deficits in SZ due to a decrease in PFC local and thalamocortical circuit function. However, we are still lacking an understanding of how cells in the MD and PFC contribute to cognitive control and how their dysfunction contributes to cognitive control deficits in SZ.

Animal model of cognitive control deficits in SZ

What is missing in our understanding of schizophrenia as a disease is how the function of neurons is altered at the cellular level to produce cognitive deficits and symptoms. To answer these questions requires animal models that allows us to reliably and validly translate cognitive deficits from patients to animal models and back-translate neural deficits (and eventually treatments) from animal models to patients (Averbeck and Chafee, 2016; Mitchell et al., 2018; Heilbronner and Chafee, 2019). Developing animal models of SZ is particularly challenging because many of the symptoms (including affective and perceptual changes that are expressed primarily through language) are difficult if not impossible to model in any nonhuman species. Another factor limiting the chances that results will effectively translate between animal models and patients is the

extent to which neural architecture and computations differ between species. There are two primary dimensions along which animal models and patients with SZ need to be matched: behavioral manifestations of SZ such as cognitive deficits, and causal factors that increase risk of SZ, specifically genetic mutations. A number of mouse genetic models have been developed to explore the effect of risk mutations on prefrontal network dynamics and cognitive functions (Kellendonk et al., 2009; Jones et al., 2011; O'Tuathaigh et al., 2013; Leung and Jia, 2016; Simpson and Kellendonk, 2017; Van et al., 2017). However, the extent to which mice can mimic either cognitive deficits or prefrontal network dynamics in humans is not clear. It is likely that nonhuman primates are superior in this regard because monkeys can more accurately mimic cognitive deficits in patients with SZ (Blackman et al., 2013), and the degree of anatomical homology between prefrontal networks in humans and monkeys is much greater than between humans and rodents (Preuss, 1995), particularly including PFC neural networks (Preuss, 1995; Uylings et al., 2003; Carlén, 2017). The approach we, as a lab, have taken is to use NMDAR blockade to induce a state of cognitive (Blackman et al., 2013) and prefrontal network (Zick et al., 2018) failure using NMDAR antagonists that is potentially analogous to cognitive and network failures occurring in SZ.

It is important to consider the extent to which the NMDA receptor antagonist model exhibits face, construct, and predictive validity. The face validity of an animal model depends on the extent to which it can mimic outward manifestations of SZ, such as cognitive deficits that are seen in patients. The construct validity of an animal model relates to the extent to which the model replicates causal factors such as genetic mutation or underlying neural dysfunctions producing the SZ in humans. Lastly, the predictive validity of an animal model depends on the extent to which interventions that

are effective in restoring function in the animal model accurately predict how humans with the disease will respond to the same intervention. In regards to face validity, NMDA receptor antagonists, such as phencyclidine (PCP) and ketamine, reproduce the full spectrum of behavioral manifestations of SZ, including positive, negative and cognitive symptoms in humans and animal models (Luby et al., 1959; Krystal et al., 1994; Jones et al., 2011; Frohlich and Van Horn, 2014; Anticevic et al., 2015a; Lodge and Mercier, 2015; Xu et al., 2015; Cheng et al., 2018). Repeated administration of NMDA receptor antagonists acutely and chronically decreases prefrontal DA utilization and glutamate levels in the prefrontal cortex that are correlated with impairment performance on a delayed alternation T-maze task and ODR task (Jentsch et al., 1997b; Jentsch et al., 1997a; Jentsch et al., 1998; Tsukada et al., 2005) and spine density in the PFC that are similar to findings in patients with schizophrenia (Kolluri et al., 2005; Hajszan et al., 2006; Lewis and González-Burgos, 2008; Jones et al., 2011; Glausier and Lewis, 2013), supporting the construct validity of the NMDAR antagonist model. Evidence that NMDAR transmission is aberrant in patients with SZ provides additional support (Humphries et al., 1996; Sokolov, 1998; Stone et al., 2007). NMDA receptor antagonist models also have predictive validity due to data showing that atypical antipsychotics ameliorate the negative effects of NMDA receptor antagonists on spatial learning, spatial memory, and reversal learning (Abdul-Monim et al., 2006; Didriksen et al., 2007; Roberts et al., 2010; Jones et al., 2011).

To further increase the translational strength of our pharmacological monkey model, we back-translated a task that effectively targets specific cognitive deficits in context processing, working memory, and prepotent inhibition in patients with SZ (MacDonald, 2008; Jones et al., 2010). The dot pattern expectancy task (DPX) and its

counterpart, the AX-Continuous performance task (AX-CPT), consist of four different trial types that require a response to a probe stimulus based on the previously shown cue stimulus. Patients with SZ exhibit a specific error in responding when a habitual response to the probe stimulus must be countermanded based on the prior cue stimulus' identity, regardless of illness stage or medication (MacDonald et al., 2005b). Monkeys that perform the DPX task following an injection of PCP exhibit the same error pattern (Blackman et al., 2013). The experiments described in this dissertation investigate altered PFC thalamocortical function in the NMDAR antagonist monkey model, leveraging the face, construct, and predictive validity of this model to increase the probability that neural pathophysiology I find will be relevant to network failure in patients with SZ.

Specific goals and significance of the current experiments

The overarching goal of my thesis work is to characterize the role of PFC – MD network dynamics underlying the production cognitive control deficits in a monkey model of SZ. To this end, I first describe the role of the MD thalamus in cognitive control behavior as it relates to the PFC and characterize the distribution and transmission of information processing between the MD and the PFC. Then, I characterize how the MD-PFC network is changed following exposure to the NMDA receptor antagonist, PCP. To accomplish this goal, I performed large-scale recording of neural activity within the MD and PFC, simultaneously, and related this spiking activity to cognitive control performance and the subsequent changes caused by NMDA receptor blockade. As will be seen below, the MD and PFC, while similar in regard to the encoding of cognitive control, have distinct functions in the production of cognitive behavior and are

differentially affected by PCP. I am the first to perform large-scale recordings in the MD and the PFC concurrently, during performance of a context processing task, and in a model of the cognitive deficits in schizophrenia. The findings described in my dissertation will further our understanding of higher-order thalamocortical networks underlying cognitive control and how those networks may be affected in SZ. Further, this research could inform the development of therapeutics that target thalamic structures to improve functional connectivity in a manner specifically targeting pathophysiological states.

CHAPTER 2:

Thalamocortical dynamics in the healthy state: Relation of MD-PFC neural activity to computations for cognitive control

ABSTRACT

The MD thalamus has been implicated to play a role in a range of cognitive functions via reciprocal connections with the PFC (Watanabe and Funahashi, 2012; Mitchell and Chakraborty, 2013; Parnaudeau et al., 2018). Still, little is known about how the neurons in the primate MD directly participate in cognitive control. To address this question, I trained monkeys to perform a cognitive control task that reliably measures cognitive deficits in patients with schizophrenia, the dot pattern expectancy task (MacDonald et al., 2005a; Jones et al., 2010), and used linear multi-electrode arrays to record neural activity in the MD and PFC simultaneously. I found that the MD contained neurons, like their PFC counterparts, that encoded the cognitive control state (the need to override the habitual response) that did not reflect stimulus features and was not aligned to the motor response. Additionally, these state neurons modulated their activity based on the amount of cognitive control required. I report that response signals were markedly more common in the MD than the PFC, single neuron and population level representations of the response were much stronger in the MD compared to the PFC, and MD neurons did not exhibit a preference bias for the non-habitual response as did the PFC neurons. I also found that transmission of task-relevant information within and between the MD and PFC occurred while monkeys performed a task. Our data provides

evidence that the MD is recruited for cognitive control processing via PFC input and the MD plays a stronger role in response selection.

INTRODUCTION

Cognitive control is the ability to use internally stored rules or goals to modify the mapping between sensory inputs and motor outputs; It is the flexible and purposeful resolution of action conflict. The prefrontal cortex (PFC) has been implicated as a key brain region involved in a number of aspects of cognitive control (Goldman-Rakic, 1987; Miller and Cohen, 2001; Schiffer et al., 2015). Neurophysiology studies have found that spiking activity in PFC neurons encodes the state of the task (Asaad et al., 2000), rules (Wallis et al., 2001b; Buschman et al., 2012), and abstract categories (Freedman et al., 2001; Christoff et al., 2009; Goodwin et al., 2012; Crowe et al., 2013b), and they rapidly adapt to changes in rules and context by adjusting how stimulus features are mapped onto actions (Roy et al., 2010; Goodwin et al., 2012; Mante et al., 2013; Crowe et al., 2014; Blackman et al., 2016). Challenging traditional thought of cognitive control as merely a cortical phenomenon, the mediodorsal nucleus of the thalamus (MD) has arisen as potential region involved in cognitive functions for its extensive reciprocal connections to the PFC (Goldman-Rakic and Porrino, 1985; Preuss and Goldman-Rakic, 1987; Xiao et al., 2009) and its involvement in a number of aspects of cognition. MD lesions in the monkeys (Isseroff et al., 1982; Zola-Morgan and Squire, 1985; Parker et al., 1997) and inactivation of the MD in rodents (Parnaudeau et al., 2013; Bolkan et al., 2017; Schmitt et al., 2017) produce deficits in working memory. Additionally, lesions in humans restricted to the MD produce executive function deficits as measured by the WCST and Stroop Task (Van der Werf et al., 2000; Van der Werf et al., 2003).

Neurophysiological experiments have found that during working memory based tasks, primate MD neurons encode the state of the task, exhibit delay period activity, and provide impending response information to the cortex (Fuster and Alexander, 1971, 1973; Tanibuchi and Goldman-Rakic, 2003; Sommer and Wurtz, 2004b, a; Watanabe and Funahashi, 2004b, a; Tanibuchi et al., 2009b; Watanabe et al., 2009; Watanabe and Funahashi, 2018). Furthermore, the PFC and MD physiologically interact during working memory, as indicated by the finding that inactivation of prefrontal cortex attenuates working memory signals in the MD nucleus in primates (Alexander and Fuster, 1973). Rodent studies inactivating the MD have found a similar attenuation of working memory signals in the mPFC (Bolkan et al., 2017; Schmitt et al., 2017). Still, simultaneous MD-PFC recording has not been conducted in monkeys performing a cognitive control-based task, to our knowledge, leaving a gap in our understanding of the role of the MD neurons in cognitive control performance and how neurons in both regions interact during said performance.

Patients with schizophrenia exhibit deficits in cognitive control that are reliably measured by the AX continuous performance (MacDonald et al., 2005b) and dot-pattern expectancy (DPX) tasks (MacDonald et al., 2005a; Jones et al., 2010), regardless of disease state or medication. Cognitive control deficits in patients have also been associated with reduced activation of the MD nucleus and the PFC (Minzenberg et al., 2009). To relate cognitive control deficits to altered prefrontal network dynamics at the cellular level, my lab previously translated the DPX task to nonhuman primates (Blackman et al., 2013; Blackman et al., 2016; Zick et al., 2018). In order to determine how the MD-PFC network functions during performance of a cognitive control task, I recorded simultaneously in the MD and PFC using large scale recording arrays. The

goals of this experiment were to determine 1) how the MD represents cognitive control performance information and 2) the dynamics within and between the two structures underlying aspects of healthy state cognitive control behavior. I found that the MD contains neurons that reflect cognitive control in a similar manner to the PFC. However, the PFC produces strong counter-habitual signals specifically when cognitive load is high, while the MD produces signals relating to action selection based on changing contexts. I also report that MD and PFC neurons reciprocally transmit information about task variables to one another during different trial periods.

MATERIALS AND METHODS

Subjects

I recorded neural activity in the dorsolateral PFC and the MD in two male monkeys (*Macaca Mulatta*; 8-11 kg) during performance of the DPX task. All animal care and experimental procedures conformed to the National Institutes of Health guideline and compiled with protocols approved by the Animal Care and Use committee at the University of Minnesota and the Minneapolis Veterans Affairs Medical Center.

The DPX Task and Conditions

The DPX task was described in detail in a previous report from my lab (Blackman et al., 2013). Monkeys sat in a primate chair about 77.5 cm in front of a back-projection screen. An LCD projector (Dell 5100MP DLP) presented the visual stimuli. An infrared eye tracking system (ISCAN Inc. Woborn, MA) recorded eye position at 60 Hz. Each trial consisted of a cue stimulus and probe stimulus presented in sequence, followed by a

joystick response (left or right) depending on cue-probe sequence shown. Cue and probe stimuli consisted of patterns of dots: A-cues and X-probes each consisted of a single dot pattern, while B-cues and Y-probes were any of 5 dot patterns each (Fig. 2.1B). Trials began with a 500 ms period of gaze fixation of a central fixation target (cross). Gaze fixation within 3.3° of a fixation cross was required until the response was made. After the initial fixation period, a cue stimulus was presented at the center of the display for 1.0 s. Following the presentation of the cue there is a 1.0 s delay period that contained only the fixation cross. Next a probe stimulus was displayed for 0.5 s at the center of the display. The cue and probe stimuli subtended 2.7° - 4.4° of visual angle. From the time the probe stimulus was presented, the monkey had 1.0 s to move a handheld joystick to the left or right. A correct, target or nontarget response movement, determined by the combination of the presented cue and probe stimuli, was rewarded by a delivery of a drop of juice (~0.1ml) at the end of the intertrial interval (1.1 s after probe offset). Trials in which an A-cue was followed by an X-probe (AX trials) were valid trials, requiring a leftward joystick movement (target response). All other cue-probe combinations (AY, BX, and BY) were invalid trials that required a rightward joystick movement (nontarget response; Fig. 2.1C). The probe was presented for the entirety of the 0.5 s probe period, regardless of the time of the response (analogous to the way the task is administered for human subjects).

We administered the DPX task in two different trial sets, balanced and prepotent, which differed in the proportion of cue and probe stimuli. In balanced sets there were an equal proportion of the four cue-probe trial sequences (AX, AY, BX, BY). These included 80, 200, or 400 trials (in 20, 27, and 1 neural ensemble(s), respectively). In prepotent trials sets the majority of trials (69%) presented the target cue-probe sequence (AX).

The remaining trials (31%) presented nontarget cue-probe sequences (AY 12.5%, BX 12.5%, BY 6%). Prepotent trial proportions were replicated from the DPX task and AX-CPT that were administered to patients (MacDonald et al., 2005a; Jones et al., 2010). Prepotent sets included either 320 or 400 trials total (in 19 and 29 ensembles, respectively). For neural ensembles included in this study, I recorded neural activity during the performance of both a balanced and prepotent trial set. The prepotent sets presumably create a prepotent motor habit to produce the leftward joystick movement in response to the X-probe presentation, as this was the required response ~4/5 of the times the X-probe was presented. Overriding this habitual response on BX trials therefore required utilization of cognitive control to countermand a prepotent action. AY trials similarly required increased cognitive control, as the A-cue implies the target response, which the Y-probe must countermand.

Monkeys received an intramuscular injection of saline (Mk1: 0.3mL; Mk2: 0.6mL) before recording neurophysiological data for 18 of the 48 neural ensembles included in this study. These saline injections were part of a study to investigate the effects of the NMDA receptor antagonist phencyclidine on the neural activity in the mediodorsal nucleus of the thalamus and the prefrontal cortex. All neural data included in the present study were recorded before monkeys had been exposed to phencyclidine.

Neural Recording

Prior to surgery structural MRI images of monkeys were obtained at 3T to localize target recording regions: the banks of the principal sulcus in prefrontal cortex (PFC, Brodmann area 46) and the mediodorsal nucleus of the thalamus (MD) (Fig. 2.2). Recording grid and electrode penetration locations were projected onto monkey-specific

cortical surface reconstructions of the locations of cortical sulci obtained from MRI images (Fig. 2.2A, B). In order to visualize electrode trajectories in depth and target the MD, I used the Cicerone software package (Miocinovic et al., 2007) that generated 3D rotatable MRI volumes from the 2D image stack and visualized chamber placements and electrode angles. This allowed for more precise chamber placement to achieve specific electrode angles that intersected the MD in each monkey. Following recording, I obtained CT scans to visualize recording locations. I inserted stainless steel probes of approximately the same diameter as the recording electrodes passing through the center of locations and depths where MD neural recordings were conducted. The steel probe was visible in the CT scans. I uploaded the CT image stack into Cicerone and aligned the CT and pre-recording MR image stacks. I confirmed the trajectory of the electrode penetrations that intersected the MD in both monkeys (Fig. 2.2C, D; eliminating data from 2 days of recording in which the electrode missed MD).

Monkeys underwent an aseptic surgical procedure under isoflurane gas anesthesia (1-2%). Two craniotomies were made in the skull, one positioned to record from the dorsolateral PFC and one positioned to record from the MD in the left cerebral hemisphere. Five titanium posts were screwed to the surface of the skill using titanium screws. PEEK recording chambers (PFC: 19mm i.d.; MD: 16mm i.d.) were placed over the craniotomies and fixed to the screws and posts using surgical bone cement. A halo was attached to the posts using metal tabs for head stabilization. Post-surgical analgesia was maintained for several days using an injectable analgesic (Buprenex, 0.05mg/kg i.m., twice a day).

Neurophysiological recordings were obtained using dual 32-channel silicone vector arrays (Neuronexus Technologies Inc.; Acute Vector Array (Deep Brain); Ann

Arbor, MI) each advanced independently into the brain using a NAN motorized Microdrive (NAN Instruments; NAN C Drives; Nazareth Illit, Israel). Two vector array electrode geometries were used throughout the experiment ('Edge', 32 electrodes in a linear array, 100 µm spacing; and 'Poly2', 2 staggered 16 electrode linear arrays, 50 µm spacing), extending from the end of a 400 µm O.D. stainless tube support body. I advanced each electrode through a stainless-steel guide tube (600 µm O.D.) which penetrated the dura. The edge design was used for MD recording in 29 ensembles and the poly2 design was used in the remaining 19 ensembles. The poly2 design was used for all 48 ensembles in the PFC. Neural data was recorded via a 64-channel Ephys digital signal processing data acquisition system (Tucker-Davis Technologies Inc., Alachua, FL). Recorded signals on each electrode were amplified and bandpass filtered (between 100 and 5000 Hz) and monitored during neural recording for the emergence of spiking neural activity once electrodes passed from white matter into the MD nucleus and to evaluate stability of spiking activity during recording. Amplified and filtered electrode signals were sampled at a frequency of 24414.1 Hz and saved to disk along with time stamps indicating behavioral events. I sorted the action potentials of individual neurons based on a principle components analysis of recorded signals implemented by an open-source software package (Kilosort Suite) (Pachitariu et al., 2016).

Data Analysis

Behavioral Analysis

I analyzed differences in percent correct performances as a function of trial type (cue-probe sequence) using the chi-squared goodness of fit test applied to counts of

correct and error trials per trial type ($p<0.05$). I analyzed differences in response time as a function of trial type using a Kruskal-Wallis test followed by post-hoc pairwise Tukey-Kramer tests.

ANCOVA - based classification of neural activity

I applied analysis of covariance (ANCOVA) to trial-wise firing rates measured within cue, delay, probe and response windows to detect significant modulation in relation to task variables. Cue, delay and probe windows were coextensive with their corresponding task epochs (Fig. 2.1). The response window was ± 200 ms centered on the time of the joystick movement. I used firing rates in the pre-cue fixation period as the covariate to control for trial-by-trial fluctuations in baseline activity. I applied ANCOVA to firing rates for all neurons combined across prepotent and balanced trial sets. To identify neurons in which activity varied as a function of the cue stimulus during the cue or delay periods I applied a one-way ANCOVA with cue (A vs B-cue) as the single factor to firing rates in these time periods. To identify neurons in which activity varied as a function of the cue and probe stimulus during the probe period, I applied a two-way ANCOVA with the cue stimulus (A vs. B) and the probe stimulus (X vs. Y) as the factors. To identify neurons in which activity varied as a function of the response, I applied a one-way ANCOVA with response direction (target vs. nontarget) as the single factor. Neurons were classified on the basis of the trial periods and the task factors yielding significance in the ANCOVAs ($p<0.05$) and based on the preference for one of the stimuli (A vs B or X vs Y) or response (target vs nontarget) factors. I further split cue neurons in to separate classifications based on the time in the trial that their neural activity was significantly modulated in response to the cue stimulus shown: Early cue neurons were

those with a cue preference during the cue period, delay cue neurons were those with a cue preference during the delay period, and late cue neurons were those with a cue preference during the probe period.

To compare significant differences in MD and PFC population proportions of significant neurons assigned to the ANCOVA-defined categories, I performed Z-score tests of proportions across the categories in the MD and PFC (i.e. proportion of all significant neurons in the MD vs proportion of all significant neurons in the PFC, proportion of significant cue neurons in the MD vs proportion of those in the PFC, proportion of significant probe neurons in the MD vs. proportion of those in the PFC, and proportion of response neurons in the MD vs proportion of response neurons in the PFC). I also wanted to determine significant biases with ANCOVA -defined categories existed within the MD and the PFC. To do this I performed a one sample Z of proportions within each category (early A vs B cue, delay A vs B cue, late A vs B cue, probe X vs Y, and response target vs nontarget; $p<0.05$, two-tailed).

Analysis of population of average activity

To obtain continuous estimations of firing rate (spike density functions, SDFs), I convolved each neuron's spike train with a Gaussian kernel (with a SD of 40 ms) using the 'ksdensity' function in Matlab. I averaged single trial SDFs over groups of trials with the same cue-probe sequence (AX, AY, BX, BY) for each neuron and then averaged SDFs over neurons with the same cue, probe or response preference to visual population activity (Fig. 2.5).

I found that individual neurons often exhibited different stimulus preferences at different times in the trial (Fig. 2.5), producing multiple significant relationships to task

variables in the ANCOVA making it difficult to classify neurons using traditional ANCOVA-based methods. I compared activity patterns across ANCOVA defined categories and identified patterns of significant ANCOVA results that corresponded to the same functional groups of neurons. This resulted in seven neuronal groups based on unique combinations task periods (cue, delay, probe, response) and factors (cue, probe, response), combined with the specific stimulus or response preferences of each neuron during those periods (Fig. 2.6). The groups are non-overlapping and take into account all of the functional preferences I observed. Group 1 neurons ('Early A-cue') were significant for the A-cue during the cue period. Group 2 neurons were significant for the B-cue during the cue period or the Y-probe during the probe period ('Early B-cue or Y-probe'; that is, neurons with either significant result exhibited essentially the same activity profile and so were combined). Group 3 neurons were significant for the A-cue during the delay or probe periods ('Delay A-cue or Late A-cue'). Group 4 neurons were similarly defined as Group 3 neurons were but preferred the B-cue ('Delay B-cue or Late B-cue'). Group 5 neurons were significant for the X-probe during the probe period. Groups 6 and 7 were significant for the response factor during the response period and preferred target (Group 6) and nontarget (Group 7) responses respectively. If a neuron was significantly modulated based on multiple task factors as indicated by the pattern results of the ANCOVA above, assignment to one group was determined by the factor associated with the most significant p-value. This grouping scheme is a modification of one developed previously in my lab to describe the heterogeneity of neural responses in PFC (Blackman et al., 2016), modified to accommodate new patterns of activity I observed in the MD.

Cue preference Index

To further understand the nature of cue preference switching between B-cues early in the trial and A-cues late in the trial, I computed a cue preference index to quantify the cue preference of each neuron for A and B cues, during the cue or probe period, as follows:

$$Index_{cue} = \frac{(A_{cue} - B_{cue})}{(A_{cue} + B_{cue})}$$

$$Index_{probe} = \frac{(A_{probe} - B_{probe})}{(A_{probe} + B_{probe})}$$

A is the average firing rate of a given neuron during A-cue trials and B is the average firing rate of the same neuron during B-cue trials. Cue subscript indicates firing rates were taken from the cue period and probe subscript indicates firing rates were taken from the probe period. Then to capture the switch in cue preference, I computed the difference cue preference indices between the cue and probe period:

$$Index_{switch} = Index_{probe} - Index_{cue}$$

Lastly, I performed a permutation test to evaluate the significance of switch index for each neuron by shuffling firing rates between the cue and probe period (1000 iterations) and recalculating the switch index. I considered the original switch index for a given neuron significant if it was greater than the 97.5 percentile or less than the 2.5 percentile of the shuffled distribution ($p<0.05$, two-tailed). To determine if the number of neurons that significantly switched their cue preference from B-cues in the cue period to A-cues in the probe period (cognitive control encoding neurons) were more or less numerous than neurons that switched their preference in the opposite direction (from A-cue in the cue period to B-cue in the probe period), I calculated a Z-test of proportions ($p<0.05$) between proportions of each type of switch neurons. This was also performed

on proportions of switch neurons in the MD and the PFC to determine if there were region-specific differences in the number of neurons that encoded cognitive control encoding.

Analysis of cognitive control load on neural activity

During the cue period, B-cues were associated with high cognitive control load (since they countermanded the habitual target response) and A-cues with low cognitive control load. The difference in firing rate between B and A-cue trials therefore provides a measure of cognitive control encoding. Similarly, during the probe period, AY trials were associated with high cognitive control load (since the Y-probe countermanded the habitual target response implied by the A-cue), and AX trials with low cognitive control load. To measure the influence of cognitive control on neural activity, I computed the difference in firing rate during the cue period on B-cue and A-cue trials, as well as the difference in firing rate during the probe period on AY and AX trials. I then compared these rate differences on a per neuron basis between balanced and prepotent trial sets and evaluated differences between them using a permutation test in which I shuffled trials of neural activity between the two sets and recomputed rate differences (100 iterations). I considered the difference in cognitive control effects on neural activity between balanced and prepotent datasets significant if it exceeded the 95^{th} percentile of the bootstrap distribution ($p < 0.05$).

Sliding-window regression analysis

I applied a sliding-window regression analysis to evaluate the strength and significance of the relationship between neuronal activity and task variables as a function

of time within the trial. I measured firing rates of single neurons on correct trials of prepotent trial sets, separately, within a sliding 100 ms window (advanced in 20 ms steps), and at each time step regressed the trial-by-trial firing rates onto the cue, probe, and response by fitting the following linear models:

$$R = \beta_0 + \beta_1 Cue + \beta_2 Probe + \beta_3 Cue * Probe + \varepsilon$$

$$R = \beta_0 + \beta_1 Response + \varepsilon$$

R is firing rate, *Cue* (A vs B), *Probe* (X vs Y), and *Response* (target vs nontarget) were dummy coded categorical variables, and *E* is the error (residual).

Neurons were ranked according to the magnitude of the peak significant regression coefficient and neuron numbers were equalized across brain areas by restricting the analysis to equal numbers of the most significant neurons in the two areas. The results of the regression analysis were then expressed as the proportion of explainable variance (PEV) associated with each regressor (Brincat and Miller, 2016), computed using the formula of (Olejnik and Algina, 2003):

$$\omega^2 = \frac{SS_{between\ groups} - df\ \times MSE}{SS_{total} + MSE}$$

To determine if there was a significant difference in the timing of signals across brain areas, I applied a Kolmogorov–Smirnov test to the cumulative distributions of the time to peak PEV. Additionally, I evaluated the significance of differences in population average PEV across the trial period between areas using a permutation test. I randomly shuffled regression results (PEV time series) between brain areas on a per neuron basis (1000 iterations) and compared the original difference between MD and PFC to the differences obtained from the bootstrap distribution. Area differences were considered

significant if they exceeded the 95th percentile of the bootstrap distribution and FDR corrected.

Population decoding analysis

To quantify information encoded by population activity patterns in the MD and PFC about the cue, probe, and response, I performed time-resolved pattern classification (Klecka, 1980; Johnson and Wichern, 1998; Crowe et al., 2010). I used the 'classify' Matlab function with empirical prior probabilities derived from the frequency of trials with level of the decoded variable in the training data and the diagonal covariance matrix estimate (diaglinear) options. I measured the firing rates of all significant neurons or neurons in specific functional groups in a sequence of 50 ms time bins throughout the trial. At each 50 ms time step, I used population activity patterns to decode the cue, probe and response on individual trials by constructing a vector of firing rates representing the population activity pattern at that time point. To construct this vector, I matched trials over recording days according to the trial repetition number of each of the decoded task variables (the first A-cue trial for each neuron, for example) and included firing rates in 3 consecutive 50 ms time bins from each neuron comprising a 150 ms sliding window. I used leave-one-out cross validation to perform the decoding; All trials (except the trial being decoded) were used as the training set to compute the mean (centroid) and covariance matrix of population activity patterns for subsets of trials corresponding to the potential values of the decoded variable (A and B-cue when decoding cue, for example). I then computed the Euclidean distance between the population activity pattern on the decoded trial in a specific time bin and the two group centroids computed using neural activity in the same time bin. That is, I allowed the

group centroids defining the population codes for the decoded variable to change over time and always compared population activity patterns to group centroids computed using training data at the same time point. I then converted the distance between the population activity pattern and the group centroids to posterior probabilities of the trial belonging to each of the two groups under the assumption that the distribution of population activity patterns in each group was multivariate normal. I assigned the trial to the group with the higher posterior probability. Repeating the decoding over time bins produced a time series of posterior probabilities quantifying fluctuations in the strength of population signals encoding specific items of task-defined information.

I included neurons in the populations if they had been recorded for a minimum number of trials in each set (70 trials for balanced and 230 trials for prepotent sets). I then ranked neurons in the two areas according to the significance of the p-value defining their group membership, and selected matching numbers of the most significant neurons in both the MD and the PFC. Equalizing neuron numbers and trial numbers removed differences between them as potential factors that would confound comparison between the strength of population encoding in the MD and the PFC. I used a permutation test repeating the decoding analysis after randomly shuffling trials of posterior probability time series between brain areas (1000 permutations). I considered original differences in decoding between brain areas significant if they exceeded the 95^{th} percentile of the bootstrap distribution (FDR corrected) of differences obtained after shuffling trials.

Signal Transmission analysis

Signal transmission analysis functions under the assumption that temporal correlations in the information that two different patterns of activity encode about the task (such as cue identity) results from physiological interactions between those two groups of neurons. Correlations in temporal patterns of information can thus allow the identification of functional linkages between two groups of neurons that are recorded simultaneously. In order to determine whether functional linkages exists within and between the MD and PFC, I applied signal transmission analysis to sets of simultaneously recorded neurons (neural ensembles) (Crowe et al., 2013b) that encoded the cue, probe and response. This allowed me to capture physiological interactions between neurons encoding different task variables that may implement conditional computations required by the task (such as, if A-cue, and X-probe, then target response). First, I identified subsets of neurons within each ensemble that encoded task variables of interest (as determined by ANCOVA-based classification above). Next, I applied time-resolved pattern classification to decode task variables using activity patterns in the neural subsets. This is analogous to the population decoding above except that neurons were limited to the sets of neurons in the PFC and MD that were recorded simultaneously. The decoding produced two posterior probability time series that capture moment-to-moment fluctuation in the strength of neural signals encoding different task variables in different brain structures. The question I addressed is whether these fluctuations were correlated in time, and if so at what lag, to infer the direction of flow of information through networks. To obtain unbiased estimates of correlation between the two time series, I first removed linear trends and autocorrelation in the time series by fitting an ARIMA (autoregressive, integrated moving average) model to the

probability time series. ARIMA models capture the variation in each time series explainable by its own prior history. The first step is to difference the time series to remove time trends. Next a regression is performed to predict the value at each time step as a weighted sum of prior values. Finally, additional regression coefficients are obtained to improve the prediction of the value at each time step by including a weighted sum of prior errors in prediction. I employed ARIMA models of order [10,2,2], including regressors for the 10 prior values in the time series in the autoregressive model, fitted the model after differencing the times series twice, and included regressors for the errors in estimation obtained for the prior 2 values. At this point, the residuals do not contain any variation based on its own history and are therefore likely to capture variation based on an outside source. I then used the residual values after fitting the ARIMA model to evaluate correlation between time series. I regressed one residual posterior probability time series onto the other within a sliding window of 500ms advanced in 50 ms time steps (at a lag of either plus or minus one 50 ms time bin). This produced a time series of F-statistics that measured fluctuation in the strength of functional coupling between groups of neurons that encoded task variables of interest in the same area or in different brain areas. When evaluating information transmission within area, the two groups of neurons were exclusive, eliminating the chance of the same neuron contributing to both times series in the final regression step. The significance of signal transmission was evaluated by comparing the transmission time series to a bootstrap distribution of time series obtained after randomly shuffling post-ARIMA probability time series between neural groups and repeating the sliding window regression analysis. I considered transmission significant if it exceeded the 95^{th} percentile of the bootstrap distribution, applying an FDR corrected method to maintain the overall Type 1 error rate at 0.05.

RESULTS

Behavioral Performance

The DPX task consists of four trial types based on four possible combinations of the cue (A, B) and probe (X, Y) stimuli (AX, AY, BX, BY; Fig. 2.1A-C) in sequence. Monkey 1 (Mk1) performed an average of 92% of DPX trials correctly and Monkey 2 (Mk2) performed an average of 90% of trials correctly. For both monkeys, performance varied as a function of trial type (Chi Squared Test: Mk1: AX=93%, AY=96%, BX=80%, BY=99%, X^2=269.41, p<0.001; Mk2: AX=90%, AY=92%, BX=83% BY=99%, X^2=364.81, p<0.001). There was an increased error rate on BX trials in both monkeys, indicating they occasionally released the prepotent target response to the X-probe. However, performance was maintained at 80% correct or greater for each of the trial types (Fig. 2.1D). Reaction time (RT) varied significantly based on the trial type for both monkeys (Fig.1E; Kruskal-Wallis test; Mk1 X^2 =2640.73, p<0.001; Mk2 X^2 =1401.61, p< 0.001). Post Hoc testing using multiple comparisons of mean ranks (p<0.01) indicated that for Mk1 RTs were significantly different across trial types, with RT being greatest on AY trials. Mk 2 RTs for A-cue trials were significantly longer than B-cue trials and RT was greatest on AX trials (BX and BY were not significantly different from each other).

Neural Database

I recorded 48 neural ensembles in the PFC and MD simultaneously, during the performance of one balanced and one prepotent set each. A total of 1,105 neurons in the PFC and 1,402 neurons in the MD (Mk1: 29 ensembles of 577 PFC neurons and 887 MD neurons; Mk2: 19 ensembles of 528 PFC neurons and 515 MD neurons) were

recorded. This included an average of 29 neurons in the MD (range 16 to 50) and 23 neurons in the PFC (range 9 to 52) per ensemble. In order to target the PFC and MD reliably and reproducibly, I inserted a grid into each recording chamber (Fig 2.2A, B, small black circles within each chamber indicates grid hole locations). Each recording location (Fig. 2.2A, B, red circles) produced between 1 – 6 ensembles (average of 2 ensembles per recording day). I confirmed that electrode penetrations successfully reached the MD by obtaining CT images of a metal probe inserted to the depth of the MD during neural recording inserting and co-registering the CT images with the pre-surgical MR images (Fig. 2.2C, D).

Neurons encoding cue, probe, and response in MD and PFC

I applied ANCOVA to identify neurons in which firing rate varied significantly ($p < 0.05$) as a function of the cue (A vs. B; during the cue, delay, or probe periods), the probe (X vs. Y; during the probe period), or the response (T vs NT; during the response period). Both the PFC and the MD contained neurons that significantly modulated their firing rates depending on the cue (Fig. 2.3, light blue), the probe (pink), and response (purple). Across the population of sampled neurons, 71% of PFC neurons and 84% of MD neurons exhibited cue, probe or response-selective activity. The proportion of sampled neurons that encoded task-related information was significantly higher in the MD than the PFC (Z-test of proportions; $Z = -7.63$, $p < 0.01$). The PFC (86%) and the MD (84%) had similar proportions of neurons that encoded cue information (Fig. 2.3A, B, blue circles; $Z = 1.44$, $p = 0.15$). The proportion of probe-selective neurons were significantly higher in MD (40%); Fig. 2.3A, B pink circles) than PFC ($Z = -4.20$, $p < 0.001$; PFC (30%). Lastly, the MD had a significantly higher proportion of response

neurons (66%) than the proportion in the PFC (48%; $Z = -7.57$, $p < 0.001$; Fig. 2.3A, B, purple circles). Overall, this data indicated variation in MD and PFC neural population recruitment for the encoding of the probe and response and similar recruitment for cue encoding.

Bar graphs in Figure 2.3 illustrate the numbers of cue, probe, and response-selective neurons that preferred A vs B-cues, X vs Y-probes, and T vs. NT responses in the PFC (Fig. 2.3C) and the MD (Fig. 2.3D). Cue neurons were split into three groups depending on the trial epoch during which their activity was significantly modulated by the cue. Early cue neurons (selective during the cue period) were biased to prefer B-cues in the PFC ($Z = -2.43$, $p < 0.05$) and the MD ($Z = -11.17$, $p < 0.001$). This bias switched during the probe period – late cue neurons were biased to prefer A-cues in both areas (PFC: $Z = 7.04$, $p < 0.001$; MD: $Z = 8.41$, $p < 0.001$). In the delay period, PFC neurons were biased to prefer A-cues ($Z = 5.56$, $p < 0.001$), whereas MD neurons were biased to prefer B-cues ($Z = 2.15$, $p < 0.05$). In the PFC probe neurons were significantly biased to prefer Y-probes ($Z = -3.66$, $p < 0.001$) and response neurons were significantly biased to prefer nontarget responses ($Z = -3.49$, $p < 0.001$). MD probe and response neurons did not show these biases (probe: $Z = -1.39$, $p = 0.164$; response: $Z = -0.90$, $p = 0.368$).

Individual neuron activity patterns during the DPX task

Next, I examined the diversity of firing patterns of individual neurons by plotting rasters and spike density functions (SDFs) of their activity separated by cue-probe sequence (trial type) in PFC (Fig. 2.4A-C) and MD (Fig. 2.4D-F). Some neurons modulated their firing rate in response to only one task factor during a single trial period.

Other neurons modulated their firing rate in response to multiple task factors during multiple trial periods. For example, the PFC neuron in Figure 2.4A primarily modulated firing rate during the cue period (B-cue preference), whereas the PFC neuron in Figure 4B modulated firing rate during both the cue period (B-cue preference) and the probe period (A-cue preference). I refer to neurons exhibiting early (cue period) B-cue preference and late (probe period) A-cue preference as 'switch neurons', as was reported previously (Blackman et al., 2016). I found that switch neurons exist also in the MD thalamus (Fig. 2.4D). Other neurons exhibited selectivity for the probe (Fig. 2.4E, F) and response (Fig. 2.4C).

Population neural activity patterns evoked by the DPX task

I first examined population activity of neurons separated according to the cue, probe or response preference of the neuron in addition to the trial epoch when selectivity was evident as detected by ANCOVA (Fig. 2.5). This revealed some general trends in population activity. Many ANCOVA-defined neural populations exhibited early B-cue preference, either during the cue period or delay period. This gave over to higher levels of activity during the probe period on A-cue trials (demonstrating the general 'switch' pattern in cue preference noted above). In addition, several of the neural populations that exhibited the switch pattern exhibited the overall highest activity during the probe period on AY trials in particular. Generally, these features of population activity were similar in the PFC and MD, suggesting that neurons in both areas were activated by stimulus combinations that instructed the necessity to override the prepotent, target response. Therefore, activity in these neurons generally correlated with the necessity to engage cognitive control. In addition, since many neurons tended to respond to multiple

task stimuli at different times in the trial, populations defined by significant ANCOVA results often exhibited similar activity profiles. Therefore, I combined populations with similar activity patterns into functional groups. This allowed for a more simplified classification without the loss of information contained within each group, as has been done with previous data sets recorded during DPX performance (Blackman et al., 2016). I adjusted this previously defined grouping scheme to account for the new activity patterns found in the MD. Neurons were assigned to one of seven non-overlapping functional groups based on the task factor significantly modulating their respective activity (cue, probe, or response), the trial period that activity modulation occurred (cue, delay, probe, or response), and the task condition associated with highest activity (A or B-cue, X or Y-cue, T or NT-response).

Group 1 (Fig. 2.6A: MD, and 2.6H: PFC) consisted of neurons with an early A-cue preference. These neurons exhibited a higher activity rate on A-cue than B-cue trials. Interestingly, Group 1 neurons in both the MD and the PFC population exhibited primarily a suppression of activity compared to the fixation period on B-cue trials.

Group 2 (Fig 2.6B: MD, and 2.6I: PFC) and Group 3 (Fig 2.6C: MD and 2.6J: PFC) populations exhibited the ‘switch’ in cue preference from B-cues during the cue period to A-cues during the probe period. Notably, probe period activity was better aligned to the onset of the cue (Fig 2.6B, C, I, J, left panels) than the timing of the motor response (right panel), suggesting that these neurons don’t play a direct role in motor control. Collectively switch neurons comprised a large fraction of task-related neurons in both areas. Group 2 was made up of neurons with an early B-cue preference or a late Y-probe preference and generally exhibited a switch from early B-cue to late AY trial selective activity. Group 3 was made up of neurons with either delay or late A-cue

preference. These neurons exhibited attenuated B-cue selective activity during the cue period that switched to A-cue selective activity during the probe period. The PFC population exhibited a decrease in delay period activity relative to baseline on B-cue trials (Fig. 2.6J), while the MD population did not (Fig. 2.6C).

Group 4 (Fig 2.6D: MD and Fig 2.6K: PFC) neurons were those with a preference for B-cues during the delay and probe periods. The MD and the PFC populations showed strong sustained delay period activity, classically associated with maintenance of information in working memory.

Group 5 (Fig 2.6E: MD and Fig 2.6L: PFC) neurons exhibited X-probe preference during the probe period. This group was much more prominent in the MD than the PFC, providing a clear distinction between these areas. Activity in Group 5 neurons was better aligned with the response (Fig. 2.6E, L; right panel) than probe onset (left panel), suggesting a role in response control.

Group 6 (Fig 2.6F: MD and Fig 2.6M: PFC) and group 7 (Fig 2.6G: MD and Fig 2.6N: PFC) were made up of neurons exhibiting response selectivity activity for T (Group 6) and NT (Group 7) motor responses. Neurons exhibiting response-selective activity were much more prominent in MD (Fig. 2.6F, G) than PFC (Fig. 2.6M, N), both in terms of numbers of neurons and strength of signal. This suggests that MD plays a more direct role in response programming and or selection than PFC.

Quantification of the population of switch neurons

To quantify ‘switch neurons’ in the MD and PFC, I computed cue preference indices that captured neural preferences of A vs. B-cues in the cue and probe periods (difference in firing rate divided by the sum for each pair of conditions, Fig. 2.7). Neurons

significant for the pattern of activity associated with encoding of cognitive control load (Early B-cue to late A-cue preference switch; MD - 106 out of 248 neurons encoding the cue during both the cue and probe periods; PFC - 70 out of 133) were significantly more numerous than neurons that switched in the opposite direction (Early A-cue to late B-cue preference; MD - 26 out of 248; PFC - 18 out of 133; Fig. 2.7, red circles vs. blue circles) in the PFC (Fig 2.7A; z-test of proportions: $Z = 6.78$, $p<0.001$) and MD (Fig. 2.7B; $Z = 6.95$, $p < 0.001$). There were no significant differences in the proportion of significant 'switch' neurons between the MD and PFC ($Z = 1.85$, $p = 0.064$).

Influence of cognitive control load on switch neuron activity

To investigate whether modulation of cognitive control load at the behavioral level influenced information processing in the MD-PFC network, I contrasted neural activity on balanced and prepotent trial sets. In balanced trial sets, all four cue-probe sequences occurred with equal probability. In prepotent trial sets, the majority of trials (69%) presented the AX cue-probe sequence, increasing the strength of the target response habit (and the level of cognitive control required to override it). During the cue period, B-cues were associated with high cognitive control load because they instructed countermanding the habitual target response (whereas A-cues established expectancy of the target response). During the probe period, preceding B-cues instructed the nontarget response regardless of the probe (so that no additional cognitive control was required). On A-cue trials, the probe is relevant and dictates which response will be correct. The Y-probe countermands the expectation of the target response, so that AY trials represent high cognitive control load, whereas AX trials release the habitual target response and represent low cognitive control load. I therefore computed the difference in

firing rate on B-cue and A-cue trials during the cue period, and AY and AX trials during the probe period, to provide a measure of the strength of neural signals reflecting cognitive control. I then asked whether the strength of these neural signals differed between balanced and prepotent trial sets. I found that the B-cue signal (activity on B-cue minus A-cue trials; Fig. 2.8 blue) in Group 2 and 3 neurons was significantly larger (permutation test, $p < 0.05$) across the population of neurons on prepotent relative to balanced trial sets in both the PFC (Fig. 2.8A, C) and the MD (Fig. 2.8B, D). Similarly, I found that the AY signal (activity on AY minus AX trials) was significantly larger on prepotent relative to balanced trial sets again in both areas (Fig. 2.8A-D, pink). These data suggest that the strength of the physiological signals reflecting cognitive control at the neural level in both the PFC and MD is augmented when cognitive control demand is increased at the behavioral level.

Timing and strength of single neuron recruitment in MD and PFC

I compared the timing and strength of cue, probe and response signals in MD and PFC neurons at the population level to provide insight into the pattern of information flow between the MD and the PFC during cognitive control processing. For that purpose, I performed a regression analysis in which I regressed single neuron firing rates in the MD and PFC onto the cue (A or B), probe (X or Y), or response (T or NT) over trials within a sliding window of 100ms advanced in 20 ms steps. I quantified the strength of the relationship between single neuron firing rate and task variables by calculating PEV (proportion of explained variance). Heat maps (1 row = 1 neuron) illustrate the time course of PEV values associated with each predictor variable (cue, probe, and

response) as a function of time in the trial (Fig. 2.9A, B, C). I ranked neurons according to the time of their peak significant regression coefficient and restrict the PFC and MD populations to equal numbers of significant neurons to compare the timing of recruitment and strength of signals across the population (cue: n = 764, probe: n = 491, response: n = 362 neurons in PFC and MD). The bands of peak PEV values in the heat maps in both PFC (Fig. 2.9A-C; right) and MD (left) indicate a sequential recruitment of neurons took place during the trial in both brain areas, with each neuron modulating its firing rate in relation to task variables for a short period of time consistent with a temporally dynamic population code (Crowe et al., 2010). Additionally, neurons exhibited more extended periods of firing rate modulation (longer horizontal bands of color in the heat maps) encoding the cue (Fig. 2.9A) and response (Fig. 2.9C) in both MD (left) and PFC (right), consistent with persistent activity reflecting the maintenance of task information in working memory. The persistent representation of the response was more apparent in MD (Fig. 2.9C, left) than PFC (right), again consistent with a preference for response encoding in the MD. To compare the timing of neural recruitment in MD and PFC, I compared cumulative distributions of the time to peak PEV of all neurons recruited for each task factor. Cue signals emerged significantly earlier in the PFC in comparison to the MD (Fig. 2.9D; KS test = 0.18, n = 764 MD and PFC neurons, $p<0.001$). Probe signals emerged earlier in the MD than the PFC (Fig. 2.9E; KS test = 0.15, $p <0.001$). Response signals also emerged earlier in the MD than the PFC (KS test = 0.19, $p <0.001$). To compare the strength of neural recruitment in MD and PFC, I computed the population average PEV time course for each task variable and evaluated the significance of differences between brain areas using a permutation test (Methods; $p < 0.05$). The population average PEV attributable to the cue (Fig. 2.9G), probe (Fig. 2.9H),

and response (Fig. 2.9I) was significantly larger in the MD than the PFC during the probe period. There was no significant difference in cue related signals between MD and PFC during the cue period (Fig. 2.9G). MD contains much stronger information about all task variables during the probe period when it is critical to combine cue and probe information to correctly select the response direction.

Timing and strength of population decoding in MD and PFC

To further elucidate differences in the strength and timing of neural signals between the MD and PFC, I conducted a time-resolved decoding analysis to quantify the information about task variables encoded by patterns of neural activity in the population. In addition to decoding the cue, probe and response with all significant neurons (Fig. 2.10), I decoded cue and probe from Group 2 and 3 neurons and the response from Group 6 and 7 neurons (Fig. 2.11). For the most part, strength and timing patterns were maintained across the MD and PFC whether they were obtained with all significant neurons (Fig. 2.10) or with the group restricted neurons (Fig. 2.11). In prepotent sets, cue decoding posterior probabilities rose in the MD and PFC in parallel but were sustained at significantly higher levels during the cue period in PFC, particularly on B-cue trials (Fig. 2.10A and Fig. 2.11A, $p < 0.05$, permutation test). During the probe period, the converse was true – cue posterior probability was significantly greater in MD than in PFC (Fig. 2.10A and Fig. 2.11A), perhaps reflecting the stronger late-cue signals in MD (Fig. 2.6C, compare 2.6J). Similarly, probe posterior probabilities rose for the MD and PFC in parallel during the probe period with the MD reaching significantly higher level (Fig. 2.10B and Fig. 2.11B, $p < 0.05$, permutation test). Lastly, response posterior probabilities were significantly greater in MD than PFC (Fig. 2.10C and Fig. 2.11C),

rising first to an intermediate level during the cue period (since the cue carried partial information about the direction of the response) and rising further after the probe was presented (which determined response direction definitively). Response probabilities obtained with all significant neurons further demonstrate the fact that the cue contained partial information about the forthcoming response direction as the decoding time courses were similar between the response and cue decoding time courses (Fig. 2.10C compared to Fig. 2.10A).

Functional coupling between neurons coding the cue, probe and response within the same brain area

I next evaluated functional communication between neurons in MD and PFC during DPX task performance. For that purpose I applied an analysis my lab developed previously to measure transmission of signals containing task-relevant information between connected brain areas (Crowe et al., 2013b). This analysis measures temporal correlations in the amount of information encoded by different groups of simultaneously recorded neurons either within or between brain areas. In this analysis, I first convert time varying patterns of neural activity in two non-overlapping sets of neurons into two time series of posterior probabilities associated with the neural representation of specific task variables. I then ask whether fluctuations in the probability time series are correlated at a lag (of ± one 50 ms time bin) within a sliding window (500 ms). Transmission time series capture the strength of this correlation (indexed by the F statistic in a regression analysis). Signal transmission occurs between the two sets of neurons when the transmission time series exceeds 95th percent of the bootstrap distributions (permutation test, $p<0.05$, FDR corrected).

I first consider signal transmission between groups of neurons coding different task variables within PFC and MD. I detected significant signal transmission between distinct subsets of simultaneously recorded neurons that encoded the cue, probe and response. This may reflect integration of these signals needed to mediate logical operations (analogous to 'if-then') necessary to implement the contingencies of the DPX task. In the PFC, I observed generally a pattern of signal transmission that bore resemblance to the activity of switch neurons, in the sense that neural signals inverted between cue and probe periods of the task (in this case, referring to the direction of signal transmission between subsets of neurons). This was seen for communication between cue and probe neurons (Fig. 2.12A), where transmission from cue to probe (blue) occurred late and from probe to cue (pink) early in the trial. Likewise, signal transmission inversion was seen in the case of communication between cue and response neurons (Fig. 2.12C) and probe and response neurons, which inverted at the end of the delay period (Fig. 2.12E). In the MD, this generally held for cue-response (Fig. 2.12D) and probe-response coupling (Fig. 2.12F) but the inversion occurred during the delay period instead of the probe period. Unique to the MD, cue and probe coupling in both directions was restricted to the probe period.

Functional coupling between neurons in MD and PFC

I next considered task-related signal transmission between neurons encoding the same task variable in MD and PFC to measure communication in thalamocortical networks during cognitive control. I observed instances wherein the direction of information flow between these areas switched from cue to probe period (as I saw above, Fig. 2.12). For example, signal transmission between cue neurons occurred in

the bottom-up direction during the cue period and top-down direction during the probe period (Fig. 2.13A). Similarly, signal transmission between response neurons was both bottom-up and top-down during the cue period but only top-down during the probe period (Fig. 2.13C). Although transmission of probe signals appeared to be strong, it was not significant when compared to the bootstrap distribution generated by trial shuffling, indicating that there were time-locked events that occurred across all trials, unrelated to the task information contained in the network (Fig. 2.13B).

Next, I looked at signal transmission between the MD and PFC with neurons encoding different task variables. Significant signal transmission between MD cue and PFC probe neurons occurred in both top-down and bottom-up directions during the cue period and bottom-up at the end of the delay period (Fig. 2.14A). There was a short instance of bottom-up signal transmission from MD cue neurons to PFC response neurons in the delay period (Fig. 2.14C). Significant top-down signal transmission from PFC cue to MD response neurons occurred during the cue and delay periods (Fig. 2.14D). Finally, there was significant bottom-up signal transmission from MD response neurons to PFC probe neurons in the cue period (Fig. 2.14F). Otherwise signal transmission between neurons coding different task variables in the two structures was absent. Taken together, this data suggest that the distribution of signals between PFC and MD may be achieved by the transmission of certain signals and at certain periods of the trial (mostly relating to the cue and response during the cue and response periods) in both a bottom-up and top-down direction.

DISCUSSION

MD has long been considered an important nodal point in cognitive functions mediated PFC distributed networks due to their reciprocal connection (Goldman-Rakic and Porrino, 1985; Xiao et al., 2009), the fact that MD lesions often produce PFC-like cognitive deficits (Isseroff et al., 1982; Zola-Morgan and Squire, 1985; Parker et al., 1997; Van der Werf et al., 2000; Van der Werf et al., 2003; Zoppelt et al., 2003), and the presence of similar neural signals in the two structures during cognitive processing in primates (Fuster and Alexander, 1971, 1973; Funahashi et al., 2004; Watanabe and Funahashi, 2004a, b). To better understand MD-PFC interactions as related to cognitive control deficits in schizophrenia, and to establish the knowledge base necessary to develop new treatments targeted at improving MD-PFC communication with follow on benefits for cognitive function, I translated a task measuring cognitive control deficits in patients to monkeys and report here the pattern of neural activation and communication between MD and PFC during its performance. Toward that goal, I showed that (1) state signals (encoding countermand probability) were found in the MD and were similar to state signals in PFC, (2) working memory signals were distributed between the MD and PFC, (3) response signals were enriched in MD relative to PFC and more balanced between the two responses in the task (prepotent and counter-habitual), and (4) information about task variables was transmitted between different groups of neurons both within and between MD and PFC.

State (countermand) signals

Neurons that encode ‘state’ (the probability of having to override the prepotent response) as instructed by different stimuli (B and AY trials) at different times in the trial

(cue and probe periods, respectively) are also found in MD and were similar to their PFC counterparts. State signals were earlier and stronger during the cue period in PFC in comparison to MD (Fig. 2.9A, D, G; 2.10A; 2.11A), but in both structures were biased to prefer the B-cue early and A-cue late in the trial (Fig. 2.3C, D), exhibited similar patterns of neuronal activity at the single neuron (Fig. 4B, D) and population levels (Fig. 2.6B, C, I, J; Groups 2 and 3), modulated their level of firing in relation to cognitive control load (Fig. 2.8), and were equally prevalent among cue-responsive neurons in both structures (Fig. 2.7). The presence of neurons that directly reflect cognitive control operations in the MD has not been well explored in primates. A key aspect of cognitive control is the ability to adjust one's response to a single stimulus based on the contextual information provided and to inhibit perseverative responses within tasks that produce/exploit habitual responding patterns. The MD has been implicated in behavioral flexibility by lesion and inactivation studies in rodents (Block et al., 2007; Parnaudeau et al., 2013; Parnaudeau et al., 2015; Schmitt et al., 2017) and humans (Van der Werf et al., 2000; Van der Werf et al., 2003) demonstrating that MD lesions cause an increase in perseverative behavior during tasks that require shifting of behavioral strategies. Lesions in monkeys have indicated dysfunctional strategy adaptation in reversal learning tasks (Chudasama et al., 2001; Chakraborty et al., 2016). However, the role of the MD has not yet been explored in a cognitive control task like the DPX task or at the cellular level. A previous study reported that local field potentials (LFPs) in the PFC exhibit increased activation in response to B-cues early in the trial and AY-trials late in the trial (Dias et al., 2006). This is similar to the neural preference biases and spiking activity patterns I report here in the MD and PFC, however the prior study did not look at PFC neurons at the spiking level. The Chafee lab previously found neurons that reflected cognitive control operations in

the PFC, referred to as switch neurons as their cue preference switches from B-cue in the cue to A-cue in the probe periods of the trial, often with an additional increment in activity on AY trials (Blackman et al., 2016). Essentially, these neurons reflect cognitive control because they increase their activity at different times in the trial in response to different stimuli (or stimulus combinations) that collectively signal an increase in the probability that it will be necessary to countermand the habitual target response at the end of the trial. The activity of switch neurons is better aligned to the visual stimuli than the motor response, suggesting they are involved in estimating environmental state (countermand probability) rather that encoding the motor response itself. In the current study I found switch neurons in the MD, providing to my knowledge the first evidence of a neuronal marker of cognitive control in this thalamic structure.

Working Memory signals

In addition to switch neuron activity encoding state in MD, I also found MD neurons that exhibit persistent activity classically associated with working memory, particularly on B-cue trials (Fig. 2.5G, Fig. 2.7D, K), information about the cue is maintained throughout the delay period (Fig. 2.10) and neurons encoding the cue are continuously recruited throughout the delay period (Fig. 2.9). The primate MD has been implicated in working memory on the basis of lesion experiments (Isseroff et al., 1982; Zola-Morgan and Squire, 1985; Parker et al., 1997). MD neural recording experiments have furthered our understanding of the information contained in the MD during delay periods of spatial working memory tasks and identifying the MD as a co-contributor to working memory function alongside the PFC. This is due to the fact that the MD contains neurons that encode task information, particularly during delay periods of the oculomotor

delay response task, delayed matched to sample task, and a go/no-go task similarly to their PFC counterparts. (Fuster and Alexander, 1971, 1973; Tanibuchi and Goldman-Rakic, 2003; Watanabe and Funahashi, 2004b, a; Tanibuchi et al., 2009b; Watanabe et al., 2009; Watanabe and Funahashi, 2018). Additionally, inactivation of PFC decreases MD signals related to working memory (Alexander and Fuster, 1973; Bolkan et al., 2017; Schmitt et al., 2017), and inactivation of MD decreases PFC delay period activity as well (Bolkan et al., 2017; Schmitt et al., 2017). My data add to this prior evidence that MD and PFC jointly participate in the network basis of working memory and further support of the MD's involvement in working memory in general, not just in spatial working memory.

Decision and response signals

The most notable differences between the activity of MD and PFC neurons related to signals encoding the motor response. Motor response signals were stronger (Fig. 2.9I; Fig. 2.10C; Fig. 2.11C), more frequent (Fig. 2.3A), and emerged earlier (Fig. 2.9F) in MD compared to PFC. Additionally, the population representation of the response in MD was more balanced between neurons preferring target (habitual) and the nontarget (counter-habitual responses), whereas PFC neurons were preferentially engaged for nontarget responses (Fig. 2.3C, D; Fig, 2.6F, G, M, N). Prior neural recording studies in monkey MD and PFC during an oculomotor delayed response task provided consistent evidence of a stronger role of MD in motor programming (Sommer and Wurtz, 2004b, a; Watanabe and Funahashi, 2004a; Tanibuchi et al., 2009b; Watanabe et al., 2009; Watanabe and Funahashi, 2018). In a series of studies, more presaccadic neurons were found in MD than PFC and MD neurons appeared to

transform working memory signals from stimulus-based to response-based spatial coding during the delay period earlier than the PFC (Watanabe and Funahashi, 2004a; Watanabe et al., 2009; Watanabe and Funahashi, 2018). The MD has also been implicated to be update the cortex about motor responses by conveying corollary discharge of motor plans (Sommer and Wurtz, 2004b, a).

Unlike prior studies, in the DPX task response direction is dictated conditionally by combinations of (cue and probe) stimuli. Consistent with a stronger role in response selection in the MD, I found that 'late' cue signals (neural signals that ramped up to the probe period but encoded the identity of the preceding cue) were stronger in MD than PFC (Fig. 2.9G; Fig. 2.10A; Fig 2.11A). In addition, MD probe signals emerged earlier (Fig 2.9E), were stronger (Fig. 2.9H; Fig. 2.10B; Fig. 2.11B), and were more balanced in their preference for X and Y-probes (Fig. 2.3 C, D) compared to probe signals in PFC. The relative enhancement of late cue and probe signals in MD suggests a more direct role in combining these signals to correctly select a response (target or nontarget). One prior study did look at thalamocortical relay neurons in the MD that project to the PFC and found that these neurons encode stimulus information and also the impending motor response (Tanibuchi et al., 2009b). Put together, a picture of the MD's role in response selection begins to emerge. In addition to inputs from the PFC, the MD also receives anatomical inputs directly from the basal ganglia, specifically the globus pallidus interna and the substantia nigra reticulata (Alexander et al., 1986; Haber and McFarland, 2001; Haber and Calzavara, 2009). This basal ganglia projection to the MD has been thought to be involved in a loop of information about impending behavioral responses (Haber and McFarland, 2001; Tanibuchi et al., 2009b) and potentially contains information specifically about the habitual response, as the basal ganglia has been implicated to a

play a large role in habit formation (Yin and Knowlton, 2006). Therefore, the MD may be a node in a distributed response selection network where information about habitual responses from the basal ganglia and state-based responses from the PFC converge to mediate the competition between habit and cognitive control.

Neural communication

The DPX task requires an 'if-then' conditional computation (e.g. if A-cue and X-probe, then target response). Implementing this logical operation in a neural circuit is likely to involve physiological interaction between groups of neurons encoding cues, probes and responses (because the decision how to respond was contingent on combinations of cues and probes). By analyzing temporal correlations in coded information, I found that neurons in the PFC and the MD that encoded the state transmitted information to probe and response neurons within their respective local circuits (Fig. 2.12), indicating within area physiological interactions required for logical operations. Additionally, I found evidence that neurons encoding state in PFC (as instructed by cues) provided top-down input to MD neurons and that this interaction was reciprocal (Fig. 2.13A, 2.14D). In addition, PFC neurons transmitted information about the response to MD when the response decision was being made (Fig. 2.13C). Studies have looked at spike phase locking to local field potentials (LFPs) between the MD and PFC during working memory performance (delayed nonmatch to sample T-maze task) (Parnaudeau et al., 2013; Bolkan et al., 2017). They reported that mPFC spikes lock to MD beta oscillations: mPFC spikes lag during the delay period, indicating a MD-mPFC drive, mPFC spikes lead during the choice phase, indicating a mPFC-MD drive (Bolkan et al., 2017). This indicates that top-down synchronization from the PFC to the MD is

strongest at the time the animal makes its response choice. However, there are no studies looking at functional coupling of MD-PFC neurons during context processing task performance at the cellular level in both areas. My data indicate that neurons in the MD-PFC network transmit information both in the top-down and bottom-up directions at pointedly important periods of task performance, potentially to influence the response selection.

Conclusion

In conclusion, I found that the MD contains neurons that reflect logical operations as they relate to performance on a context processing task and serves a response selection node within the network. Differences in the state of the network between situations of high and low cognitive load indicate that the PFC is involved when cognitive demand is high, represents cue information early on, and transmits information to the MD when it comes online for response selection. The MD, on the other hand, plays a more balanced role in representing both habitual and counter-habitual responses, and may participate in the mediating the competition between them. In patients with Schizophrenia the MD is typically smaller (Pakkenberg, 1992; Popken et al., 2000; Young et al., 2000), has decreased activation during performance of cognitive control tasks that is correlated with decreased activation of the PFC (Minzenberg et al., 2009), and has decreased connections with the PFC (Welsh et al., 2010; Woodward et al., 2012; Anticevic et al., 2014b; Anticevic et al., 2014a). These data suggest the MD-PFC network is particularly affected by the disease. Since the MD projects broadly to PFC, treatments that target this nucleus could have wide-ranging modulatory effects on PFC function, particularly as it relates to cognitive deficits in patients.

FIGURES

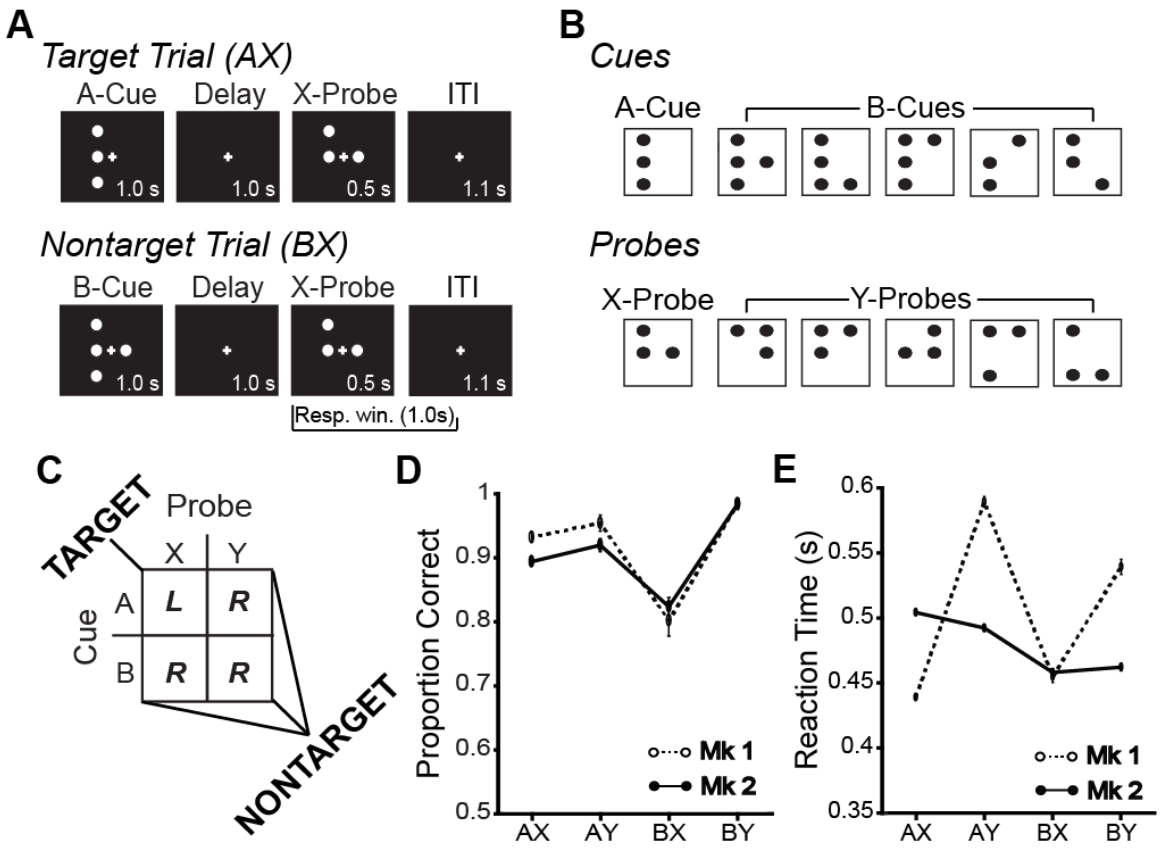

Figure 2.1. The DPX task and behavioral performance. A. Cue-probe sequence on AX and BX trials. The cue was presented for 1.0 s, followed by a 1.0 s delay period, followed by a 0.5 s presentation of the probe. The monkey could respond from probe onset until 0.5 s following probe offset. The intertrial interval was 1.1 s. Top Row: 'AX' valid sequence requiring leftward (target; T) joystick movement. Bottom Row: 'BX' invalid sequence requiring rightward (nontarget; NT) movement. (ITI: intertrial interval). **B.** All cue and probe dot patterns used. A-cue and X-probe consisted of a single dot pattern each, while B-cues and Y-probes consisted of 5 different dot patterns each. **C.** The correct movement direction was dependent on the combination of the cue and probe

stimuli. The combination of an A-cue and an X-probe required the target, left (L) response. All other combinations (AY; BX; BY) required a nontarget, right (R) response. **D, E.** Mean (±2 standard error of the mean, SEM) proportion of trials correct (**D**) and reaction time in seconds (**E**) is shown split by trial type (cue-probe sequence) and by monkey (Mk 1 - open circles and dashed lines; Mk 2 - closed circles and solid line). Prepotent and balanced sets combined.

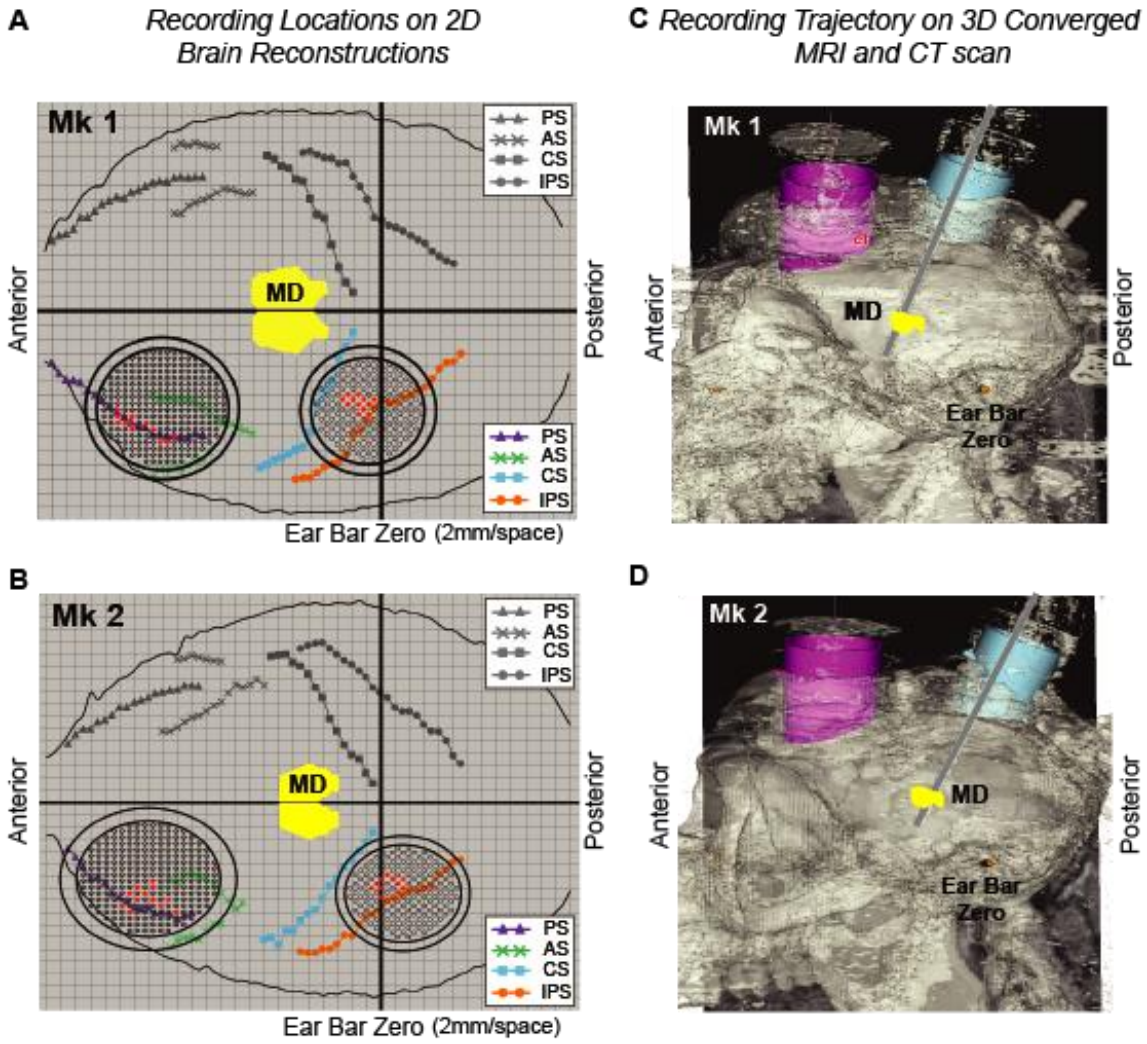

Figure 2.2. Reconstructions of electrode array recording sites. A, B. Two-dimensional (2D) reconstructions of chamber and grid locations (red dots indicate recording sites) superimposed on a dorsal view of sulcal anatomy in Mk1 (**A**) and Mk 2 (**B**). MD: Mediodorsal nucleus of the thalamus, PS: Principal sulcus, AS: Arcuate sulcus, CS: Central Sulcus, IPS: Intraparietal sulcus. **C, D.** Images show superposition of electrode penetration (gray line through blue chamber) targeting MD in three-dimensional (3D) reconstruction of MR image sequence with co-registered CT images in Mk 1 (**C**) and Mk 2 (**D**). Magenta chambers = prefrontal chamber, blue chambers =

thalamic chambers. Yellow region indicates location of MD in the Cicerone brain atlas after fitting the thalamus in atlas to each monkey's thalamus in the MR sequence.

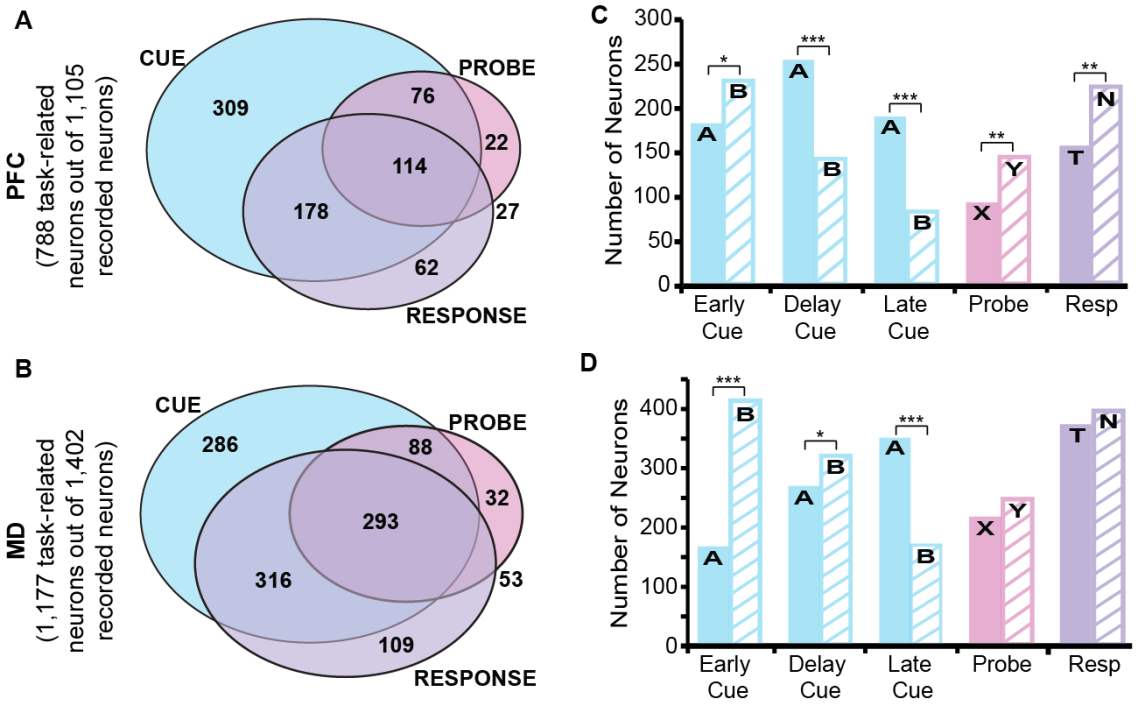

Figure 2.3. Numbers of neurons selective for cue, probe and response in MD and PFC. A, B. Venn diagrams depict the numbers of neurons exhibiting significant selectivity (ANCOVA, $p < 0.05$) for the cue (blue), probe (pink), and/or response (purple) in MD (**A**) and PFC (**B**). Area of circles is proportional to neuron number. **C, D.** Bars indicate the number of neurons in the PFC (**C**) and MD (**D**) that exhibit preference for specific cues (A or B), probes (X or Y), and responses (T or N). Asterisks indicate significant biases in preference for specific cue, probes, and responses in the neural population (One sample Z-test of proportions: *$p < 0.05$, **$p < 0.001$, ***$p < 0.0001$).

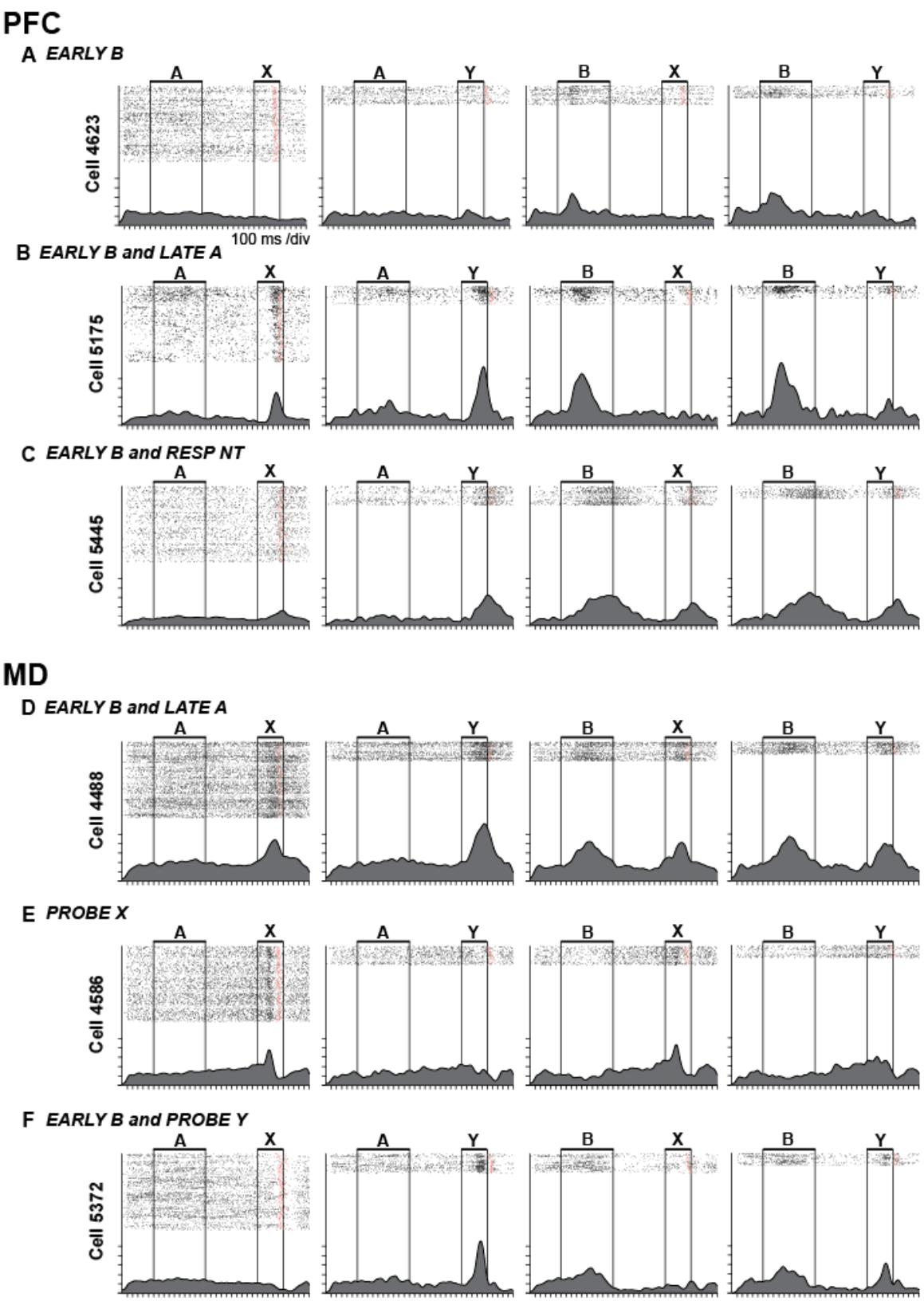
PFC
A EARLY B
A
X
A
Y
B
X
B
Y
Cell 4623
100 ms /div
B EARLY B and LATE A
Cell 5175
C EARLY B and RESP NT
Cell 5445
MD
D EARLY B and LATE A
Cell 4488
E PROBE X
Cell 4586
F EARLY B and PROBE Y
Cell 5372

Figure 2.4. Single neuron activity during DPX task performance. Each row of panels illustrates the activity of a single neuron in PFC (**A-C**) or MD (**D-F**). Individual panels indicate activity on a single trial type defined by cue-probe sequence. Rasters indicate timing of action potentials, spike density functions (solid gray; σ = 40 ms; 10 Hz/div) show modulations in average firing rate. Red tick marks indicate the time of the response in each trial. **A.** Early B-cue neuron: PFC cell 4623 is an example of a neuron whose firing rate during the cue period is greater on B-cue trials than A-cue trials. **B.** Early B-cue and Late A-cue neuron. PFC cell 5175 is an example of a 'switch' neuron that switches its cue preference from B-cues during the cue period to A-cues during the probe period. **C.** Early B-cue and NT-response neuron: PFC cell 5445 is an example of a neuron whose firing rate is greater on B-cue than A-cue trials during the cue period and is also greater on invalid NT-response than T-response trials during the response period. **D.** Early B-cue and Late A-cue neuron: MD cell 4488 is an example of a 'switch' neuron that switches its cue preference from B-cues during the cue period to A-cues during the probe period. **E.** X-probe neuron: MD cell 5486 is an example of a neuron whose firing rate during the probe period is greater on X-probe than Y-probe trials. **F.** Early B-cue and Y-probe neuron: MD Cell 5372 is an example of a neuron whose firing rate during the cue period is greater on B-cue than A-cue trials, and during the probe period is greater on Y-probe than X-probe trials.

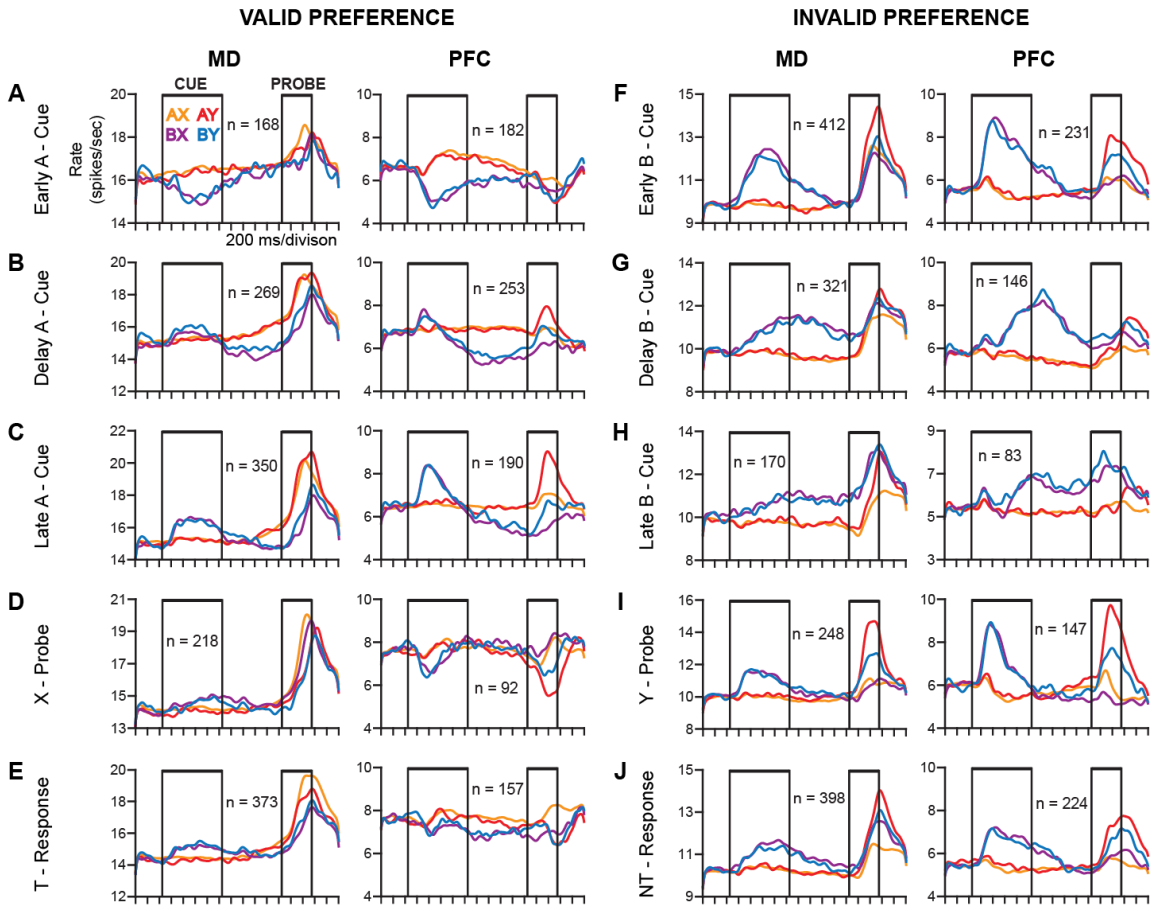

Figure 2.5. Task-defined population activity patterns on prepotent trial sets. Population spike density functions (SDFs; δ = 40 ms) display average population activity as a function of time on subsets of trials defined by cue-probe sequence (AX: orange, AY: red, BX: purple, BY: blue). Neurons are assigned to populations in this figure based on their cue, probe, and response preference as well as the trial epoch in which activity was modulated as determined by ANCOVA ($p<0.05$). Each neuron could belong to multiple populations so defined. The left column of panels (**A-E)** illustrate the activity of populations that preferred valid stimuli and responses (A-cue, X-probe, T-response). The right column of panels (**F-J**) illustrate the activity of populations that preferred invalid stimuli and responses (B-cue, Y-probe, NT-response). In each panel, MD and PFC

population activity are shown on the left and right, respectively. All SDFs are aligned to the cue onset. The stimulus or response preference defining each population is illustrated on the left margin of each pair of panels.

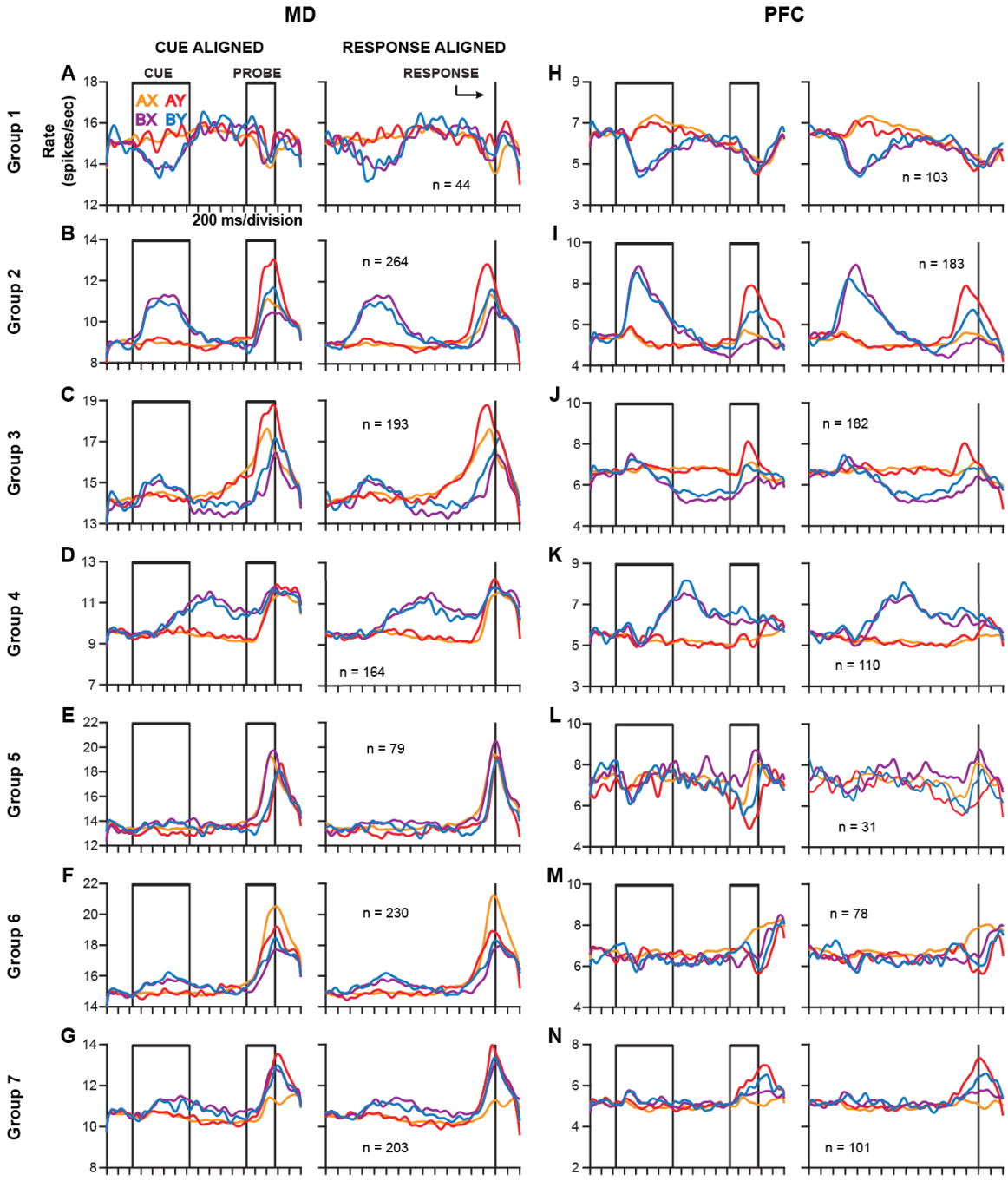

Figure 2.6. Population activity patterns in functionally defined neural groups in prepotent trial sets. Population spike density functions (SDF; δ = 40 ms) display average population activity patterns on subsets of trials defined by cue-probe sequence (AX: orange, AY: red, BX: purple, BY: blue). Neurons were divided into seven non-

overlapping functional groups (see Results text) depending on the specific preference for individual cues, probes and responses as well as the trial period that neurons exhibited selective activity as defined by ANCOVA. Population activity in MD (**A - G**) and PFC (**H - N**) is shown aligned to cue onset (left panels) and time of the response (right panels) of Groups 1-7.

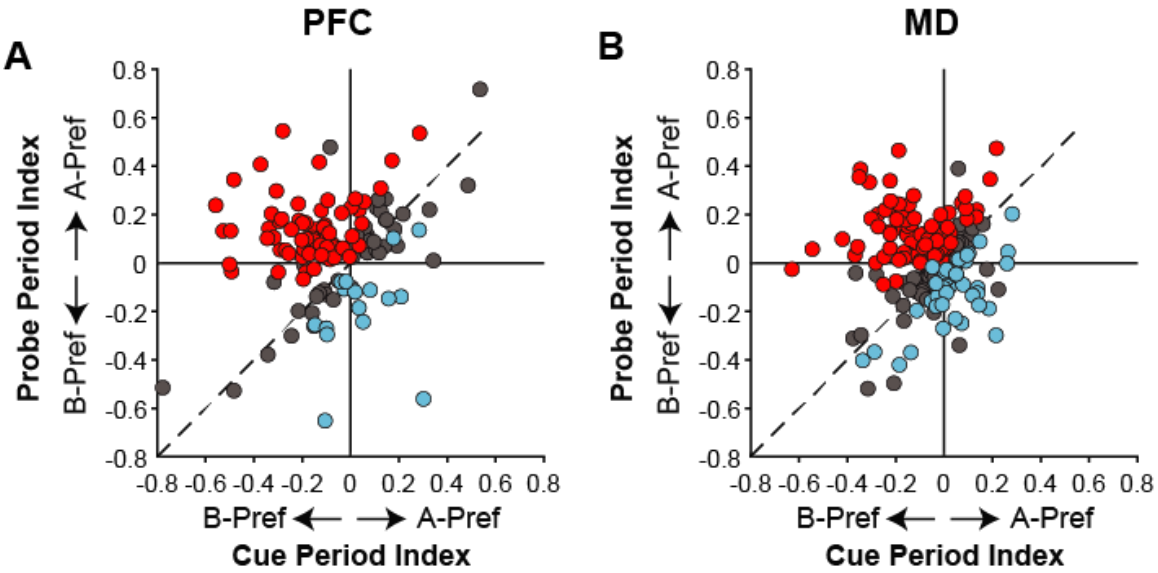

Figure 2.7. Quantification of switch in cue preference from the cue to the probe period in single neurons on prepotent trial sets. I computed an index quantifying cue preference (B-cue – A-cue) / (B-cue + A-cue) using cue and probe period firing rates for each neuron. **A, B.** Colored symbols indicate neurons with a significant switch from B-cue to A-cue preference between the cue and probe periods (red circles), or the opposite switch in preference (blue circles). Gray symbols indicate neurons that encoded the cue during both cue and probe periods but did not switch preference. Data are displayed separately for PFC neurons (**A**) and MD neurons (**B**) recorded during the performance prepotent trial sets.

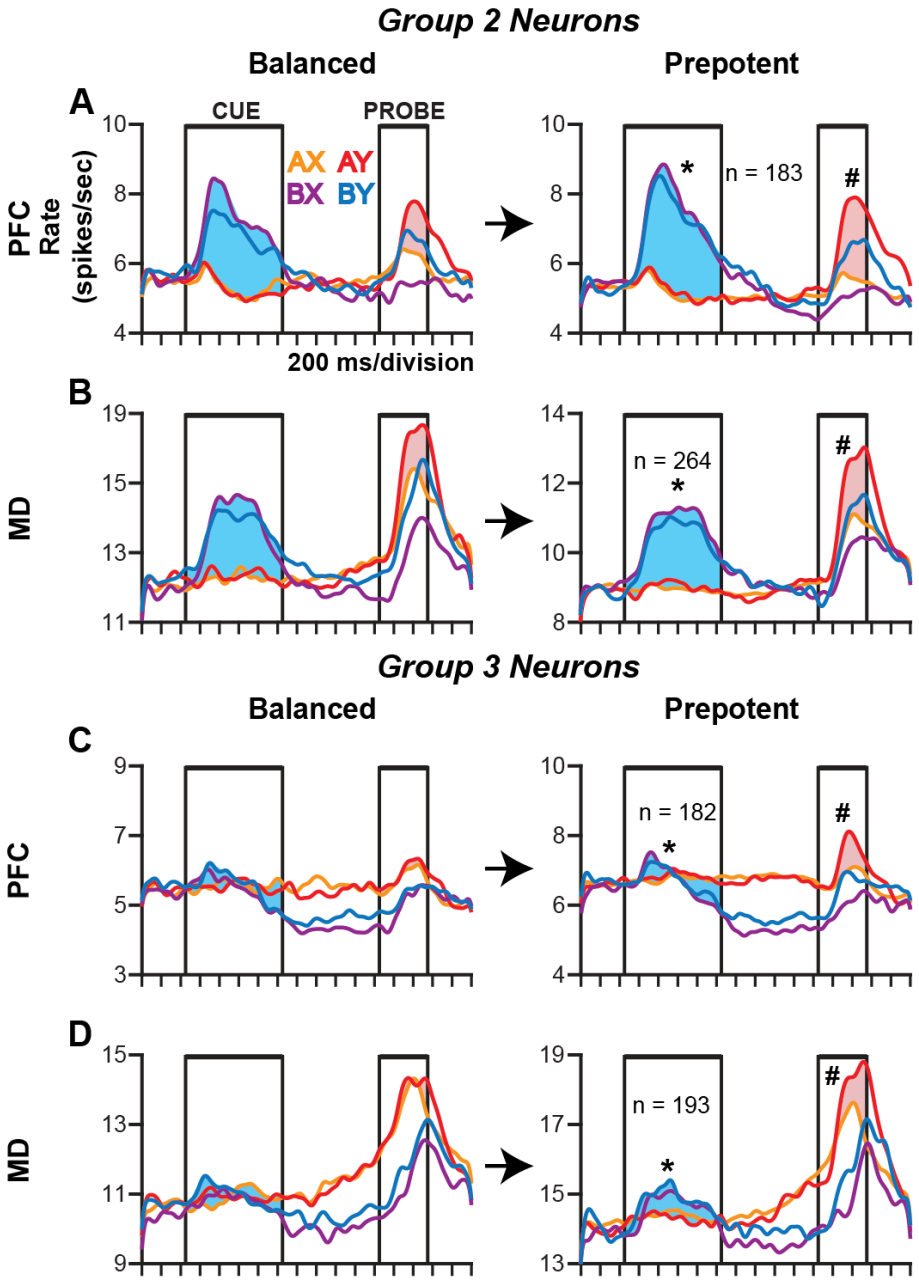

Figure 2.8. Modulation of cognitive control neural signals with cognitive control load. Blue shading indicates difference in cue period firing rates on B-cue and A-cue trials. Pink shading indicates difference in probe period firing rates on AY and AX trials. **A, B.** Population activity of Group 2 neurons in PFC (**A**) and MD (**B**) on balanced (left) and prepotent (right) trial sets. **C, D.** Population activity of Group 3 neurons in PFC (**C**)

and MD (**D**) on balanced (left) and prepotent (right) trial sets. Asterisks (*) indicate a significant increase in the difference in cue period firing rate on B-cue and A-cue trials on prepotent relative to balanced trial sets ($p < 0.05$, permutation test). Pound symbols (#) similarly indicates a significant increase in the difference in probe period firing rate on AY and AX trials in prepotent relative to balanced trial sets ($p < 0.05$).

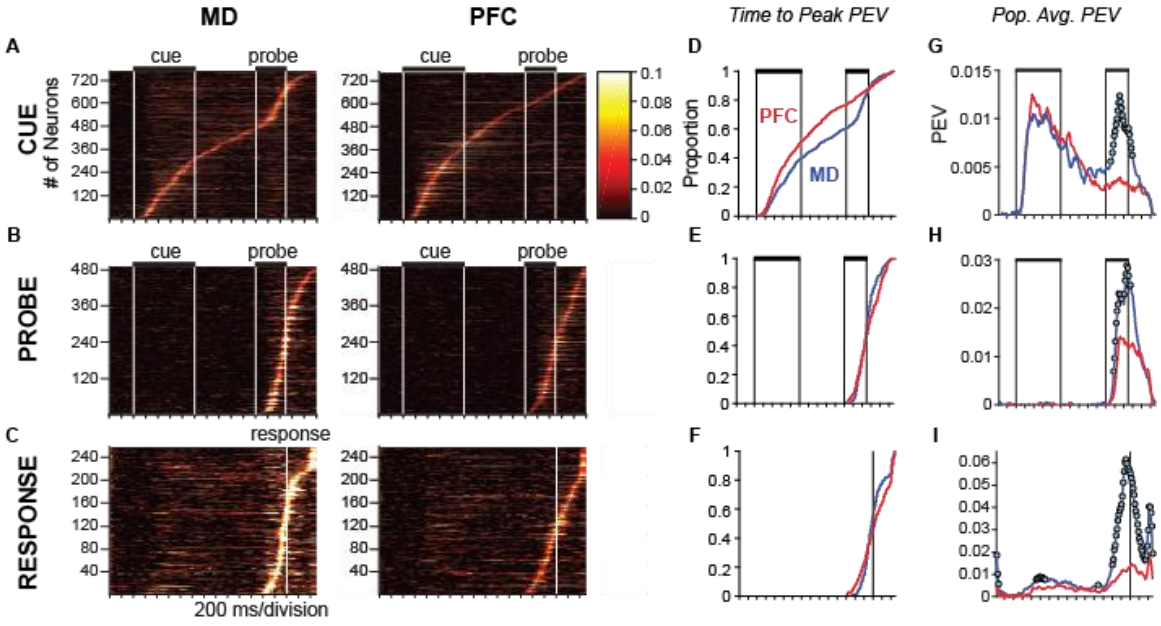

Figure 2.9. Proportion of explained variance (PEV) in firing rate over trials as a function of time in prepotent trial sets. A-C. Warmer colors in the heat maps represent greater PEV values associated with the cue (**A**), probe (**B**), and response (**C**). Neurons were ranked according to the time of their peak significant regression coefficient during the trial and populations in MD and PFC were restricted to equal numbers of significant neurons to facilitate comparison of the timing of neural recruitment between brain areas. PEV values were obtained by regressing the firing rate of each neuron onto the appropriate task factor over trials within a sliding 100 ms window (advanced in 20 ms steps). MD data is on the left and PFC data on the right. **D-F.** Cumulative distributions of time to peak PEV attributable to the cue (**D**), probe (**E**), and response (**F**) in MD neurons (blue) and PFC neurons (red). **G-I.** Population average PEV attributable to the cue (**G**), probe (**H**), and response (**I**) in MD neurons (blue) and PFC neurons (red). Significant differences in population average PEV time courses are indicated with circles (blue circles indicated MD > PFC; permutation test, $p < 0.05$).

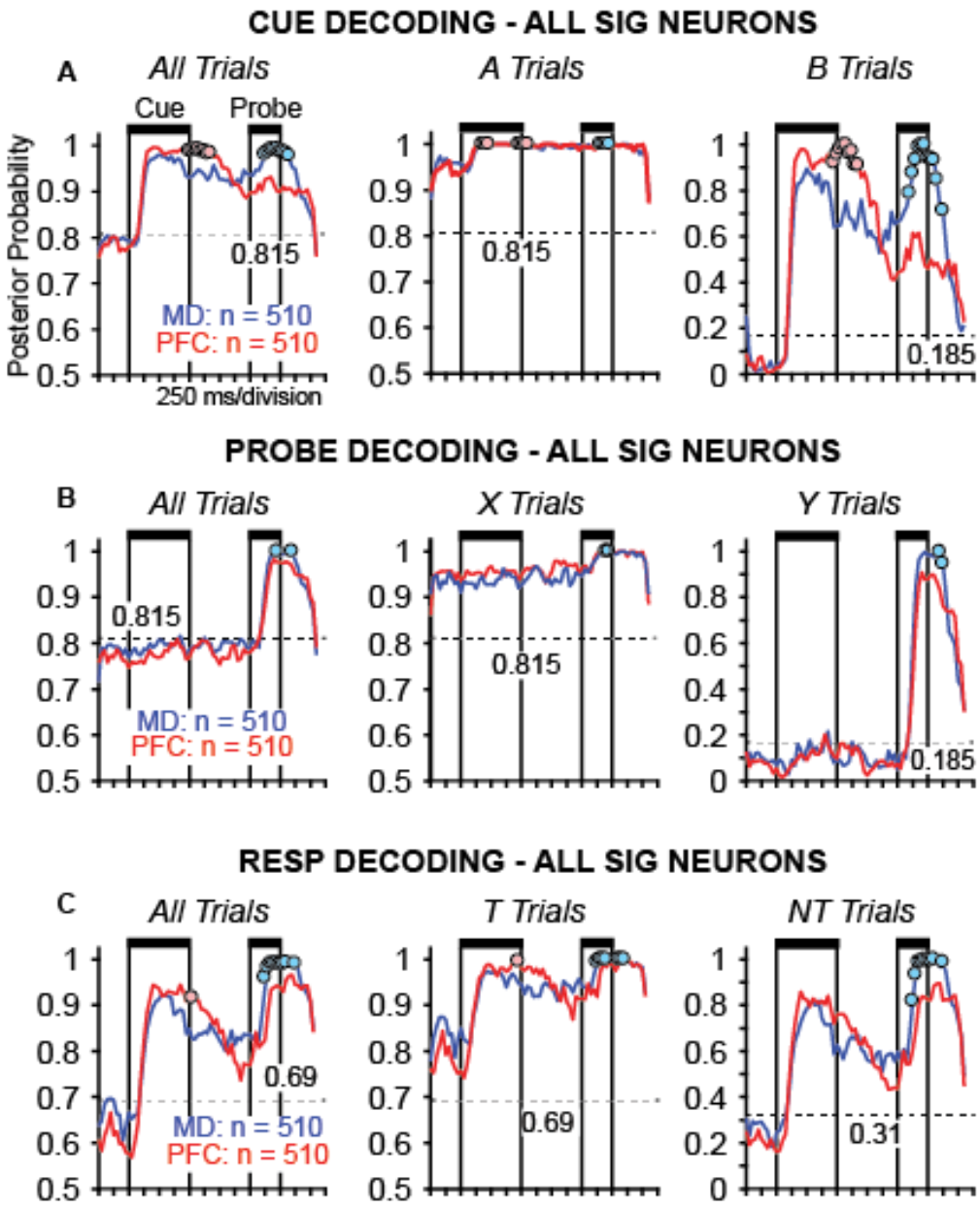

Figure 2.10. Time-resolved population decoding of cue, probe and response MD and PFC neurons using all significant neurons. Functions plot the population average posterior probability associated with the neural representation of the cue (**A**), probe (**B**), and response (**C**) as a function of time in the trial, based on neural population activity in MD (blue) and PFC (red). Neural data recorded on prepotent trial sets. Left

panels illustrate posterior probability averaged over all trials, center and right panels plot posterior probability averaged over the subsets of trials indicated above. Horizontal dashed lines indicate chance decoding based on the prior probabilities of cue, probe and response in prepotent trial sets. Circles indicate significant differences in decoding strength between areas ($p < 0.05$, MD > PFC in blue, PFC > MD in red, permutation test, FDR corrected, Methods). Dashed lines indicate prior probabilities. For example, before the cue appeared and neural signals encoding the cue developed, the prior probability of the A-cue was 0.81 (AX and AY trials comprised 81% of trials in prepotent sets). Baseline decoding (before cue onset) reflects the prior probability of the decoded task variable.

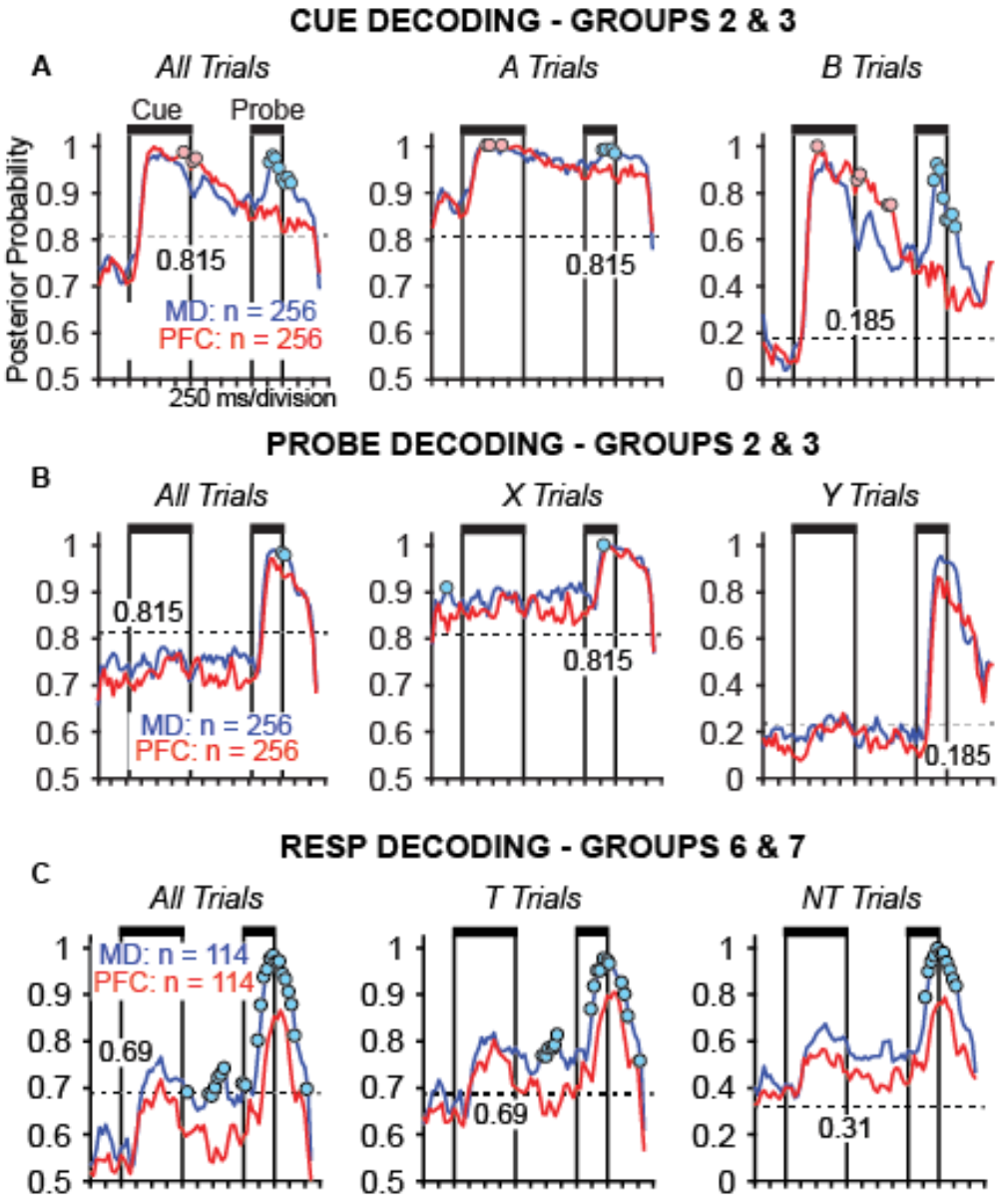

Figure 2.11. Time-resolved population decoding of cue, probe and response MD and PFC using neurons in Groups 2 and 3. Functions plot the population average posterior probability associated with the neural representation of the cue (**A**), probe (**B**), and response (**C**) as a function of time in the trial, based on neural population activity in MD (blue) and PFC (red). Neural data recorded on prepotent trial sets. Left panels illustrate posterior probability averaged over all trials, center and right panels plot

posterior probability averaged over the subsets of trials indicated above. Horizontal dashed lines indicate chance decoding based on the prior probabilities of cue, probe and response in prepotent trial sets. Circles indicate significant differences in decoding strength between areas ($p < 0.05$, MD > PFC in blue, PFC > MD in red, permutation test, FDR corrected, Methods). Dashed lines indicate prior probabilities. For example, before the cue appeared and neural signals encoding the cue developed, the prior probability of the A-cue was 0.81 (AX and AY trials comprised 81% of trials in prepotent sets). Baseline decoding (before cue onset) reflects the prior probability of the decoded task variable.

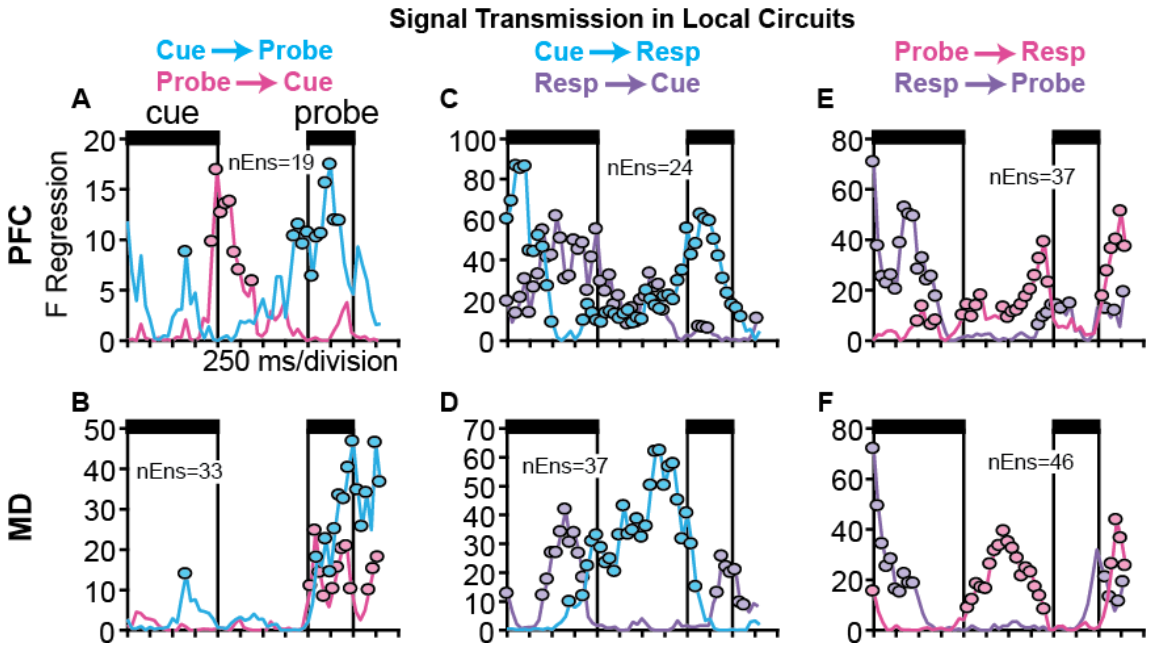

Figure 2.12. Task signal transmission between subsets of neurons within MD and PFC encoding the cue, probe and response. Functions illustrate the time course of signal transmission between subsets of neurons located within the same brain area that encoded different task variables. The direction of signal transmission between neural subsets is indicated by color (see legend above each column). Circles indicate time points where the strength of transmission was significantly nonzero, defined as time points where the F-statistic exceeded the 95th percentile (FDR corrected) of a bootstrap distribution of F-statistics at that time point generated after shuffling trials of posterior probability time series to break the simultaneity of the underlying neural data and repeating the regression analysis. **A, C, E.** Transmission between subsets of neurons in prefrontal cortex encoding the cue and probe (**A**), cue and response (**C**) and probe and response (**E**). **B, D, F**. Corresponding data for MD.

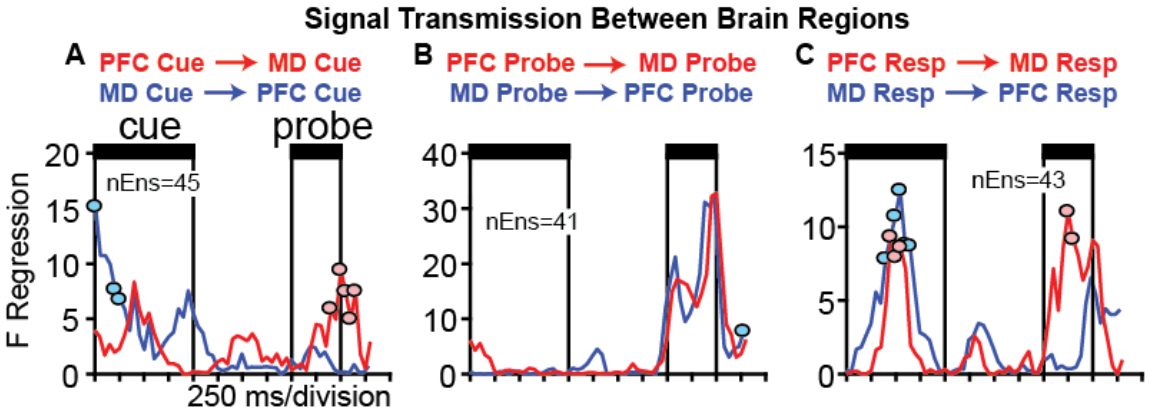

Figure 2.13. Signal transmission between PFC and MD neurons encoding the same task variable. Functions plot is the time course of transmission of (**A**) cue, (**B**) probe, and (**C**) response signals between neurons in the MD and PFC. Top-down (PFC to MD) transmission in red and bottom-up (MD to PFC) in blue. Signal transmission is indicated by circles, where regressions were significantly above the bootstrap regressions ($p < 0.05$; permutation test evaluating transmission in trial-shuffled data).

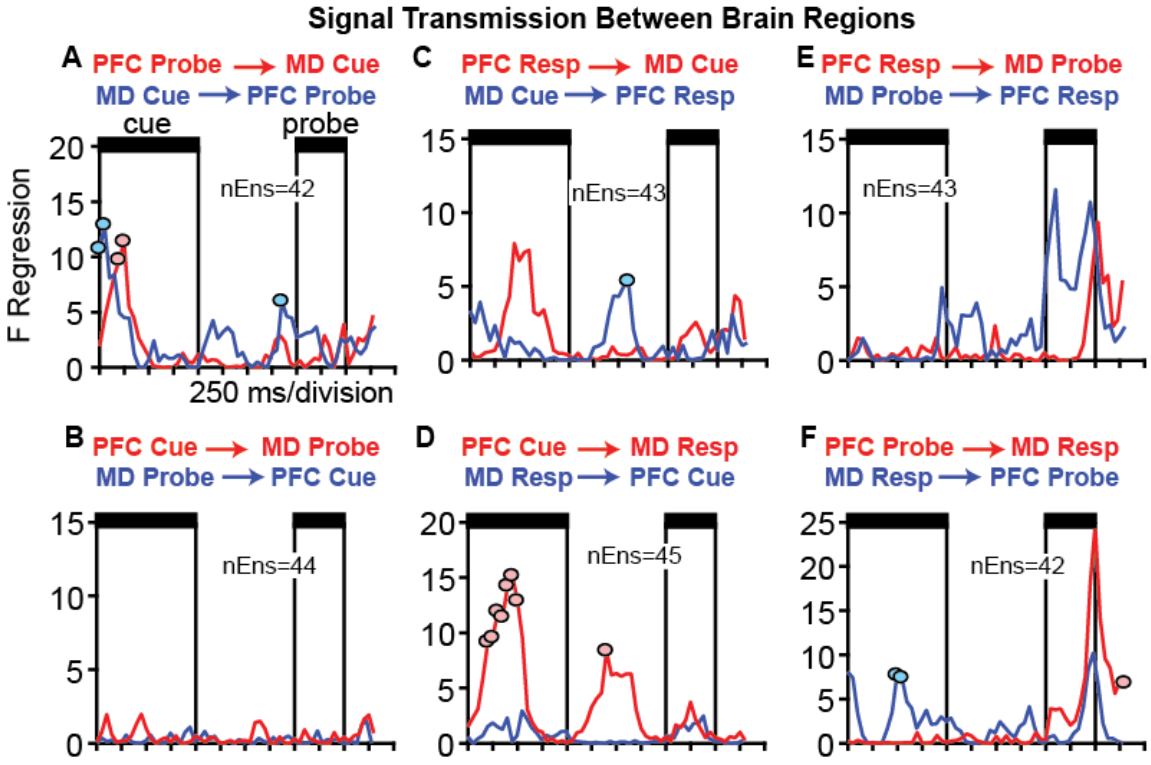

Figure 2.14. Signal transmission between PFC and MD neurons encoding different task variables. Functions illustrate the time course of signal transmission between subsets of neurons located in different brain areas that encoded different task variables. The direction of signal transmission between neural subsets is indicated by color (see legend above each column). Circles indicate time points where the strength of transmission was significantly nonzero. **A, B.** Signal transmission between (**A**) PFC probe and MD cue neurons, and (**B**) MD probe and PFC cue neurons. **C, D.** Signal transmission between (**A**) PFC response and MD cue neurons, and (**B**) MD response and PFC cue neurons. **E, F.** Signal transmission between (**A**) PFC response and MD probe neurons, and (**B**) MD response and PFC probe neurons.

CHAPTER 3:

Thalamocortical dynamics in a schizophrenia-relevant state: Disruption of MD-PFC network activation relates to cognitive control errors following NMDAR blockade

ABSTRACT

Functional imaging studies have shown that cognitive control deficits in patients with schizophrenia (SZ) are correlated with decreased activation within and functional coupling between the mediodorsal nucleus of the thalamus (MD) and the prefrontal cortex (PFC) (Minzenberg et al., 2009; Welsh et al., 2010; Woodward et al., 2012; Anticevic et al., 2014b; Anticevic et al., 2014a). However, little is known about how neural activity, information processing, and network dynamics are affected at the cellular level in the MD and PFC by the disease. To begin to understand how neurons in the MD and PFC are functionally changed in a SZ-like disease state, I blocked NMDA receptors while monkeys performed a cognitive control task and related changes in neural activity and network dynamics to patient-like cognitive deficits in monkeys' performances on the dot pattern expectancy task (MacDonald et al., 2005a; Jones et al., 2010). I found that blocking NMDA receptors (NMDARs) caused a decrease in the number of neurons encoding task state (defined as the probability of having to produce the counter-habitual response) in the MD and PFC and that the state neurons that did emerge were delayed in their recruitment. Additionally, NMDAR blockade decreased the strength of the neural signals encoding task state at both the single neuron and population levels, although the magnitude of this effect was stronger in PFC than the MD. Changes in state

representation predicted task failure on a trial-by-trial basis more strongly in MD than PFC. NMDAR blockade strongly attenuated transmission of information in local circuits from state neurons to probe and response neurons in the PFC more than in the MD. Finally, repeated NMDAR blockade chronically disrupted both top-down and bottom-up information transmission of task state information between the PFC and MD. These data provide new insight into how NMDAR synaptic failure is thought to contribute to cognitive deficits in schizophrenia.

INTRODUCTION

Cognitive deficits in patients with schizophrenia (SZ) are wide-ranging, debilitating, and present regardless of illness stage or medication (Servan-Schreiber et al., 1996; MacDonald et al., 2005b; Jones et al., 2010; Lesh et al., 2011). The severity of cognitive deficits predicts functional outcome for patients (Green et al., 2000; Green et al., 2004; Green, 2006; Ventura et al., 2009), however current therapeutics do not effectively improve them (Mortimer, 1997; Stip et al., 2005). Dysfunction in cognitive control is likely due to the inability of patients to use internally stored goals and rules to flexibly produce an appropriate behavioral outcome, a process that is dependent on the coordination of central representations of context with sensory inputs and motor outputs. This is due to dysfunction across multiple neural systems from genetic abnormalities (Schizophrenia Working Group of the Psychiatric Genomics Consortium, 2014) to structural abnormalities (Kolluri et al., 2005; Lewis and González-Burgos, 2008; Dorph-Petersen and Lewis, 2017) to large scale network activity (Fornito et al., 2012; Sheffield and Barch, 2016). The dorsolateral prefrontal cortex (PFC) has been implicated as the main region integrating rule and goal information with sensory and motor input from

multiple other brain regions to influence behavioral outcomes via appropriate action selection (Miller and Cohen, 2001; Roy et al., 2010; Goodwin et al., 2012; Mante et al., 2013). Patients with SZ exhibit decreased activation of the dorsolateral PFC in fMRI studies during performance of rule switching (Berman et al., 1986; Weinberger et al., 1986), context processing (Barch et al., 2003; MacDonald and Carter, 2003; MacDonald et al., 2005b; Yoon et al., 2008; Richard et al., 2013), prepotent inhibition (Perlstein et al., 2003) and working memory (Glahn et al., 2005; Van Snellenberg et al., 2006; Van Snellenberg et al., 2016) tasks. Multiple lines of evidence suggest that these deficits extend to include interactions with the mediodorsal nucleus of the thalamus (MD), which provides the primary thalamic input to PFC (Goldman-Rakic and Porrino, 1985; Preuss and Goldman-Rakic, 1987). For example, in schizophrenia, decreased activation in MD and PFC are correlated across patients and tasks during performance of many executive functioning tasks (Minzenberg et al., 2009), and the disease is associated with a decrease in functional connectivity between the PFC and MD, compared to health controls. Additionally, patients with schizophrenia exhibit structural abnormalities in the MD (Smith et al., 2011), and post-mortem tissue assessments found loss of dendritic spines in layer 3 of the PFC (Kolluri et al., 2005; Lewis and González-Burgos, 2008) that are thought to reflect, in part, loss of MD glutamatergic input to PFC (Cobia et al., 2017; Dorph-Petersen and Lewis, 2017). Taken together, these data indicate that cognitive deficits in schizophrenia likely derive in part from disrupted engagement of this thalamocortical network.

It is not possible to obtain information regarding changes in brain function at the cellular level in patients with SZ, necessitating the development of animal models to investigate this question. I trained monkeys to perform the dot pattern expectancy task

(DPX). The DPX task, and its analogous counterpart the AX-Continuous Processing Task, have been used to study cognitive deficits in patients with SZ (MacDonald et al., 2005b; Jones et al., 2010) due to their ability to expose a specific (as opposed to generalized) cognitive deficit in patients, which manifests as the inability to use internal representations of state to modify behavioral responses to stimuli (MacDonald et al., 2005a; MacDonald, 2008). Monkeys trained to perform the DPX task exhibit the same behavioral deficit when given acute subanesthetic injections of ketamine or phencyclidine (PCP) (Blackman et al., 2013). Using this primate model, I sought to determine how information processing in the MD and PFC network is affected at the cellular level following drug administration. This information could point to the nature of the specific disturbance in cellular activity dynamics responsible for cognitive control failure in patients with schizophrenia. In this experiment I recorded from the primate MD and PFC, simultaneously, following injections of PCP or saline. I found that NMDAR blockade strongly reduced the information about task state (the probability of having to produce a counter-habitual response) encoded by neurons in prefrontal cortex, as well as delaying their recruitment. Neurons in MD, in contrast, were less affected, with signals encoding both the habitual and counter-habitual states and responses persisting after NMDAR blockade. Additionally, transmission of information about the task state was decreased in both the top-down and bottom-up directions, indicating faulty thalamocortical network communication that could contribute to cognitive deficits like those seen in schizophrenia.

MATERIALS AND METHODS

Neurophysiological recording and data analysis methods were as described in greater detail in Chapter 2. I describe NMDAR pharmacological manipulation and new analyses here.

Subjects

The same two male monkeys (*Macaca Mulatta*; 8-11 kg) were used to record neurophysiological data. All animal care and experimental procedures conformed to the National Institutes of Health guideline and complied with protocols approved by the Animal Care and Use committee at the University of Minnesota and the Minneapolis Veterans Affairs Medical Center.

The DPX Task and Conditions

Monkeys were trained to perform the DPX task (Fig. 2.1). Each trial consisted of a cue (A or B) and probe (X or Y) dot pattern stimulus, presented in sequence (cue for 1.0 s and probe for 0.5 s), and separated by a 1.0 s delay period. The cue-probe sequence instructed movement direction of the joystick: either the target left response left following an AX sequence or a nontarget right response following an AY, BX, or BY sequence. Monkeys could respond within a 1.0 s window starting at the onset of the probe stimulus and continuing for 0.5 s after probe offset. The intertrial interval (between probe offset to the onset of the fixation target for the next trial) lasted 1.1 s.
Monkeys performed 2 sets of different trial proportions of DPX trials per ensemble of recorded neural data: a balanced and a prepotent trial set. Balanced sets contained an equal proportion of each cue-probe sequence (25% each of the four) and prepotent sets

contained a majority of AX target response trials (69%) with the remained 31% split amongst the nontarget trials (AY: 12.5%, BX: 12.5%, and BY: 6%). Prepotent trial proportions were replicated from the DPX task and AX-CPT that were administered to patients (MacDonald et al., 2005b; Jones et al., 2010). Balanced sets included 80 trials for all 53 drug and 43 saline post-drug ensembles. Prepotent sets included 320 or 400 trials (in 20 and 33 drug ensembles, respectively, and 19 and 24 saline ensembles, respectively).

Drug and Saline Injection Protocol

Here I contrast neural activity under three drug conditions: naïve, drug, and saline. In the naïve condition, I recorded neural activity in the MD and PFC either without any injection (30 of 48 neural ensembles) or an injection of saline (18 of 48 neural ensembles; i.m., Mk1: 0.30mL and Mk2: 0.6mL). (Data from the naïve condition is presented in Chapter 2). Once enough neural data in the naïve condition was collected, alternating daily injections of phencyclidine (PCP; Sigma-Aldrich Co. LLC; i.m. Mk1: 0.42 – 0.69 mL; Mk2: 0.26 – 0.32 mL) or saline (i.m. volumes were replicated from the most recent PCP injection volume administered to each monkey) commenced. Neural recording was conducted after each injection. In contrast to the naïve data, neural data in the saline condition was recorded immediately after an injection of saline but after initial exposure to PCP on a prior recording day.

I tested the PCP dose prior to the start of the recording experiment in order to determine the correct dosage needed to elicit a consistent deficit over multiple hours of the recording session. In Monkey 1 doses of 0.20 mg/kg, 0.25 mg/kg and 0.30 mg/kg were used for 3, 3, and 27 ensembles, respectively. In Monkey 2 doses of 0.15 mg/kg

and 0.18 mg/kg were used for 8 and 12 ensembles, respectively. Following an injection of PCP, the recording session began when monkeys were able to maintain eye fixation and respond consistently. Drug effects on behavior were gone by the next day and therefore did not affect behavioral performance on saline days following drug days (Fig. 3.1).

Neural Recording

Neural recording and signal sorting were completed using the methods described in Chapter 2. For this experiment, all neural data recorded in the MD and PFC was collected with the 'Poly2' vector array electrode geometry (53 drug ensembles and 43 saline ensembles).

Data Analysis

In order to assess acute effects of PCP on the neurophysiology underlying cognitive control performance I compare neural data collected on PCP days to neural data collected on saline days. These saline days were all collected after the initial PCP injection (as described above). The Chafee lab previously reported that this drug protocol produced chronic changes in PFC local circuit dynamics (Zick et al., 2018). Therefore, in order to determine if there were chronic effects on the neurophysiology underlying cognitive control performance in the PFC and MD, I compared naive data (data discussed in Chapter 2) to saline data collected following the initial PCP exposure.

Behavioral analysis

I analyzed the effects of PCP injections on the trial outcome (success or failure) as a function of trial type ('AX', 'AY', 'BX', 'BY') using a logistic regression. The equation was as followed:

$$\ln\left(\frac{p(correct)}{1-p(correct)}\right) = b_0 + b_1 Condition + b_2 Type + b_3 Condition * Type$$

where 'Condition' refers to drug condition (drug vs saline) and 'Type' refers to the trial type. I applied a two-way ANOVA to reaction time (RT) data on correct trials using drug condition and trial type as the factors.

ANCOVA – based classification of neural activity

I applied analysis of covariance (ANCOVA, $p < 0.05$) to firing rates of neurons recorded during the drug and saline days to detect significant modulation of firing activity in relation the cue, probe, and response task variables. I applied separate ANCOVAs (listed below) to firing rates in the cue, delay, probe and response windows of the trial. Firing rates in the pre-cue fixation period were used as the covariate to control for trial-by-trial fluctuations in baseline activity. Balanced and prepotent set firing rates were combined in the ANCOVA. I applied a one-way ANCOVA to firing rates in the cue and delay periods to identify neurons whose activity varied as a function of the cue stimulus (A vs. B). I applied a two-way ANCOVA to firing rates in the probe period to identify neurons whose activity varied as function of the cue stimulus (A vs. B) or probe stimulus (X vs. Y). Lastly, I applied a one-way ANCOVA to firing rates in the response period (± 200ms centered on the time of the joystick movement) to identify neurons whose activity varied as a function of the response direction (target vs. nontarget). Cue neurons were

split into separate classifications based on the trial epoch in which their neural activity was significantly modulated in response to the cue stimulus: early cue neurons modulated their activity during the cue period, delay cue neurons modulated their activity during the delay period, and late cue neurons modulated their activity during the probe period.

To determine if there were acute effects on the proportions of significant neurons within the MD and PFC, I performed a Z-test of proportions on the counts of neurons in different ANCOVA-defined categories in the drug and saline conditions. To determine if there were chronic effects of the drug, I performed a Z-test of proportions on counts of neurons in the naive and saline conditions. Lastly, I tested whether biases in the numbers of neurons preferring different cues (A vs. B), probes (X vs. Y) or responses (target vs. nontarget), I performed a one sample Z-test of proportions on counts of neurons with each preference in the drug and saline conditions.

Analysis of population average activity

Continuous estimations of firing rate (population spike density functions, SDFs) were obtained via the methods described in Chapter 2. SDFs were generated using the 'ksdensity' function in Matlab with a kernel width of 40 ms. SDFs are presented in the functionally defined, non-overlapping groups. Group 1 neurons were cue selective during the cue period and preferred the A-cue. Group 2 neurons were cue selective during the cue period and preferred the B-cue and/or were probe selective during the probe period and preferred the Y-probe. Group 3 neurons were cue selective during delay or probe period and preferred the A-cue. Group 4 neurons were similarly defined as Group 3 neurons but preferred the B-cue. Group 5 neurons were probe selective during the probe

period and preferred the X-probe. Groups 6 and 7 were response selective during the response period and preferred target and nontarget responses, respectively.

Analysis of cognitive control load dependent neural activity across drug and saline conditions

I examined whether NMDAR blockade affected the degree to which neural signals were modulated by cognitive control load. For that purpose, I contrasted the activity of Group 2 and 3 'switch' neurons encoding task state (defined as the probability that the counter-habitual response will be required based on cues and probes shown) on balanced and prepotent trials. Specifically, I computed the difference in mean firing rate during trial types that evoked the counter habitual versus habitual responses (B-cue compared to A-cue trials during the cue period and AY compared to AX trials during the probe period). The significance of cognitive control effects on firing rate modulation was determined by a permutation test in which I randomly shuffled firing rates between trial sets (balanced and prepotent) recalculating firing rate differences across trial types (100 iterations). I considered the difference in cognitive control effects on neural activity between balanced and prepotent data sets to be significant if it exceeded the 95^{th} percentile of the bootstrap distribution ($p < 0.05$).

Cue Preference Index

To quantify the influence of drug condition on the propensity of single neurons to switch cue preference between the cue and probe periods, I calculated the switch index as described in Chapter 2 for neurons that were cue selective during both the cue and probe periods. I first computed the cue preference index (A-B/A+B) using firing rates in

the cue and probe periods. I then defined the switch index as the difference between them. To identify neurons with significant switch activity I performed a permutation test by shuffling firing rates between the cue and probe periods (1000 iterations) and recalculating the switch index. Neurons were considered to have significant switch indices if their index was either greater than the 97.5 percentile, or less than the 2.5 percentile, of the distribution of the shuffled data ($p < 0.05$). To determine if the number of neurons that significantly switched their cue preference from B-cues in the cue period to A-cues in the probe period (task state neurons) were more or less numerous than neurons that switched their preference in the opposite direction (from A-cue in the cue period to B-cue in the probe period), I performed a Z-test of proportions ($p<0.05$) between proportions of each type of switch neurons in the drug and saline conditions, separately. To determine whether NDMAR blockade influenced the prevalence of switch neurons in the MD and PFC, I performed a chi-square analysis on 2 X 2 contingency tables with counts of switch and nonswitch neurons in the drug and saline (acute) or naive and saline (chronic) conditions.

Sliding window regression analysis

To evaluate the timing and strength of neural signals in the MD and PFC in saline and drug conditions, I applied a sliding-window regression analysis. I advanced a 100 ms wide sliding window at 20 ms steps through firing rates of single neurons on correct trials in prepotent and balanced trial sets and then regressed the trial-by-trial firings rates onto the cue, probe, and response. The results of the regression analysis were then expressed as the proportion of explained variance (PEV) associated with each regressor. To determine if there was an effect of PCP on the timing of neural signals in

the PFC and MD, I applied a Kolmogorov-Smirnov test to the cumulative distributions of the time to peak PEV across the neural populations recorded on drug, saline and naive conditions (drug vs saline for acute effects, and saline vs. naive for chronic effects). To determine if there was an effect of PCP on the strength of neural signals in the PFC and MD, I compared the difference between time courses of population average PEV across drug conditions in each area at each time point to a bootstrap distribution of differences obtained by randomly shuffling single neuron regression results between the drug conditions (1000 iterations; $p < 0.05$, FDR corrected).

Population decoding analysis

To quantify information encoded by population activity patterns in the MD and PFC about the cue, probe, and response in the drug and saline conditions, I performed time-resolved pattern classification (Klecka, 1980; Johnson and Wichern, 1998; Crowe et al., 2010) as described in Chapter 2. I measured the firing rates in all significant neurons in a sliding window of 150 ms comprised of three consecutive 50ms time bins. I decoded the cue, probe, and response on individual trials using a population activity vector made up of the mean firing rate of each neuron within the 3-bin window. All trials, except the trial being decoded, were used as the training set to compute the mean and covariance matrix of population activity patterns for subsets of trials corresponding to the potential values (A or B, X or Y, T or NT) of the decoded variable (leave-one-out cross validation). I then computed the Euclidean distance between the population activity pattern on the decoded trial in a specific time bin and the two group centroids corresponding to the two values of the decoded variable computed using firing rates in the same time bin. These distances were then converted to posterior probabilities of the

trial belonging to each of the two groups. I assigned that trial to the group with the higher posterior probability. I repeated the decoding over time bins at each step in the trial to quantify the fluctuations in the strength of population signals encoding task-defined information. I defined differences across drug conditions in cue, probe and response decoding time courses as significant if they exceeded the 95th percentile ($p < 0.05$) of a bootstrap distribution obtained by randomly shuffling trials of posterior probabilities between conditions (drug vs. saline or saline vs. naive; 1000 permutations).

The decode analysis described above was performed on correct trials only, since error trials were sparse in the naive and saline conditions. However, in the drug condition there were a significant number of BX errors. To determine the influence of elevated B-cue trial errors on neural decoding, I also performed time-resolved pattern classification training the classifier using all trials (error and correct combined).

Finally, I tested whether differences in neural activity could predict the commission of behavioral errors on a trial-by-trial basis in the drug condition. For that purpose, I decoded trial outcome (correct versus error) from the activity of neurons coding task state (Groups 2 and 3), the response (Groups 6 and 7) or all neurons on BX trials. I restricted this analysis to neural activity on 15 error and 15 correct trials per neuron. I identified differences in outcome decoding time courses between MD and PFC as significant if they exceeded the 95th percentile of a bootstrap distribution of differences obtained by randomly shuffling trials of posterior probabilities between conditions (1000 permutations).

Signal Transmission Analysis

To determine the effect of PCP exposure on functional connectivity within and between the MD and PFC, I applied a signal transmission analysis to sets of simultaneously recorded neurons (neural ensembles) (Crowe et al., 2013b). Signal transmission analysis captures temporally correlated fluctuations in information about task variables encoded by groups of simultaneously recorded neurons. This may capture physiological interactions between neurons encoding different task variables such as are likely required to implement conditional computations to determine the response in the DPX task (for example, if A-cue and X-probe, then target response). To measure signal transmission, first I applied time-resolved pattern classification to decode the cue, probe and response from subsets of neurons encoding each of these task variables that were recorded simultaneously in MD and PFC. This produced posterior probability time series associated with the neural representation of each task variable. To obtain unbiased estimates of temporal correlation between posterior probability time series, I first removed linear trends and autocorrelation in the time series by fitting them with ARIMA (autoregressive, integrated moving average) models of order [10,2,2]. I then took the residuals from the ARIMA fits. This provided a time series of variation in task information coded by the activity of a group of neurons that could not be predicted by its own history (autocorrelation) and may therefore reflect the influence of an external input. I then determined whether fluctuations in the residual posterior probability time series derived from the activity of two groups of neurons (either within or between areas) was significantly correlated in time, by regressing one time series onto the other within a sliding window of 500 ms advance in 50 ms time steps (at a lag of either plus or minus one 50 ms time bin). The resulting time series of F-statistics measures the strength of

temporal correlation between time series, and hence effective coupling between the underlying groups of neurons. Significant coupling was identified at time points ($p < 0.05$; FDR corrected) where F-statistics exceeded the 95th percentile of a bootstrap distribution of F-statistics obtained after randomly shuffling post-ARIMA probability time series between neural groups and repeating the sliding window regression analysis.

RESULTS

Behavioral Performance

The DPX task consists of four cue-probe sequence trial types (AX, AY, BX, BY; Fig. 2.1). Proportion correct data is displayed separated by monkey, trial type, and drug condition (Fig. 3.1A). Mk1 performed an average of 87% on all trials during the drug condition (AX = 95%, AY = 92%, BX = 41%, BY= 96%) and 94% on all trials during the saline condition (AX = 95%, AY = 97%, BX= 82%, BY = 99%). Performance was significantly dependent on the drug condition, the trial type, and their interaction (Z-test on logistic regression model coefficients: condition: $z = 17.62$, $p < 0.001$; trial type: $z = 10.19$, $p<0.001$; condition X trial type interaction: $z = 24$, $p<0.001$). Mk2 performed an average of 88% correct on all trials during the drug condition (AX = 95%, AY = 83%, BX = 60%, BY = 94%) and 92% on all trials during the saline condition (AX = 93%, AY = 93%, BX = 78%, BY=99%). Performance was significantly dependent on the drug condition, the trial type, and their interaction (condition: $z = 8.84$, $p < 0.001$; trial type: $z = 14.52$, $p<0.001$; condition X trial type interaction: $z = 24.01$, $p<0.001$). Proportion correct was significantly dependent on the drug condition and trial type in both monkeys, with BX trials being associated with the highest error rate. This demonstrates the ability to

recreate the BX error phenotype via PCP injections in monkeys used in this experiment that mimics BX error behaviors in a previous cohort of monkeys (Blackman et al., 2013) and human patients with SZ (Jones et al., 2010).

RTs were significantly dependent on drug condition, trail type, and their interaction for both Mk 1 (condition: $F = 248.37$, $p < 0.001$; trial type: $F = 273.38$, $p<0.001$; condition X trial type: $F = 3.91$, $p<0.01$) and Mk 2 (condition: $F = 89.021$, $p < 0.001$; trial type: $F = 398.66$, $p<0.001$; condition X trial type: $F = 22.26$, $p<0.01$). Overall, monkeys were significantly slower across all trial types during the drug condition and were slowest on AY trials compared to other trial types during both the drug and saline post-drug conditions.

Neural Database

I recorded 53 ensembles in the PCP drug condition in the PFC and MD simultaneously, during the performance of one balanced and one prepotent set (Mk1: 33 ensembles and Mk2: 20 ensembles). These 53 ensembles included a total of 1,246 neurons in the PFC (Mk1: 706 neurons and Mk2: 540 neurons) with an average of 24 neurons (range 6 – 43) per ensembles and 1,211 neurons in the MD (Mk1: 728 neurons and Mk2: 483 neurons) with an average of 23 neurons (range 12 -42) per ensemble. In the saline condition, I recorded 43 ensembles (Mk1: 24 ensembles and Mk2: 19 ensembles) in the PFC and MD simultaneously during performance of a balanced and prepotent set. This consisted of a total of 981 PFC neurons (Mk1: 542 neurons and Mk2: 439 neurons) with an average of 23 neurons (range 14 – 44) per ensemble and 1,057 MD neurons (Mk1: 595 neurons and Mk2: 462 neurons) with an average of 25 neurons (range 12 – 48) per ensemble. Each sampled recording location in the grid (drug: Fig.

3.2A, C and saline: Fig. 3.2B, D) yielded 2 – 6 ensembles (average of 2 ensembles per recording day). The naïve dataset, utilized for some comparisons here, is described in Chapter 2.

Stimulus encoding across brain areas and drug conditions

In order to identify neurons that significantly varied their firing rate as a function of the cue (A vs. B; during the cue, delay, or probe period), probe (X vs. Y; during the probe period), or response (target (T) or nontarget (NT); during the response period), I applied ANCOVA ($p < 0.05$) to neuron firing rates in the drug and saline conditions. In both conditions, the MD (Fig. 3.4A, B) and PFC (Fig. 3.3A, B) contained neurons that significantly modulated their firing rates depending on the cue (light blue), probe (pink), and response (purple). Across the population of sampled neurons in the drug condition, 57% of PFC neurons and 70% of MD neurons exhibited modulations in firing rate in relation to at least one of the task factors. In the saline condition, 66% of PFC neurons and 75% of MD neurons exhibited modulations in firing rates in relation to at least one of the task factors. Table 3.1 shows the results for all statistical comparisons between the proportions of significant neurons observed in each drug condition and area (Z-test proportions, $p < 0.05$). PCP exposure affected the proportion of neurons encoding the cue, probe, and response in the PFC and MD variably within each area.

To determine bias preferences in the drug and saline conditions, I performed a one-sample Z-test of proportions (on neurons preferring A vs. B-cue, X vs. Y-probe, T vs. NT-response) separated by trial period (cue, delay, probe, and response) in the MD (Fig. 3.4 C, D) and PFC (Fig. 3.3C, D). In the PFC during PCP exposure (Fig. 3.3C), early B-cue ($Z = -3.2596$ $p<0.01$) and late A-cue ($Z = 8.2156$ $p<0.001$) biases were the

only significant biases present, as there was no significant bias in delay cue ($Z = 1.5607$ $p = 0.12$), probe ($Z = 0.3312$ $p = 0.74$), or response (resp $Z = 0.0519$ $p = 0.96$) neurons. In the saline condition (Fig. 3.3D), PFC neurons in all groups were biased towards valid stimuli that indicated a target response (A-cue: early – $Z = 4.1697$ $p < 0.001$, delay – $Z = 13.9975$ $p < 0.001$, and late – $Z = 8.3753$ $p < 0.001$; and X-probe: 5.6845 $p < 0.001$; T-response: $Z = 2.6510$ $p < 0.01$). These biases are opposite to trends observed in the naïve data (Fig. 2.3C). In the MD during PCP exposure (Fig. 3.4C) neurons encoding the cue in the cue period and in the delay period were biased to prefer the B-cue (early – $Z = -4.4887$ $p < 0.001$; delay – $Z = -3.1021$ $p < 0.01$) and neurons encoding the response were biased to prefer the NT response ($Z = -2.9733$ $p < 0.01$). There were no significant biases in the late cue ($Z = 0.2551$ $p = 0.80$) or probe neuron ($Z = 0.7576$ $p = 0.45$) populations. In the saline condition, MD neurons (Fig. 3.4D) were biased to prefer the B-cue in the cue period ($Z = -3.3796$ $p < 0.001$) and delay period ($Z = -4.9573$ $p < 0.001$), the A-cue in the probe period ($Z = 2.1489$ $p < 0.05$), and X-probe in the probe period ($Z = 2.4711$ $p < 0.05$). There was no bias in the response neuron population ($Z = 1.8189$ $p = 0.07$).

Individual neuron activity patterns during the DPX task in drug and saline conditions

Next, I plotted rasters and individual spike density functions (SDFs), separated by trial type in the PFC (Fig. 3.5) and the MD (Fig. 3.6) to examine the influence of drug condition on single neuron activity patterns. I found that activity patterns reflecting combinations of stimulus and response preferences at different times in the trial that were present in the naïve condition, were also present in the drug and saline conditions. For example, neurons in the PFC and MD that encoded task state and switched their

cue preference from B-cue early to A-cue late in the trial persisted in the drug (PFC: Fig. 3.5B; MD: Fig. 3.6A) as well as the saline (PFC: Fig. 3.5C; MD: Fig. 3.6C) conditions. Also, individual neurons in both drug and saline conditions encoded multiple (PFC: Fig 3.5A; MD: Fig. 3.6B. D) or single (PFC: Fig. 3.5D) task factors. Therefore, I was able to demonstrate that individual neurons recorded during the drug condition modulated their activity in much the same manner as neurons in the saline and naïve conditions. Therefore, NMDAR blockade did not globally suppress task-related activity in either brain area.

Population neural activity patterns during DPX task performance in drug and saline conditions

Neurons were assigned to one of the seven, non-overlapping functional groups based on task factor preferences and trial periods that resulted in the modulation of neural activity (Chapter 2). Generally, basic functional categories of neural response during DPX performance were found to persist in all three drug conditions (naïve, saline, and drug) corresponding to three non-overlapping neural samples, both in PFC (Fig. 3.7, 2.6) and MD (Fig. 3.8, 2.6). This indicates that the various types of modulation of neuronal firing rate throughout the trial that were present in the control data were robust to NMDAR blockade. Group 1 in MD (Fig. 3.8A, H; Fig. 2.6A) and PFC (Fig. 3.7A, H; Fig. 2.6H) exhibited a decrease in activity during the cue period on B-cue trials. Group 2 neurons in MD (Fig. 3.8B, I; Fig. 2.6B) and PFC (Fig. 3.7B, I; Fig. 2.6I) exhibited a switch in cue preference from B-cue in the cue period to AY trials in the probe period. Group 3 neurons in MD (Fig. 3.8C, J; Fig. 2.6C) and PFC (Fig. 3.7C, J; Fig. 2.6J), firing rate was modestly elevated during the cue period and suppressed during the delay period on B-

cue trials. Group 4 neurons in MD (Fig. 3.8D, K; Fig. 2.6D) and PFC (Fig. 3.7D, K; Fig. 2.6K) exhibited persistently elevated activity during the delay period selectively on B-cue trials. Group 5 neurons in MD (Fig. 3.8E, L; Fig. 2.6E) and PFC (Fig. 3.7E, L; Fig. 2.6L) exhibited increased firing rate on X-probe trials that was better aligned to the response time (Fig. 3.7, 3.8, 2.6; right panels) than probe onset (left panels). Group 6 and 7 neurons in MD (Fig. 3.8F, G, M, N; Fig. 2.6F, G) and PFC (Fig. 3.7F, G, M, N; Fig. 2.6M, N) exhibited increased activity for target trials around the response time. The only apparent differences in population activity firing patterns attributable to the drug condition were the blunting of the neural response to the B-cue during the cue period in PFC (Group 2; compare Fig. 3.7C to 3.7J and 2.6J) and the loss of AY-selective activity in the probe period in MD (Group 3; compare Fig. 3.8B to 3.8I and 2.6I).

Quantification of the population of switch neurons in drug and saline conditions

To determine if the number of 'switch neurons' was affected by NMDA receptor blockade, I computed cue preference indices that captured the switching in cue preference between cue and probe periods and compared the numbers of neurons with significant switch indices in the drug and saline conditions. As I saw in the naive condition (Fig. 2.7), there were significantly more neurons that encoded cognitive control load (early B-cue to late A-cue preference) than neurons that switched in the opposite direction (early A-cue to late B-cue preference) in the drug (PFC: Fig 3.9A, 42 neurons compared to 9 neurons, $Z = 5.3629$ and $p < 0.001$; MD: 3.9C, 60 neurons compared to 26 neurons, $Z = 4.3409$ and $p< 0.001$) and saline (PFC: Fig 3.9B, 30 neurons compared to 1 neuron, $Z = 6.0143$ and $p< 0.001$; MD: D, 37 neurons compared to 17 neurons, $Z = 3.2038$ $p < 0.01$) conditions. There were no significant effects of drug condition on the

number of cognitive control neurons in the PFC (X^2 = 2.3683 p = 0.30601) or MD (X^2 = 0.7 p = 0.7). Additionally, there was no significant difference in the proportion of cognitive control neurons between the MD and PFC in the drug (Z = -0.3807 p = 0.70394) or saline (Z = -1.2758 p = 0.20054) conditions. Therefore, the number of switch neurons in each brain region and their relative distribution was not affected by NMDA receptor blockade.

Condition effects on the influence of cognitive control load on switch neuron activity

To investigate if NMDAR blockade influenced the modulation of neural activity by cognitive control load, I contrasted neural activity on balanced and prepotent trials in each of the drug conditions. Prepotent sets represent higher cognitive control load than balanced because the target AX trial type occurs 69% of the time creating a habitual response to the A-cue and X-probe that doesn't exist in balanced sets where all trials are presented equally. This habitual response requires an increase in cognitive control strength to override it. During the cue period, the B-cue is associated with high cognitive control load because it represents an impending need to countermand the target response, regardless of the probe identity. In the probe period, the Y- probe that follows an A-cue is associated with high cognitive control load because it instructs the inhibition of the habitual response to the previously presented A-cue. I computed the difference in firing rates of neurons in Groups 2 and 3 (the switch neurons that encode cognitive control state per Chapter 2) between the B-cue trials and A-cue trials during the cue period and between AY trials and AX trials during the probe period. I then compared these differences across trial set types. In general, neural signals that reflected cognitive control (probability to countermand the habitual response) were augmented under

conditions of greater cognitive control demand (prepotent relative to balanced trial sets) in the PFC (Fig. 3.10) and MD (Fig. 3.11), both under saline and drug conditions ($p < 0.05$; permutation test). Therefore, NMDAR blockade did not strongly influence the effect of cognitive control load on neural activity.

Effects of PCP on the timing and strength of single neuron recruitment in MD and PFC.

To determine the effects of PCP on the timing and strength of cue, probe, and response neural signals in the MD and PFC, I compared the time to peak and magnitude of proportion explainable variance (PEV) attributable to the cue, probe and response. Heat maps show PEV values associated with each predictor variable as a function of time, with neurons ordered according to the time of their peak significant regression coefficient. PFC and MD neural populations recorded in drug (Fig. 3.12A-C and Fig. 3.13A-C; left panels) and saline (right panels) conditions exhibited a sequential recruitment of neurons throughout the trial period as indicated by the diagonal band of warmer color in the heat maps. This demonstrates that the drug did not prevent the network from generating a temporally dynamic population code wherein neurons modulate their firing rate in relation to task variable for a short period of time at staggered times of onset. I also found that PCP did not affect the ability of neurons to exhibit persistent activity outside of their peak PEV time point, illustrated by the more extended period of firing rate modulation present in the heat maps (longer horizontal bands of color in the heat map for the cue and response).

To determine if PCP affected the timing of neural recruitment within the MD and PFC, either chronically or acutely, I compared cumulative distributions of the time to peak PEV for each task factor (cue, probe, or response) of all neurons between drug

conditions. I found that the emergence of cue signals in PFC were chronically delayed following exposure to PCP as indicated by significantly slower time to onset in saline relative to naïve, with no difference between saline and drug (Fig. 3.12D; Drug vs. Saline: KS test = 0.05, $p = 0.4$; Saline vs. Naive: KS test = 0.09, $p < 0.01$). Response signals were similarly chronically delayed (Fig. 3.12F Drug vs. Saline: KS test = 0.08, $p = 0.21$; Naive vs. Saline: KS test = 0.12, $p < 0.05$). NMDAR blockade delayed probe signals acutely (Fig. 3.12E; Drug vs. Saline: KS test = 0.13, $p < 0.001$) but not chronically (Naive vs. Saline: KS test = 0.06, $p = 0.54$). In the MD, cue (Fig. 3.13G; Drug vs. Saline: KS test = 0.07, $p < 0.05$; Naive vs. Saline: KS test = 0.07, $p < 0.05$), probe (Fig. 3.13H; Drug vs. Saline: KS test = 0.15, $p < 0.001$; Naive vs. Saline: KS test = 0.02, $p = 1$), and response (Fig. 3.13I; Drug vs. Saline: KS test = 0.011, $p < 0.01$; Predrug vs. Saline: KS test = 0.09, $p < 0.01$) signals were all delayed acutely and chronically following PCP exposure.

To characterize the effect of PCP exposure on the strength of neural recruitment within the MD and PFC, I computed the population average PEV time course for each condition and task variable. I then evaluated the significance of differences between drug and saline conditions to examine acute drug effects and between naïve and saline conditions to examine chronic drug effects ($p < 0.05$; permutation test). In the PFC, the population average PEV attributable to the cue was acutely decreased in the drug condition, during the cue period and the probe period (Fig. 3.12G). Population average PEV attributable to the probe was higher at the end of the trial in the drug condition compared to the saline condition (Fig. 3.12H). Lastly, population average response PEV in the drug condition was reduced relative to saline and naïve conditions at different times in the trial (Fig. 3.12I). In the MD, as was the case in the PFC, the population

average PEV attributable to the cue was acutely decreased in the drug condition relative to saline during the cue period and the probe period (Fig. 3.13G). Probe (Fig. 3.13H) and response (Fig. 3.13I) PEV were reduced around the time of the response and increased later in the intertrial interval.

NMDAR blockade reduces population encoding of the cue, probe and response in the PFC and MD

To further examine the chronic and acute effects of PCP exposure on the strength and timing of neural signals within the MD and PFC, I conducted a time-resolved decoding analysis. This quantified the information about task variables encoded by patterns of neural activity. Following the decoding analysis, I calculated significant differences in the decoding results between the drug and saline (acute effects) conditions and naive and saline (chronic effects) conditions obtained from MD and PFC. In the PFC, cue signals were chronically reduced in the saline relative to the naïve drug condition (Fig. 3.14A, left panel), a pattern that was particularly prominent on B-cue trials (Fig. 3.14A, right). In the drug condition, the decoder reached ceiling and nearly always decoded neural activity to the A-cue (Fig. 3.14A, left and middle panels), reflecting the much weaker B-cue representation (Fig. 3.14A, right panel). This was generally true for probe representation in the drug condition as well, and the decoder reached ceiling and nearly always decoded neural activity to the X-probe (Fig. 3.14B, left and middle panels), reflecting the weaker Y-probe representation relative to saline (Fig. 3.14B, right). Y-probe representation was significantly weaker in saline relative to naïve indicating a chronic effect (Fig. 3.14B, right). Response decoding exhibited a similar pattern, with the decoder most often decoding activity to target trials with a markedly weaker

representation of nontarget trials in the drug condition and exhibiting chronic decreased in nontarget representation in the saline relative to naïve data (Fig. 3.14C). Overall, during acute PCP exposure PFC neurons mostly represented information about the valid stimuli and responses (A, X, and T), indicating the loss of neural signals encoding invalid stimuli and responses (B, Y, NT). Finally, there was evidence that repeated PCP exposure chronically reduced representation of invalid stimuli and responses. In the MD, there was a much stronger residual B-cue representation in the presence of NMDAR receptor blockade (Fig. 3.15A, right; red) in comparison to the near total elimination of the B-cue representation in prefrontal cortex (Fig. 3.14A, right). Consequently, the decoder did not peg at ceiling. In addition, the neural representation of valid stimuli and responses was chronically reduced for cue, probe and response signals (Fig. 3.15A-C, middle panels). Finally, B-cue signals were chronically reduced during the probe period (Fig. 3.15A, right). Overall, NMDAR blockade affected the neural representation of task stimuli much less in MD than that in the PFC.

To determine if the weak B-cue representation in the PFC in the drug condition reflected the greater number of errors committed on B-cue trials or the fact that I used only neural data on correct trials to train the decoder, I reran the analysis using both correct and error trials in the training data. Inclusion of errors in the training data marginally increased the strength of the signal (posterior probability) in the PFC coding the B-cue (Fig. 3.16A) but decoding still did not approach the level achieved in the naïve or saline conditions (Fig. 3.14A, right). This indicates that the decrease in B-cue decoding was not attributable to the fewer number of correct trials or the increased number of errors only. In the MD, inclusion of error trials in the training data modestly decreased the strength of B-cue representation during the probe period (Fig. 3.16B).

Including error trials into the training data did not modify Y-probe or NT-response posterior probabilities in the PFC or the MD (Fig. 3.16C-F).

Changes in population activity predict errors in the drug condition

To determine if trial outcome was represented in the MD or PFC during the drug condition, I conducted time-resolved pattern classification on BX trials only, using an equal number of error and correct trials in the analysis. Overall the MD contained a stronger representation of the outcome of the trial (error or correct) in the cue period and probe period (Fig. 3.17, blue), while neural activity in the PFC bore a weaker relation to trial outcome (red). This indicates that the MD contained reliably different patterns of activity on error trials versus correct trials, potentially reflecting its stronger representation of the response (and hence outcome).

Effects of PCP on functional coupling between neurons coding the cue, probe and response within the same brain area.

To determine if PCP exposure resulted in acute or chronic effects on information transmission within local PFC and MD circuits during DPX task performance, I applied a signal transmission analysis (Crowe et al., 2013b). This analysis measures correlations in temporal fluctuations related to the amount of information encoded by different groups of simultaneously recorded neurons (see Methods). In the PFC under the saline condition, cue neurons transmitted significant information to probe and response neurons during the cue period (Fig. 3.18B, D; light blue circles), which was absent in the drug condition (Fig. 3.18A, C; light blue, note lack of significant transmission during cue period). Transmission of information from probe (Fig. 3.18A, B; pink) and response

neurons (Fig. 3.18C, D; purple) to cue neurons persisted in the drug condition relative to the saline and in some cases was enhanced (Fig. 3.18C). Transmission of information between probe and response neurons was comparable across conditions (Fig. 3.18E, F). Transmission of information from cue to probe and response neurons in the saline condition (Fig. 3.18B, D; blue) was chronically reduced relative to the naïve condition (Fig. 2.12A, C; blue). In the MD, acute PCP exposure reduced signal transmission from cue to probe neurons in the cue period (Fig. 3.19A, B; blue), while cue to response signal transmission was stronger in the drug condition during the probe period (Fig. 3.19C, D; blue). As in the PFC, there was little effect of drug on probe and response signal transmission (Fig. 3.19E, F). Overall, signal transmission in the PFC and the MD indicated that transmission of information between cue, probe, and response neurons that would be needed to mediate logical operations for cognitive control was reduced following NMDA receptor blockade.

Effects of PCP on functional coupling between neurons in MD and PFC.

To determine the effect of NMDAR blockade on thalamocortical network communication during cognitive control, I measured signal transmission between the MD and PFC in neurons encoding the same task variable. In the saline condition, I found evidence of robust top-down transmission (red) of information from PFC to MD involving neurons encoding the probe and response, that occurred during the late delay and probe periods (Fig. 3.20D, F), which was largely abolished in the drug condition (Fig. 3.20C, E). Instead, the drug condition was associated with the emergence of both top-down and bottom-up transmission between cue, probe, and response neurons that occurred later in the trial during the intertrial interval (Fig. 3.20A, C, E). Transmission of information

during the cue period between cue and response neurons was chronically reduced in the saline condition (Fig. 3.20B, F) compared to the naïve condition (Fig. 2.13A, C). This indicates a selective loss of information transmission across the MD and PFC during the cue period when neurons encoding the cue (and hence task state) would normally interact with other neurons in the circuit. This could lead to a failure to encode cue-instructed context and communicate this information between MD and PFC, leading to the inability to inhibit a prepotent response based on contextual information (BX error).

DISCUSSION

Thalamocortical dysfunction has been implicated in patients with SZ, with different patterns of deficits found in sensory relay thalamocortical networks, which exhibit increased functional coupling and activity in patients and association thalamocortical networks, which exhibit the reverse. The MD thalamic nucleus provides the primary thalamic input to the prefrontal cortex (PFC), and it receives reciprocal input from PFC in return (Goldman-Rakic and Porrino, 1985; Preuss and Goldman-Rakic, 1987; Xiao et al., 2009). Functional connectivity in fMRI (Woodward et al., 2012; Anticevic et al., 2014b; Anticevic et al., 2014a; Tu et al., 2015) and anatomical connectivity evaluated with diffusion tensor imaging (Giraldo-Chica et al., 2018) provide evidence that communication between the MD and PFC is decreased in the disease. Additionally, both the PFC and the MD exhibit decreased activation in fMRI studies of patients performing a gamut of cognitive control tasks (Minzenberg et al., 2009). Although the above data point to dysfunctional dynamics within the MD-PFC network, they do not provide information about network failure at the cellular level. To better understand distributed processing and interactions across the MD-PFC network and

relate it to the neural pathophysiology of SZ, I recorded from monkeys in both areas simultaneously following an injection of PCP (a potent NMDA receptor antagonist) during performance of a cognitive control task translated from patients with SZ. PCP exposure in monkeys reliably produces an error pattern (increased 'BX' errors) in cognitive control that is found in patients with SZ performing the same DPX task (Blackman et al., 2013). My results show NMDAR blockade produced distinct effects on neurons in the MD relative to the PFC, both acutely and chronically. I found that blocking NMDAR synaptic transmission systemically: (1) both acutely and chronically reduced the strength and prevalence of neural signals encoding task state ('countermand probability') both at the single neuron and population levels, (2) more strongly degraded state signals in the PFC than the MD, (3) delayed the emergence of task-related signals in both structures, (4) increased the occurrence of BX errors that were better predicted by changes in neural activity in the MD than the PFC, and (5) disrupted the pattern of information transmission between neurons in local circuits within each structure as well as transmission of information between the MD and PFC.

State signals

Task-related signals in the MD-PFC circuit can be broadly classified as encoding task 'state' and the behavioral response. 'State' neurons exhibited a switch in their preference for the identity of visual stimuli appearing during the cue and probe periods in the trial which instructed the nontarget, counter-habitual response (B-cues during the cue period, AY cue-probe sequence during the probe period). The activity of these neurons is not time-locked to the motor response (Fig. 3.7, 3.8), but rather appears to encode 'countermand probability' (e.g. task state) more than the identity of individual

stimuli. I found that following NMDAR blockade, neurons that encode task state were differentially affected in the MD and the PFC. In the PFC, little residual representation of B-cues and Y-probes persisted following NMDAR blockade (Fig. 3.14A, right) whereas in the MD, the B-cue and Y-probe signals were largely intact (Fig. 3.15A, right). This suggests that circuits in the MD and PFC are differentially sensitive to NMDAR synaptic failure. Moreover, at the single neuron level, effects of NMDAR blockade on state neurons in the PFC and MD appeared comparable (as indicated by approximately equivalent reductions in cue PEV in the two structures, for example; Figs. 3.12G, 3.13G). This suggests that the neural representation at the population level is more adversely affected by NMDAR blockade in the PFC than the MD. One such aspect of population encoding that could contribute to the reduction in population decoding is an increase in noise correlation between neurons, suggesting a potential role for decreased attention following NMDAR blockade in the production of BX errors (Cohen and Maunsell, 2009). The population representation of state appeared to use a temporally dynamic code (in which individual neurons carried signal for brief periods at staggered times of onset). Blocking NMDAR modestly delayed the dynamic recruitment of state signals (as instructed by the cue and probe) both in PFC (Fig. 3.12) and MD (Fig. 3.13). One key question is what change in neural activity contributes to the elevation of BX errors seen in the drug condition. I found that changes in state representation (as encoded by Group 2 and 3 neurons) predicted BX errors on a trial-by-trial basis and that state signals in MD predicted errors better than state signals in PFC (Fig. 3.17). This is consistent with our other evidence that MD neurons are preferentially engaged to encode the response (as described in Chapter 2). The disruption of task-related activity patterns by NMDAR blockade was not absolute and many characteristics of neural

activity found in the baseline data persisted in the drug condition. For example, state neurons in the MD and PFC both continued to exhibit the 'switch' pattern of activity which was accentuated under conditions of increased cognitive control load in the drug condition (Fig. 3.9, 3.10 and 3.11).

Response signals

Interestingly, NMDAR blockade did not seem to affect signals encoding the motor response in the MD as strongly as in the PFC, even though the MD contains more overall response related signals than the PFC, at baseline (Chapter 2). For example, population representation of nontarget response information was significantly weaker in the PFC following NMDAR blockade (Fig. 3.14), while nontarget response representation in the MD remained relatively unaffected (Fig. 3.15). This is consistent with the selective degradation of state signals in the PFC encoding the counter-habitual response compared to the MD (discussed above).

Effects of NMDAR blockade on neural communication

The DPX task requires that the brain perform a logical operation to compute the correct response based on combinations of stimuli shown (e.g. if A-cue and X-probe then target response). This is likely to involve physiological interaction between groups of neurons encoding all three variables (cue, probe, and response). Evidence of interactions was found both within and between the MD and the PFC in the naïve condition (Chapter 2). I found that acute exposure to PCP modulated the flow of information between neurons encoding task variables in local circuits both with the MD (Fig. 3.19) and the PFC (Fig. 3.18). This could impair the ability of neural circuits to

perform logical operations that require combining cue and probe information to compute the conditional response. Transmission of information about the state and response in the MD-PFC thalamocortical network was diminished following PCP exposure. Top-down transmission of probe and response information during the delay and probe periods from PFC to MD was essentially abolished by acute PCP exposure (Fig. 3.20). Both top-down and bottom-up transmission of cue and response information during the cue period was chronically reduced (Fig. 3.20 compared to Fig. 2.13). These data suggest that NMDAR, in addition to influencing synaptic plasticity over longer time scales, play a direct role in neuronal communication for computations supporting cognitive control.

Relation to prior work in animal models

To our knowledge, there are no prior experiments that have recorded in the primate MD following administration of an NMDAR antagonist. Prior studies recording the monkey PFC following the administration of an NDMAR antagonist have demonstrated a decrease in the strength of task related neural signals, including delay period activity associated with working memory (Wang et al., 2013), as well as neural signals encoding rules and feedback in a delayed anti-saccade task (Skoblenick and Everling, 2012; Ma et al., 2015) and action monitoring (Skoblenick and Everling, 2014). Still, these studies did not address changes in neural activity and dynamics related to the performance on a cognitive control task translated from patients or investigate thalamocortical networks dynamics in the MD and PFC that may underlie the behavioral deficit they report.

In the rodent, studies have examined the influence of NMDAR blockade on MD-PFC activation and dynamics during spatial working memory performance (Kupferschmidt and Gordon, 2018). Acute systemic administration of NMDAR antagonists (Ketamine or PCP) produced mixed effects on the firing rate of MD and mPFC neurons (Celada et al., 2013; Furth et al., 2017), as well as increased gamma power LFP oscillations in MD and mPFC in rats (Furth et al., 2017). Injection of the NMDAR antagonist MK 801 into the rat MD increased delta power in mPFC (Kiss et al., 2011). These studies show that MD-PFC dynamics are modified by NMDAR blockade in rats, but do not relate these changes in neural function to altered cognitive control performance. In addition, I found little evidence that PCP altered firing rates of task-related neurons (Figs. 3.7, 3.8) suggesting that differences in the influence of NMDAR synaptic function on the MD-PFC network may differ between species.

Relation to schizophrenia

Functional imaging studies in SZ have repeatedly shown reduced PFC activation in patients specifically related to the neural representation of B-cues performance in the DPX task and its analogous task the AX-Continuous Processing Task (Barch et al., 2001; Perlstein et al., 2003; Yoon et al., 2008; Lesh et al., 2013; Poppe et al., 2016). Patients with SZ further exhibit a decrease in the activation of the MD during cognitive control performance (Minzenberg et al., 2009), as well as reduced MD-PFC thalamocortical functional connectivity at rest (Welsh et al., 2010; Woodward et al., 2012; Anticevic et al., 2014b; Anticevic et al., 2014a; Tu et al., 2015). Several aspects of these results have parallels in my current data. The reduction of B-cue activation in PFC of patients with SZ is consistent with the reduction in B-cue representation, as well as

state encoding generally, that I observed in monkey PFC following NMDAR blockade. A recent report used diffusion tensor imaging (DTI) to measure white matter tract integrity between PFC and MD and relate it to behavioral performance in patients with schizophrenia performing a variety of executive function tasks, including the AX-CPT (Giraldo-Chica et al., 2018). This study found that decreased thalamocortical anatomical connectivity, specifically from the MD to the PFC, was correlated with poorer working memory performance but not with poorer performance on the AX-CPT. My data suggest that functional communication between MD and PFC is disrupted by NMDAR synaptic malfunction. This may mean that even though anatomical connectivity from the MD and PFC is not related to context processing in the AX-CPT, information flow between the two areas could still be dysfunctional due to other factors, including NMDA receptor hypofunction. Generally, my data are consistent with the characterization of SZ as a functional 'disconnection' syndrome (Friston, 1998; Stephan et al., 2006) that results in altered patterns of information flow in prefrontal networks (Woodward et al., 2012).

Conclusions

Our data are unique in that they provide cell and circuit level information about the distributed processing of task state information across the MD and PFC during NDMAR disruption that underlies cognitive deficits in a pharmacological model of SZ. I provide evidence of decreased population encoding and functional connectivity in the MD-PFC thalamocortical network, specifically related to the neural representation of state that is required for correct response selection. State representation in PFC was preferentially degraded by NMDAR blockade relative to MD. This suggests that loss of top-down input of state information from PFC to MD could contribute to cognitive control

errors in patients. Conversely, the motor response and trial outcome (e.g. errors) under NMDAR blockade, were better represented in MD, suggesting this structure plays a more direct role in response selection and execution. Lack of state signal input to MD may therefore result in excessive influence of habitual response signal input from the basal ganglia (Haber and McFarland, 2001; Weickert et al., 2002; Yin and Knowlton, 2006), leading to commission of BX errors. However, future experiments will need to be done to determine the effect of NMDAR on basal ganglia input to the MD during cognitive control performance. In patients with SZ it was recently shown that improvement in cognitive control performance using cognitive behavioral therapy was correlated with an improvement in thalamocortical functional connectivity (Ramsay et al., 2017). This is further confirmation of the need to understand the nature of MD-PFC connectivity underlying cognitive control deficits for future therapeutic developments targeted at improving this network.

TABLES AND FIGURES

Z-test of Proportions Samples	All Significant Neurons	Cue Neurons	Probe Neurons	Response Neurons
PFC Naive Vs. Saline	**Z = 2.73** **p < 0.01**	**Z = 15.66** **p < 0.01**	Z = 0.49 p = 0.62	Z = 0.99 p = 0.32
PFC Saline Vs. Drug	**Z = 4.06** **p < 0.001**	Z = 1.55 p = 0.12	**Z = 3.72** **p < 0.001**	**Z = -2.34** **p < 0.05**
MD Naive Vs. Saline	**Z = 5.27** **p < 0.001**	Z = 0.63 p = 0.53	**Z = 2.69** **p < 0.01**	**Z = 3.34** **p < 0.001**
MD Saline vs. Drug	**Z = 3.11** **p < 0.01**	**Z = 3.42** **p < 0.001**	Z = -0.60 p = 0.55	Z = 0.83 p = 0.41
PFC vs. MD Drug	**Z = -6.29** **p < 0.001**	**Z = -2.50** **p < 0.05**	**Z = -6.30** **p < 0.001**	Z = -1.52 p = 0.11
PFC vs. MD Saline	**Z = 21.58** **p < 0.001**	Z = 0.26 p = 0.79	Z = -1.82 p = 0.069	**Z = -4.68** **p < 0.001**

Table 3.1. Statistical results comparing proportions of significant neurons across conditions and brain regions. Bolded results indicate significant differences via z-test of proportions, $p < 0.05$.

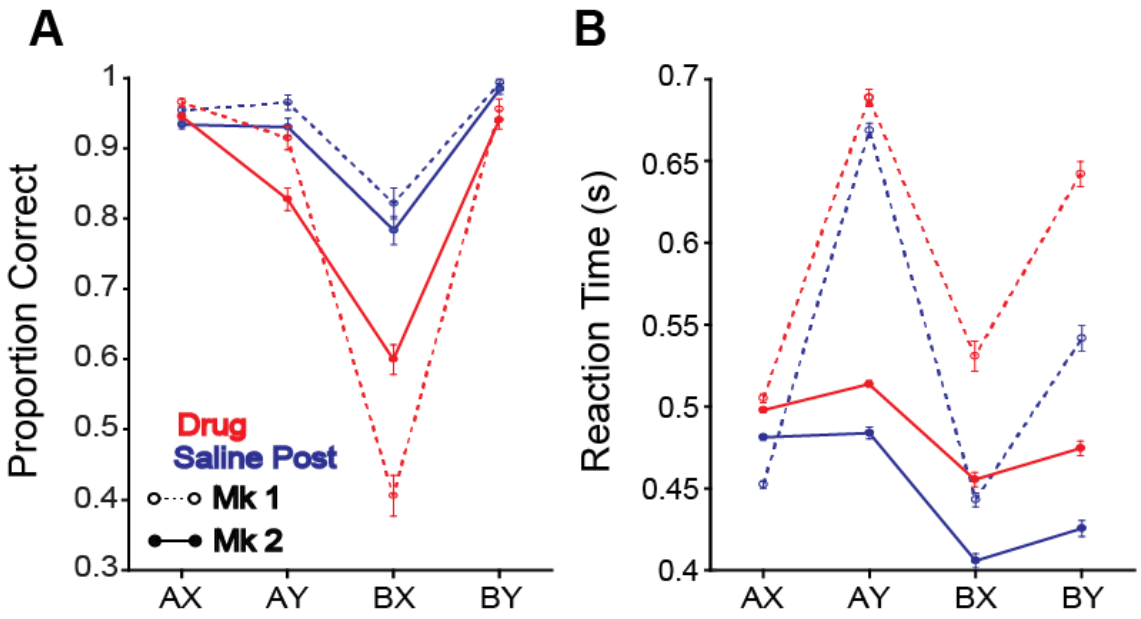

Figure 3.1. Behavioral performance in NMDA receptor blockade and saline conditions. Mean (±2 standard error of the mean, SEM) proportion of trials correct (**A.**) and reaction time (**B.**) in seconds is shown split by trial (cue-probe sequence) and by monkey (Mk 1- dashed lines and open circles; Mk 2- solid lines and closed circles; Drug – red; Saline – blue). Prepotent and balanced sets combined.

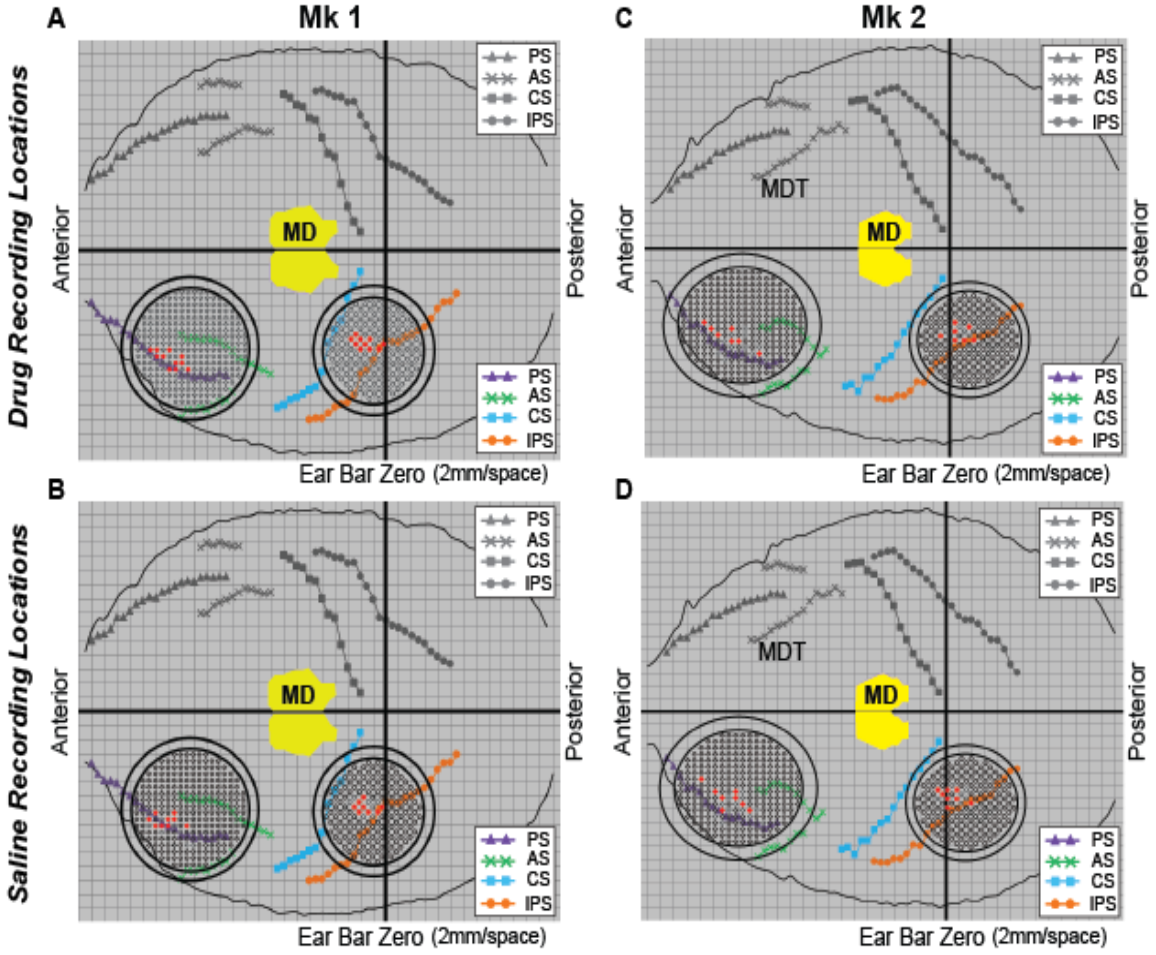

Figure 3.2. Reconstructions of electrode array recording sites. Two-dimensional (2D) reconstructions of chamber and grid locations (red dots indicate recording sites) superimposed on a dorsal view of sulcal anatomy in Mk1 (**A, B**) and Mk 2 (**C, D**) for the drug (**A, C**) and saline (**B, D**) conditions. Yellow region indicates relative location of the MD superimposed on the sulcal anatomy. MD: Mediodorsal nucleus of the thalamus, PS: Principal sulcus, AS: Arcuate sulcus, CS: Central Sulcus, IPS: Intraparietal sulcus.

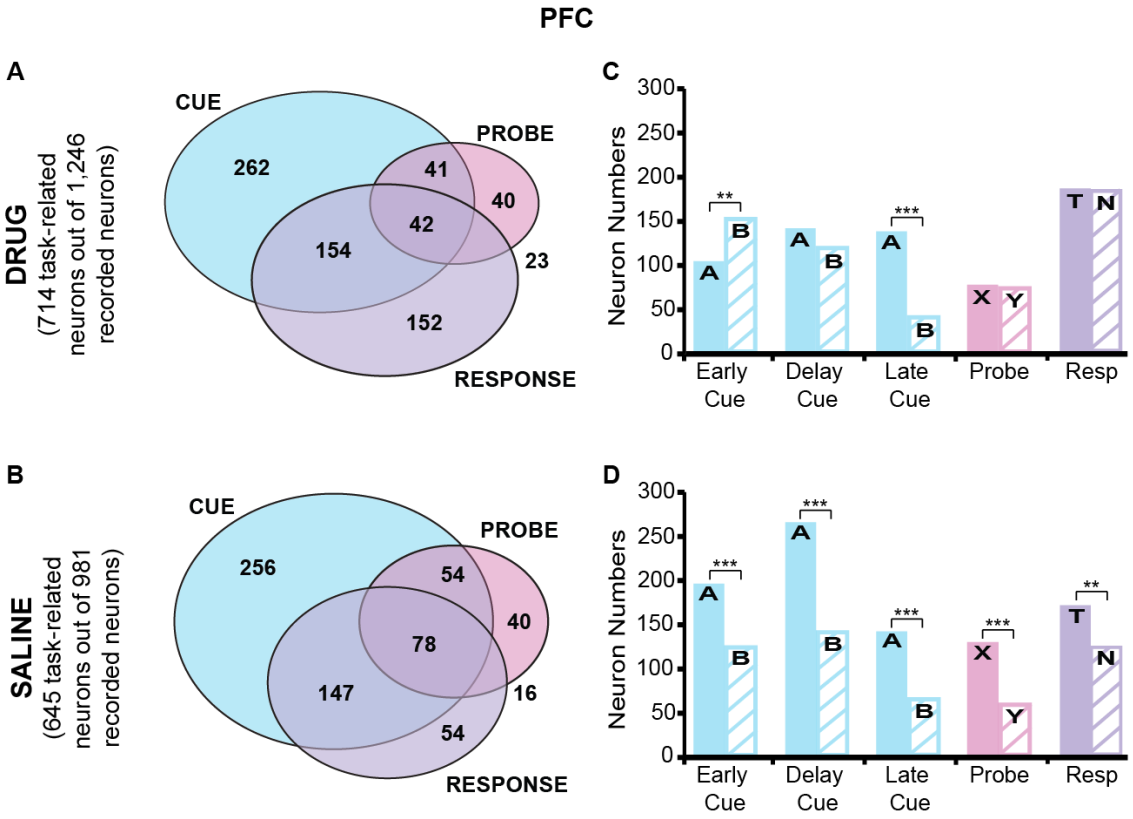

Figure 3.3. Numbers of neurons selective for cue, probe and response in the PFC during NMDA receptor blockade and saline conditions. A, B. Venn diagrams depict the numbers of neurons exhibiting significant selectivity (ANCOVA, $p < 0.05$) for the cue (blue), probe (pink), and/or response (purple) in drug (**A**) and saline (**B**) conditions. Area of circles is proportional to neuron number. **C, D.** Bars indicate the number of neurons in the drug (**C**) and saline (**D**) conditions that exhibit preference for specific cues (A or B), probes (X or Y), and responses (T or N). Asterisks indicate significant biases in preference for specific cue, probes, and responses in the neural population (One sample Z-test of proportions: *$p < 0.05$, **$p < 0.001$, ***$p < 0.0001$).

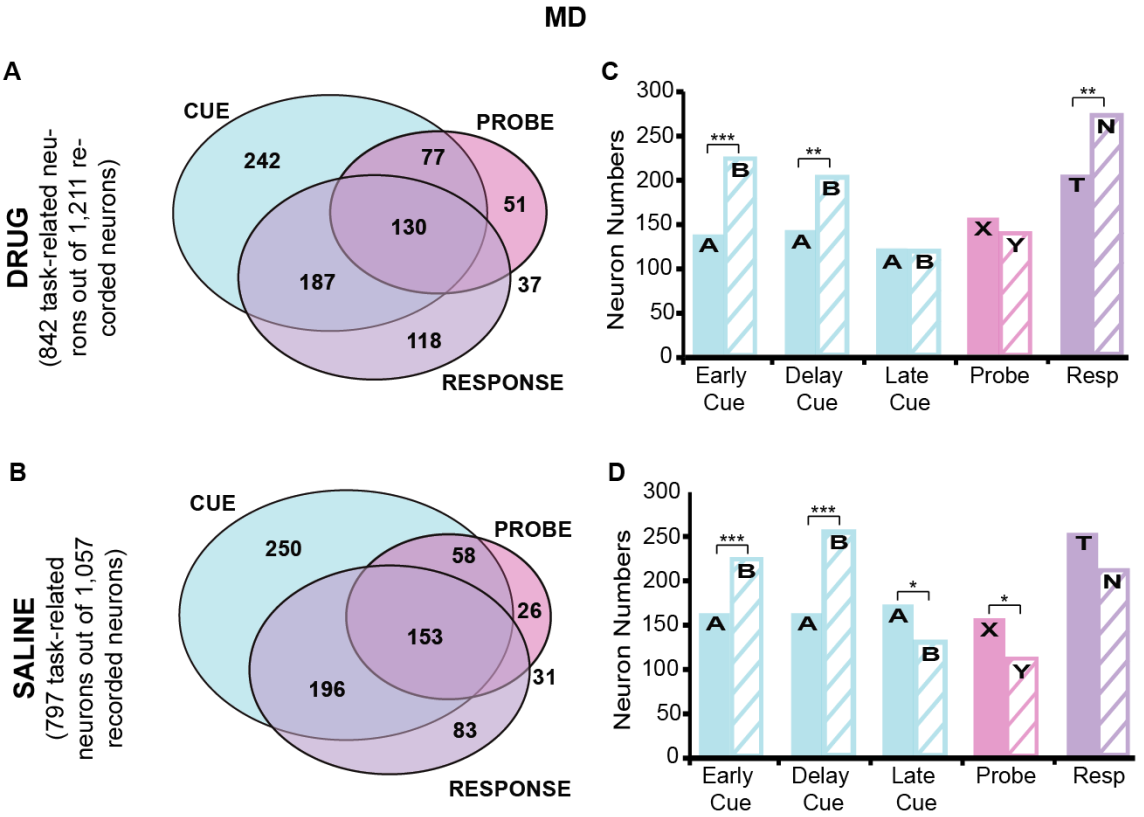

Figure 3.4. Numbers of neurons selective for cue, probe and response in the MD during NMDA receptor blockade and saline conditions. A, B. Venn diagrams depict the numbers of neurons exhibiting significant selectivity (ANCOVA, $p < 0.05$) for the cue (blue), probe (pink), and/or response (purple) in drug (**A**) and saline (**B**) conditions. Area of circles is proportional to neuron number. **C, D.** Bars indicate the number of neurons in the drug (**C**) and saline (**D**) conditions that exhibit preference for specific cues (A or B), probes (X or Y), and responses (T or N). Asterisks indicate significant biases in preference for specific cue, probes, and responses in the neural population (One sample Z-test of proportions: *$p < 0.05$, **$p < 0.001$, ***$p < 0.0001$).

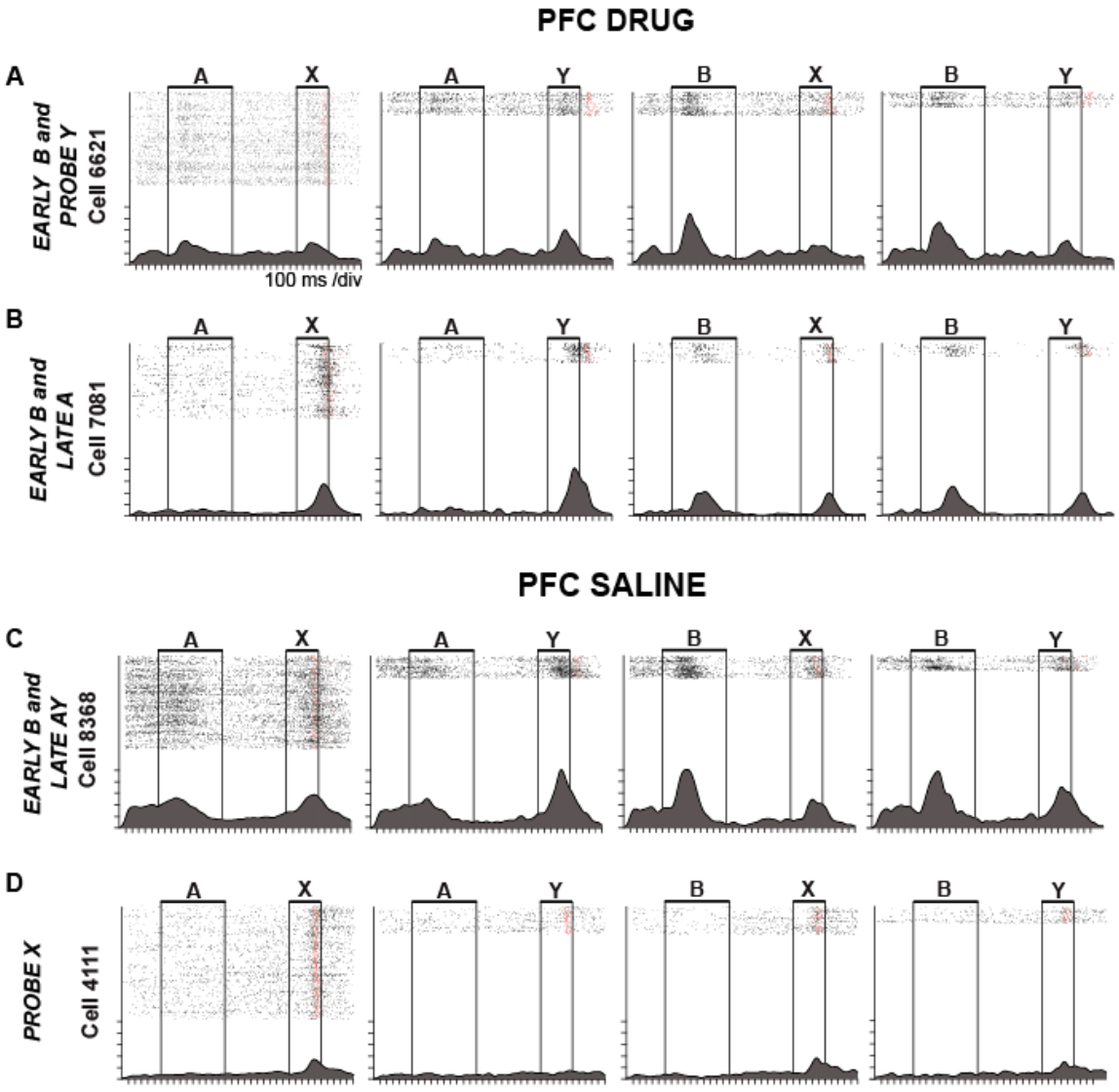

Figure 3.5. Single neuron activity during DPX task performance in the PFC during NMDA receptor blockade and saline conditions. Each row of panels illustrates the activity of a single neuron in drug (**A, B**) or saline (**C, D**) conditions. Individual panels indicate activity on a single trial type defined by cue-probe sequence. Rasters indicate timing of action potentials, spike density functions (solid gray; σ = 40 ms; 10 Hz/div) show modulations in average firing rate. Red tick marks indicate the time of the response in each trial. **A.** Early B-cue and Y-probe neuron recorded following a PCP

injection: PFC cell 6621 is an example of a neuron whose firing rate during the cue period is greater on B-cue trials than A-cue trials and activity in the probe period is greater on Y-probe trials than X-probe trials. **B.** Early B-cue and Late A-cue neuron recorded following a PCP injection. PFC cell 7081 is an example of a 'switch' neuron that switches its cue preference from B-cues during the cue period to A-cues during the probe period. **C.** Early B-cue and Late AY-trial neuron recorded following a saline injection: PFC cell 8368 is an example of a neuron whose firing rate is greater on B-cue than A-cue trials during the cue period and is greater on AY trials in the probe period. **D.** X-probe neuron recorded following a saline injection: PFC cell 4111 is an example of a neuron whose firing rate during the probe period is greater on X-probe than Y-probe trials.

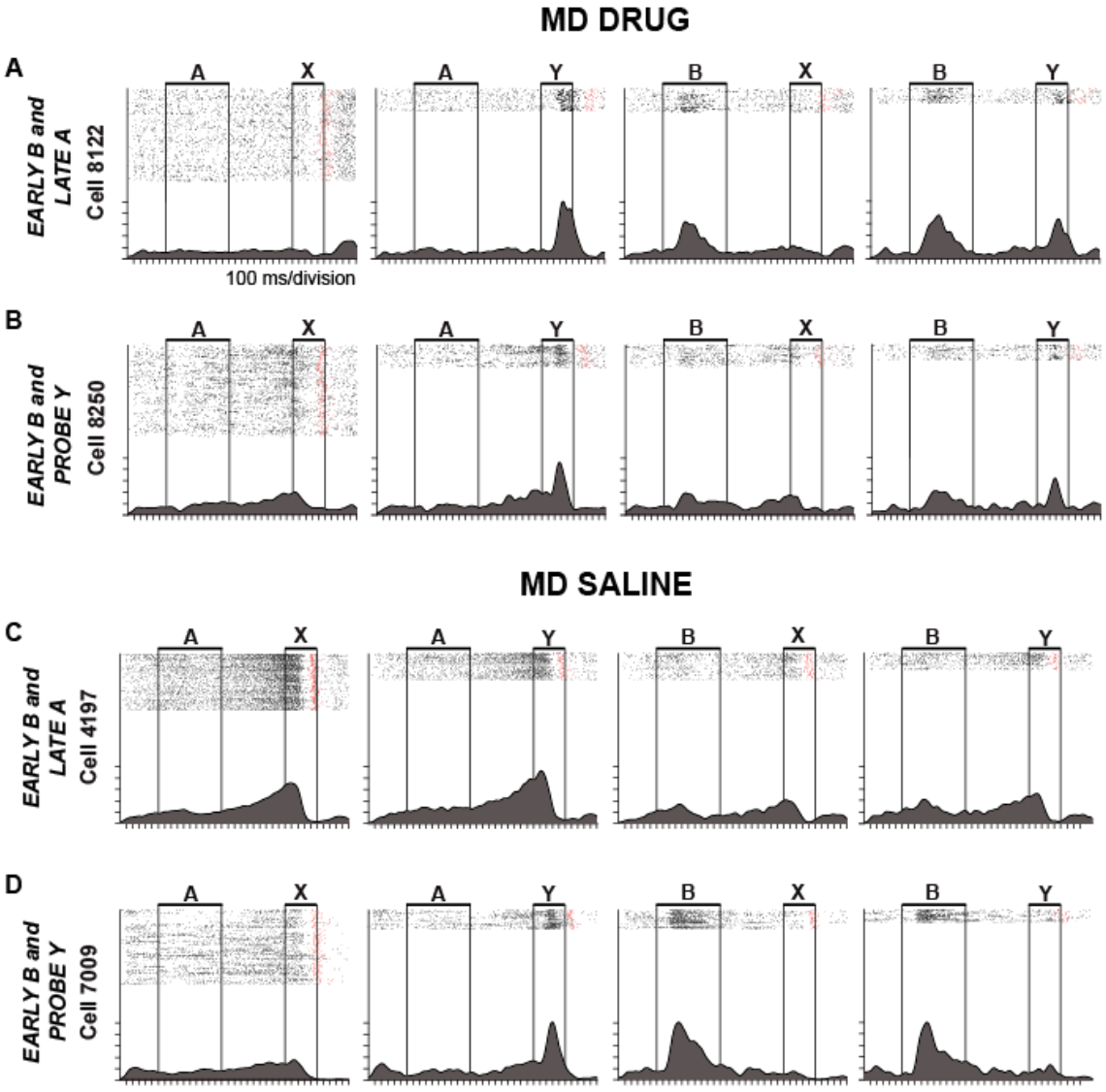

Figure 3.6. Single neuron activity during DPX task performance in the MD during NMDA receptor blockade and saline conditions. Each row of panels illustrates the activity of a single neuron in drug (**A, B**) or saline (**C, D**) conditions. Individual panels indicate activity on a single trial type defined by cue-probe sequence. Rasters indicate timing of action potentials, spike density functions (solid gray; σ = 40 ms; 10 Hz/div) show modulations in average firing rate. Red tick marks indicate the time of the response in each trial. **A.** Early B-cue and Late A-cue neuron recorded following a PCP

injection. MD cell 8122 is an example of a ‘switch’ neuron that switches its cue preference from B-cues during the cue period to A-cues during the probe period. **B.** Early B-cue and Y-probe neuron recorded following a PCP injection: MD cell 8250 is an example of a neuron whose firing rate during the cue period is greater on B-cue trials than A-cue trials and activity in the probe period is greater on Y-probe trials than X-probe trials. **C.** Early B-cue and Late A-cue neuron recorded following a saline injection. MD cell 4197 is an example of a ‘switch’ neuron that switches its cue preference from B-cues during the cue period to A-cues during the probe period. **D.** Early B-cue and Y-probe neuron recorded following a saline injection: MD cell 7009 is an example of a neuron whose firing rate during the cue period is greater on B-cue trials than A-cue trials and activity in the probe period is greater on Y-probe trials than X-probe trials.

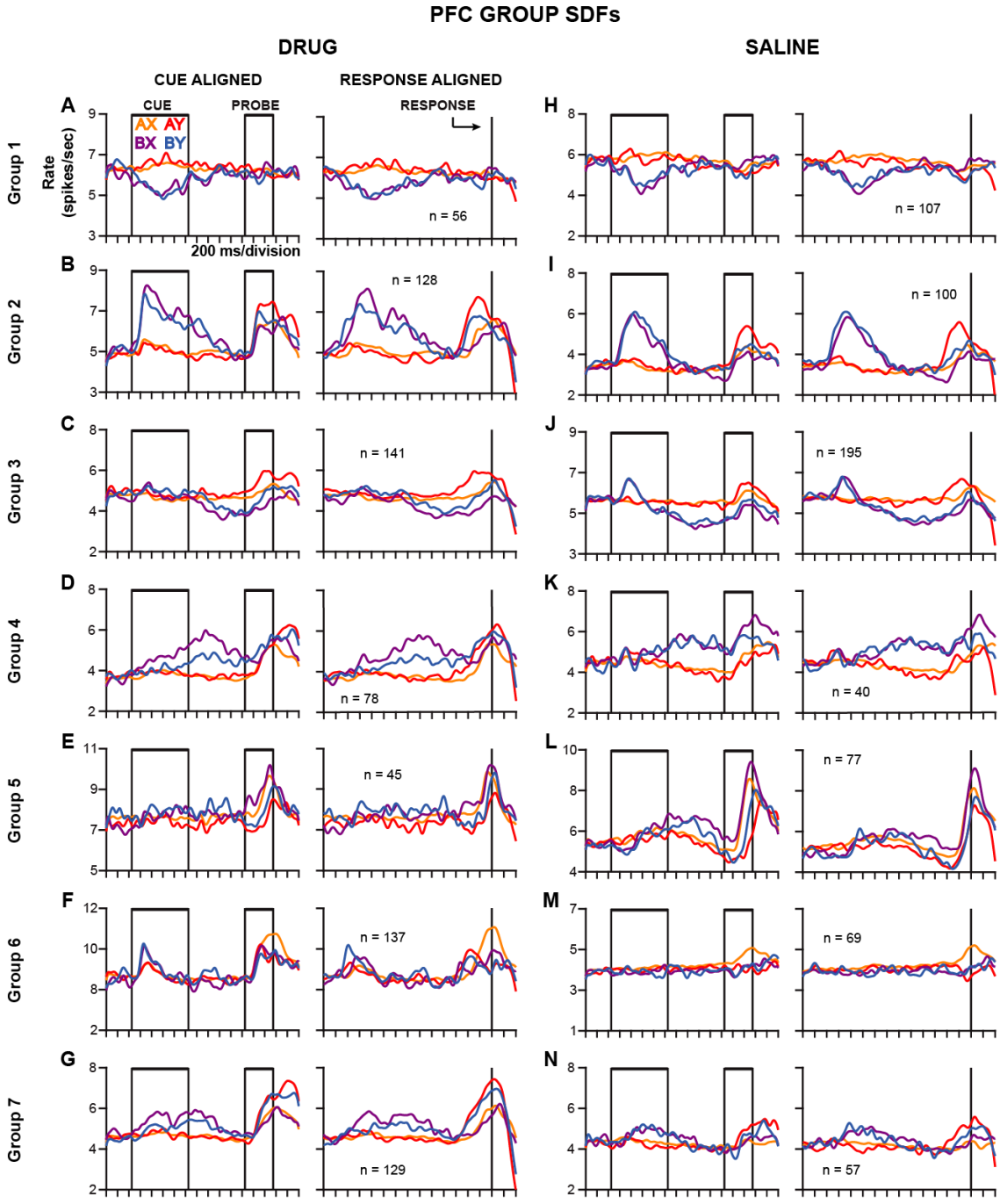

Figure 3.7. Population activity patterns in functionally defined neural groups in prepotent trial sets in the PFC during NMDA receptor blockade and saline conditions. Population spike density functions (SDF; δ = 40 ms) display average

population activity patterns on subsets of trials defined by cue-probe sequence (AX: orange, AY: red, BX: purple, BY: blue). Neurons were divided into seven non-overlapping functional groups (see Results text) depending on the specific preference for individual cues, probes, and responses as well as the trial period that neurons exhibited selective activity as defined by ANCOVA. Population activity of neurons recorded in drug (**A - G**) and saline (**H - N**) conditions is shown aligned to cue onset (left panels) and time of the response (right panels) of Groups 1-7.

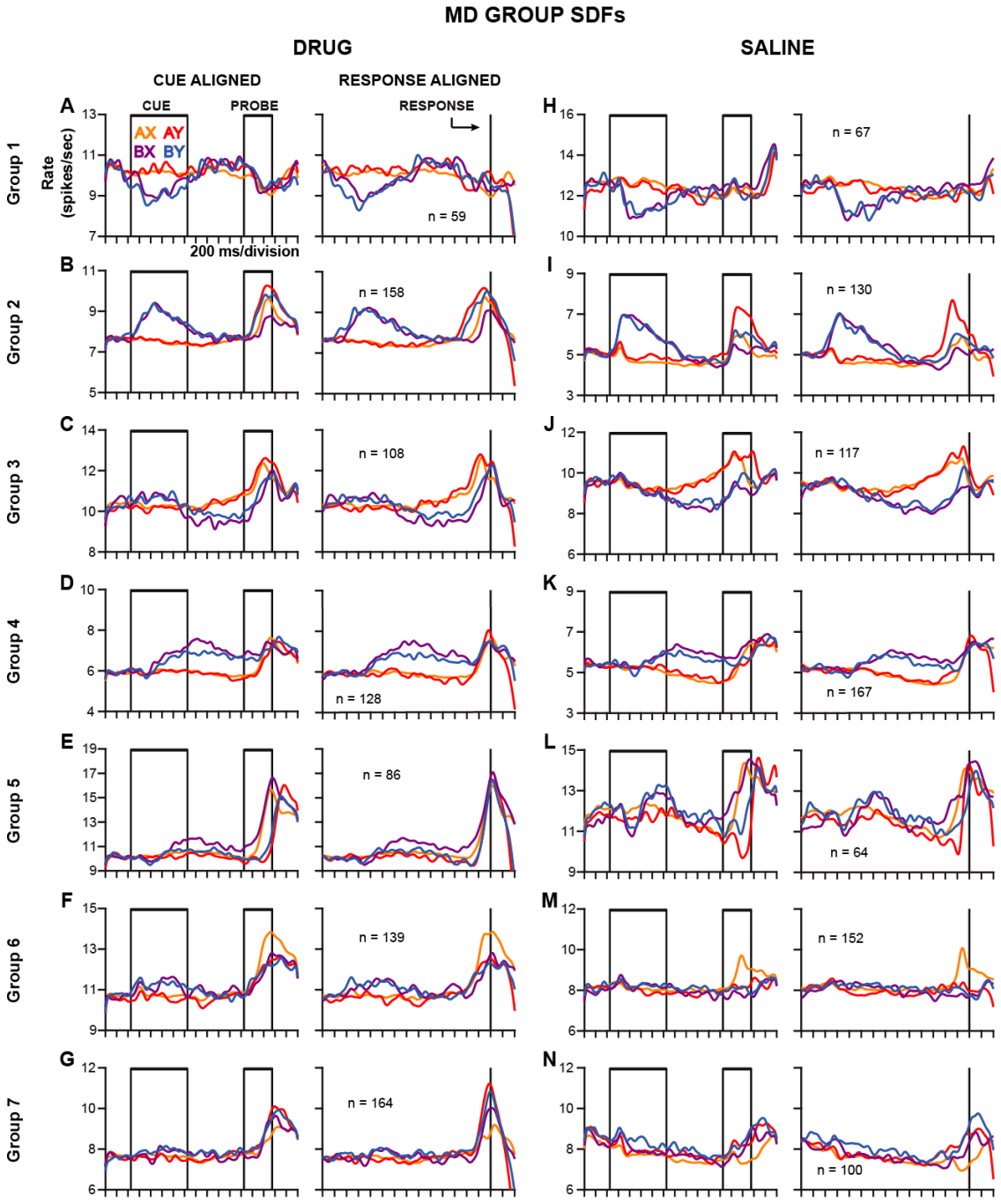

Figure 3.8. Population activity patterns in functionally defined neural groups in prepotent trial sets in the MD during NMDA receptor blockade and saline conditions. Population spike density functions (SDF; δ = 40 ms) display average

population activity patterns on subsets of trials defined by cue-probe sequence (AX: orange, AY: red, BX: purple, BY: blue). Neurons were divided into seven non-overlapping functional groups (see Results text) depending on the specific preference for individual cues, probes, and responses as well as the trial period that neurons exhibited selective activity as defined by ANCOVA. Population activity of neurons recorded in drug (**A - G**) and saline (**H - N**) conditions is shown aligned to cue onset (left panels) and time of the response (right panels) of Groups 1-7.

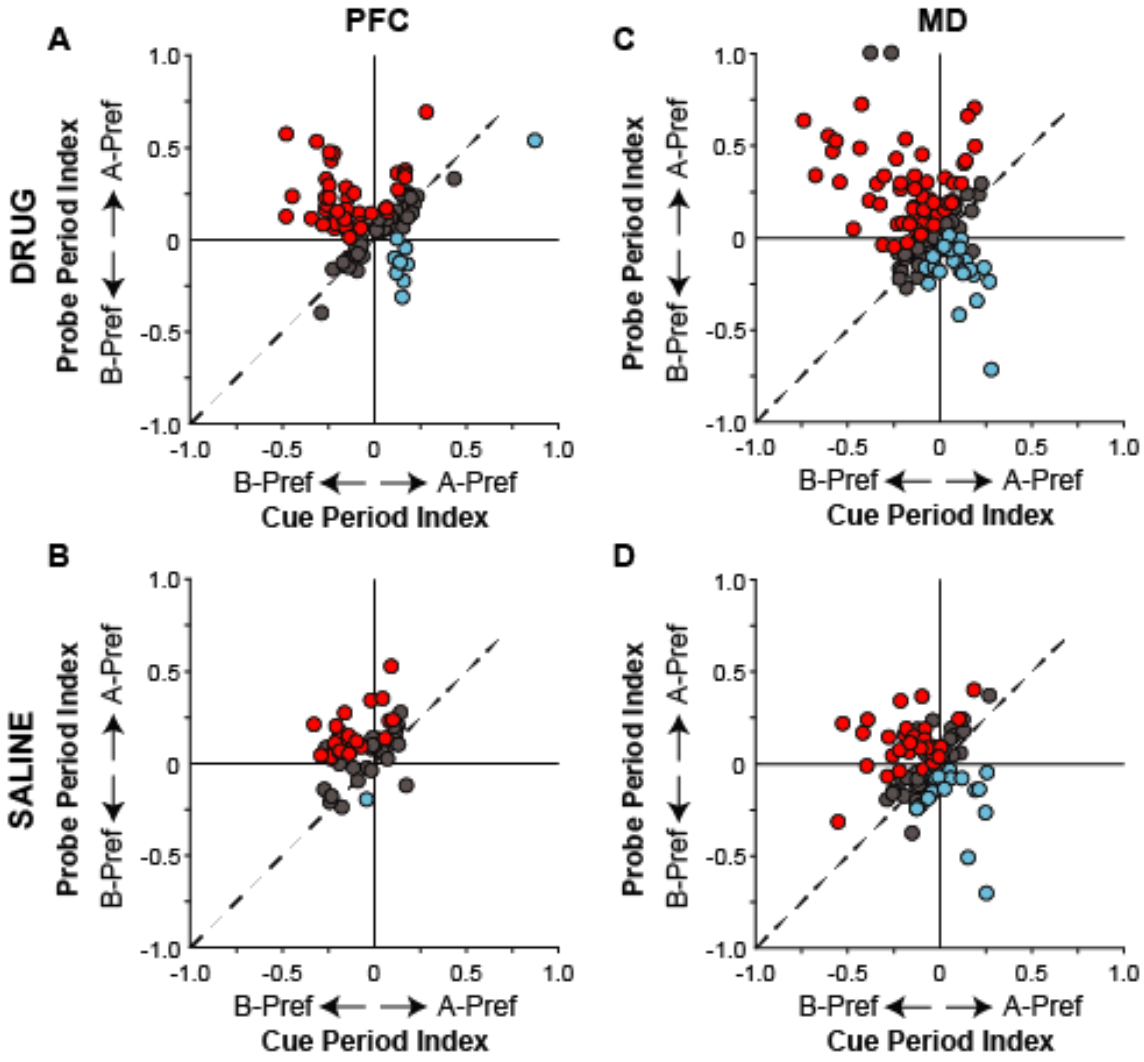

Figure 3.9. Quantification of switch in cue preference from the cue to the probe period in single neurons on prepotent trial sets during NMDA receptor blockade and saline conditions. I computed an index quantifying cue preference (B-cue – A-cue) / (B-cue + A-cue) using cue and probe period firing rates for each neuron. **A – D.** Colored symbols indicate neurons with a significant switch from B-cue to A-cue preference between the cue and probe periods (red circles) or the opposite switch in preference (blue circles). Gray symbols indicate neurons that encoded the cue during both cue and probe periods but did not switch preference. Data are displayed separately

for PFC neurons recorded following a PCP injection (**A**) and saline injection (**B**) and MD neurons recorded following a PCP injection (**C**) and saline injection (**D**) recorded during the performance prepotent trial sets.

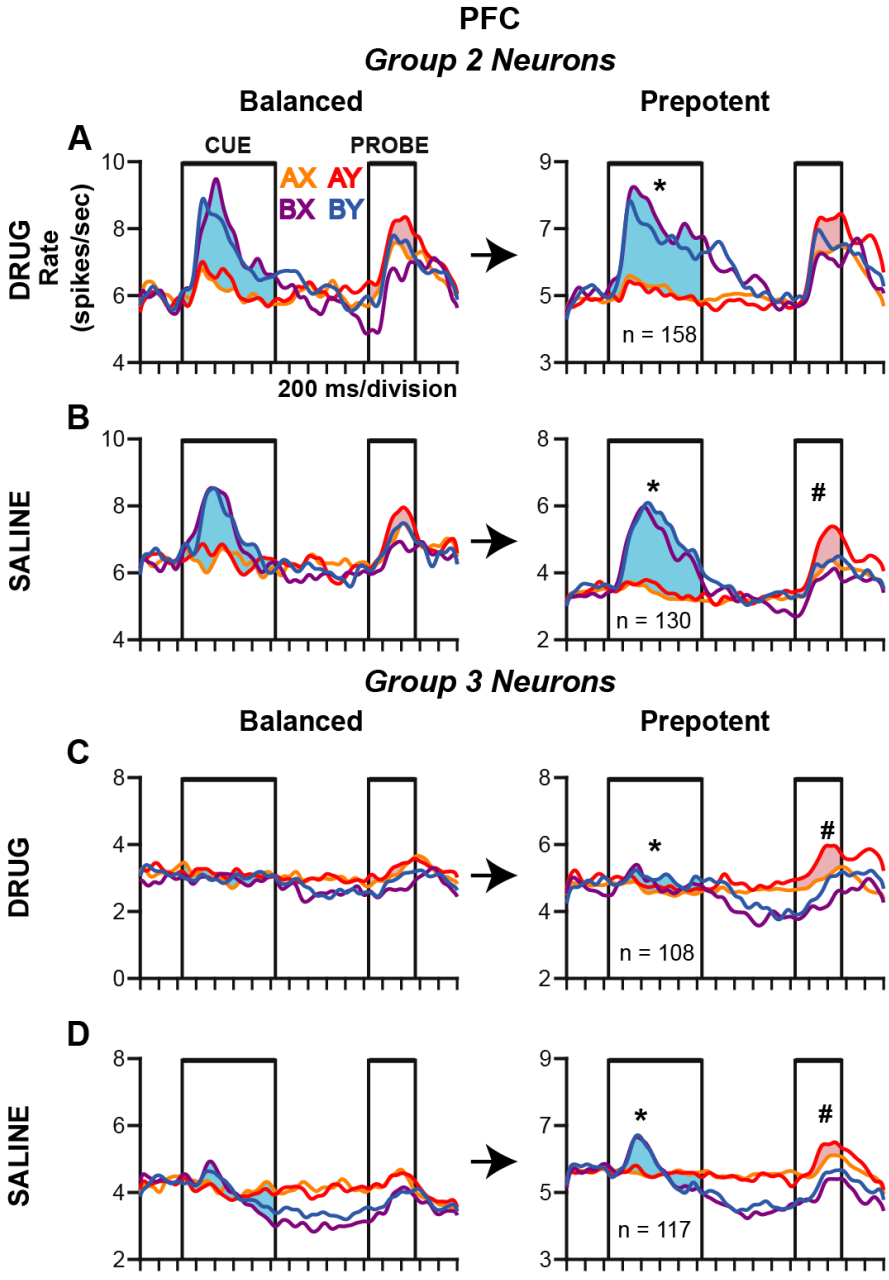

Figure 3.10. Modulation of cognitive control neural signals with cognitive control load in the PFC during NMDA receptor blockade and saline conditions. Blue shading indicates difference in cue period firing rates on B-cue and A-cue trials. Pink shading indicates difference in probe period firing rates on AY and AX trials. **A, B.** Population activity of Group 2 neurons. **C, D.** Population activity of Group 3 neurons

recorded following a PCP injection (**C**) and saline injection (**D**) on balanced (left) and prepotent (right) trial sets. Asterisks (*) indicate a significant increase in the difference in cue period firing rate on B-cue and A-cue trials on prepotent relative to balanced trial sets ($p < 0.05$, permutation test). Pound symbols (#) similarly indicate a significant increase in the difference in probe period firing rate on AY and AX trials in prepotent relative to balanced trial sets ($p < 0.05$).

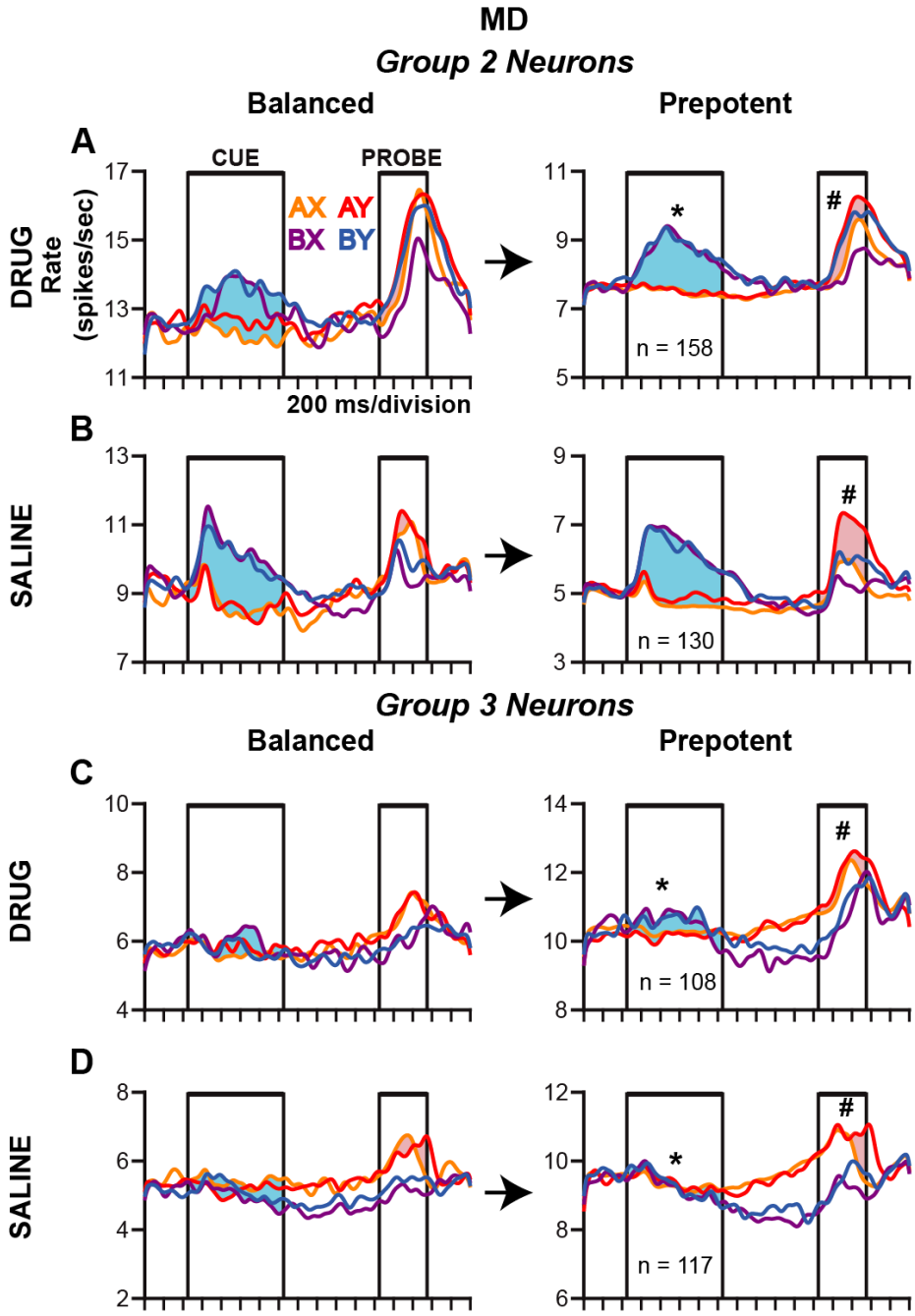

Figure 3.11. Modulation of cognitive control neural signals with cognitive control load in the MD during NMDA receptor blockade and saline conditions. Blue shading indicates difference in cue period firing rates on B-cue and A-cue trials. Pink shading indicates difference in probe period firing rates on AY and AX trials. **A, B.** Population

activity of Group 2 neurons. **C, D.** Population activity of Group 3 neurons recorded following a PCP injection (**C**) and saline injection (**D**) on balanced (left) and prepotent (right) trial sets. Asterisks (*) indicate a significant increase in the difference in cue period firing rate on B-cue and A-cue trials on prepotent relative to balanced trial sets ($p < 0.05$, permutation test). Pound symbols (#) similarly indicate a significant increase in the difference in probe period firing rate on AY and AX trials in prepotent relative to balanced trial sets ($p < 0.05$).

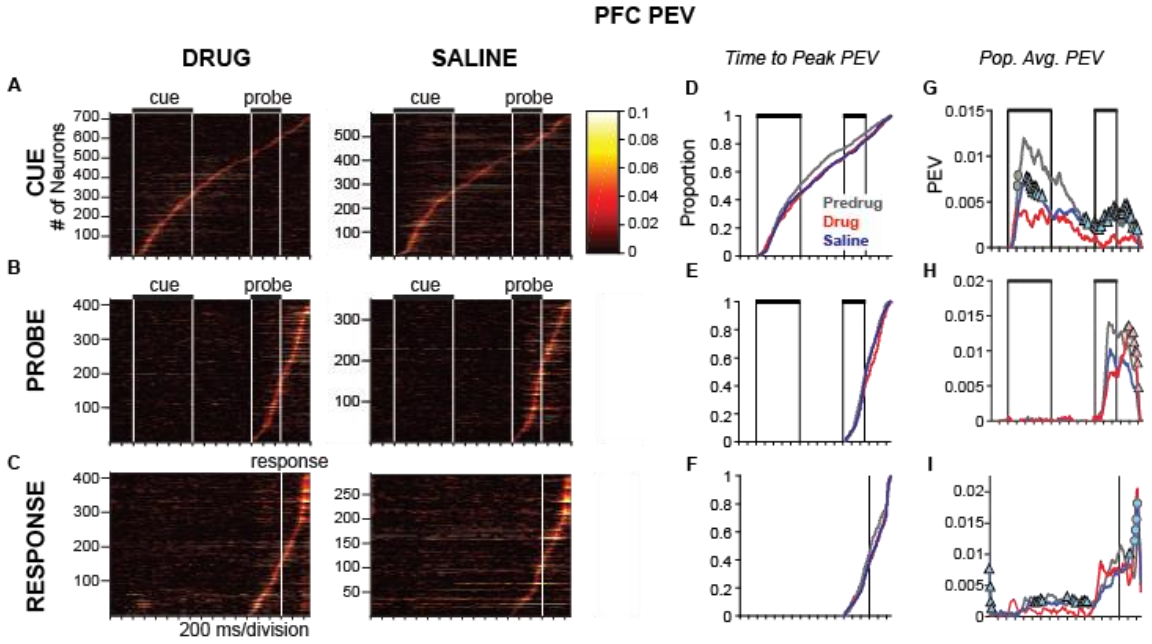

Figure 3.12. Proportion of explained variance (PEV) in firing rate over trials as a function of time in the PFC across conditions. A-C. Warmer colors in the heat maps represent greater PEV values associated with the cue (**A**), probe (**B**), and response (**C**). PEV values were obtained by regressing the firing rate of each neuron onto the appropriate task factor over trials within a sliding 100 ms window (advanced in 20 ms steps). Drug data is on the left and saline data on the right. **D-F.** Cumulative distributions of time to peak PEV attributable to the cue (**D**), probe (**E**), and response (**F**) in neurons recorded in the predrug (gray), drug (red), and saline (blue) conditions. **G-I.** Population average PEV attributable to the cue (**G**), probe (**H**), and response (**I**) neurons recorded in the predrug (gray), drug (red), and saline (blue) conditions. Significant differences in population average PEV time courses are indicated with circles (gray indicates higher population average on predrug compared to saline, blue indicates higher population average on saline compared to predrug) and triangles (blue indicates higher population

average on saline compared to drug and red indicates higher population average on drug compared to saline; permutation test, $p < 0.05$).

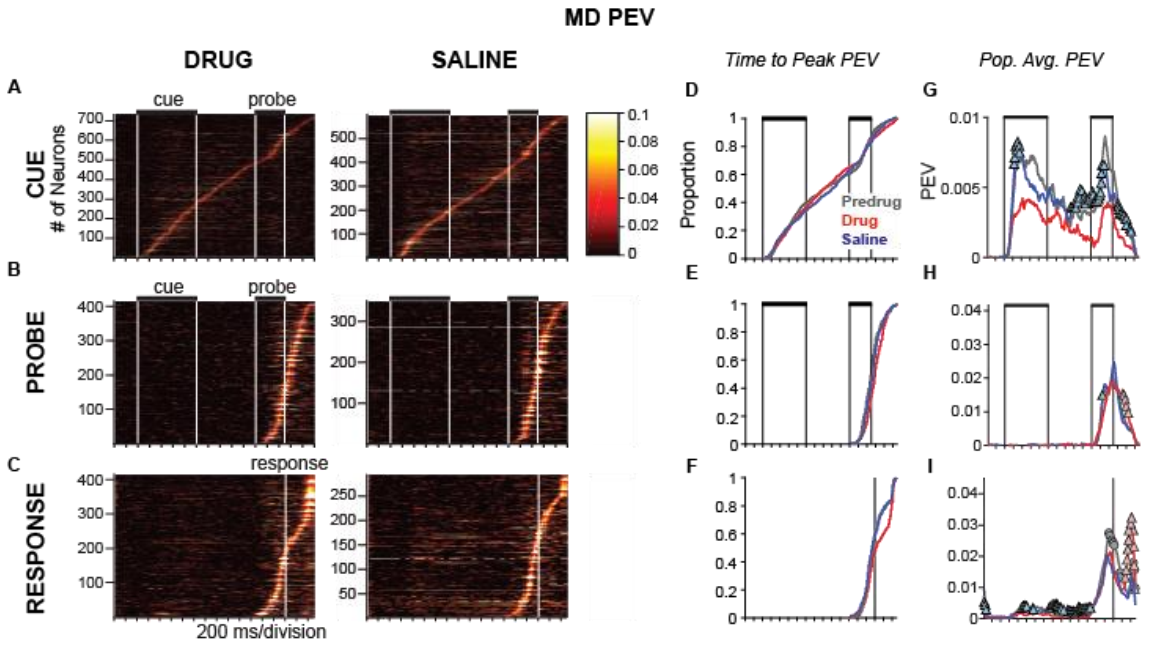

Figure 3.13. Proportion of explained variance (PEV) in firing rate over trials as a function of time in the MD across conditions. A-C. Warmer colors in the heat maps represent greater PEV values associated with the cue (**A**), probe (**B**), and response (**C**). PEV values were obtained by regressing the firing rate of each neuron onto the appropriate task factor over trials within a sliding 100 ms window (advanced in 20 ms steps). Drug data is on the left and saline data on the right. **D-F.** Cumulative distributions of time to peak PEV attributable to the cue (**D**), probe (**E**), and response (**F**) in neurons recorded in the predrug (gray), drug (red), and saline (blue) conditions. **G-I.** Population average PEV attributable to the cue (**G**), probe (**H**), and response (**I**) neurons recorded in the predrug (gray), drug (red), and saline (blue) conditions. Significant differences in population average PEV time courses are indicated with circles (gray indicates higher population average on predrug compared to saline, blue indicates higher population average on saline compared to predrug) and triangles (blue indicates higher population

average on saline compared to drug and red indicates higher population average on drug compared to saline; permutation test, $p < 0.05$).

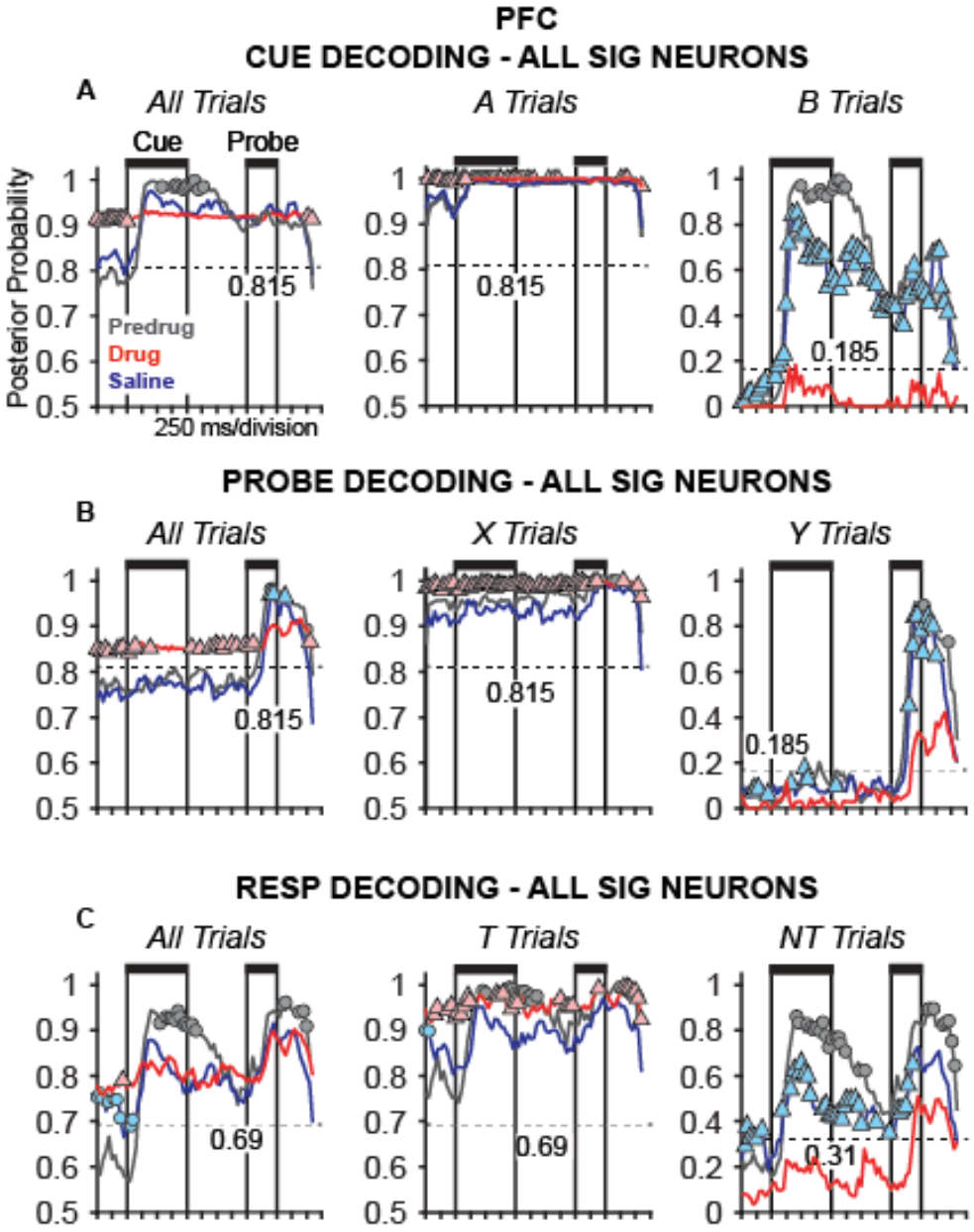

Figure 3.14. Time-resolved population decoding of cue, probe and response PFC neurons using all significant neurons across all conditions. Functions plot the population average posterior probability associated with the neural representation of the cue (**A**), probe (**B**), and response (**C**) as a function of time in the trial, based on neural population activity in predrug (gray), drug (red), and saline (blue). Neural data recorded

on prepotent trial sets. Left panels illustrate posterior probability averaged over all trials, center and right panels plot posterior probability averaged over the subsets of trials indicated above. Horizontal dashed lines indicate chance decoding based on the prior probabilities of cue, probe, and response in prepotent trial sets. For example, before the cue appeared and neural signals encoding the cue developed, the prior probability if of the A-cue was 0.81 (AX and AY trials comprised 81% of trials in prepotent sets). Baseline decoding (before cue onset) reflects the prior probability of the decoded task variable. Circles and triangles indicate significant differences in decoding strength between areas ($p < 0.05$, predrug > saline in gray circles, saline > predrug in blue circles, drug > saline in red triangles, saline > drug in blue triangles, permutation test, FDR corrected, Methods).

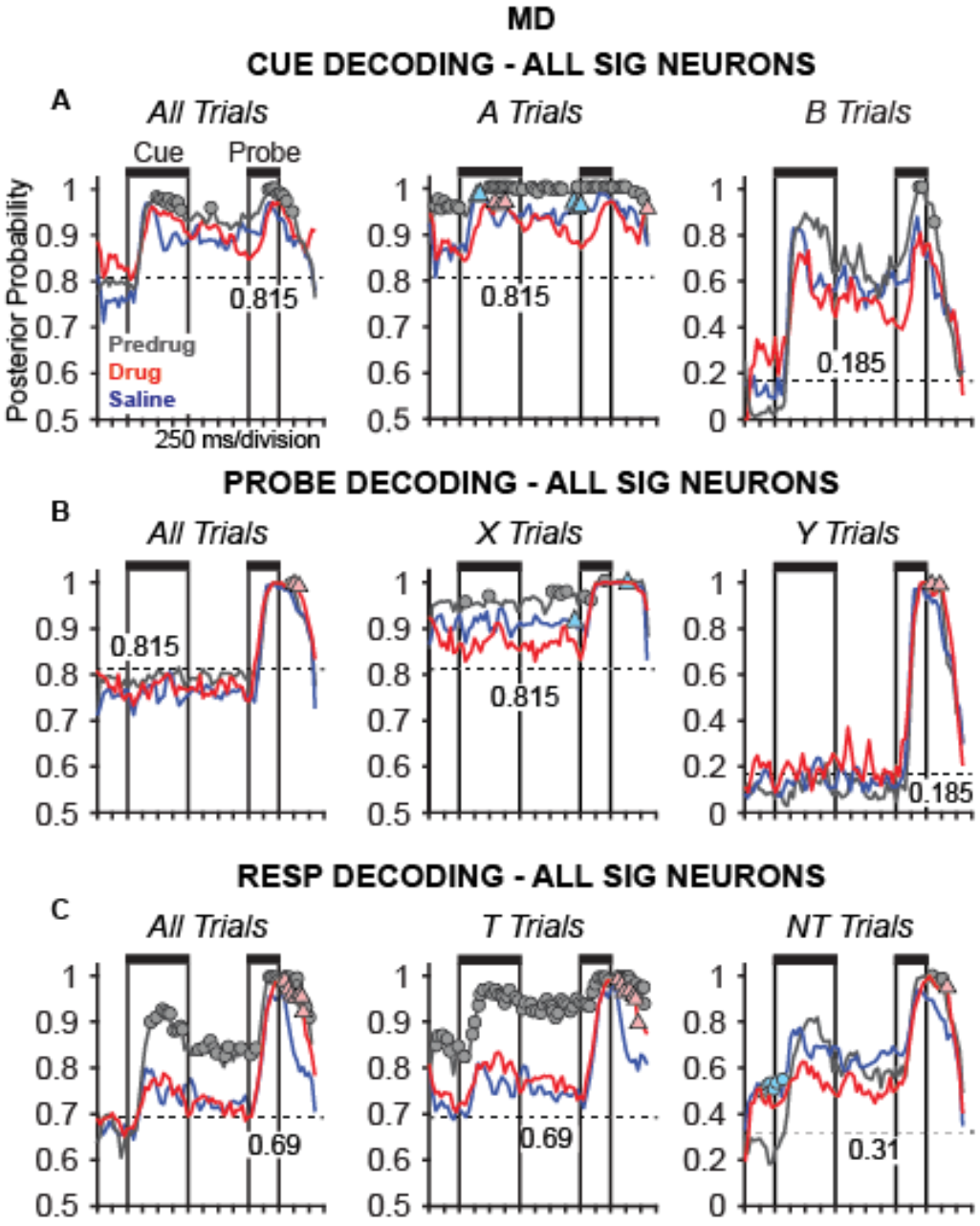

Figure 3.15. Time-resolved population decoding of cue, probe and response MD neurons using all significant neurons across all conditions. Functions plot the population average posterior probability associated with the neural representation of the cue (**A**), probe (**B**), and response (**C**) as a function of time in the trial, based on neural

population activity in predrug (gray), drug (red), and saline (blue). Neural data recorded on prepotent trial sets. Left panels illustrate posterior probability averaged over all trials, center and right panels plot posterior probability averaged over the subsets of trials indicated above. Horizontal dashed lines indicate chance decoding based on the prior probabilities of cue, probe and response in prepotent trial sets. For example, before the cue appeared and neural signals encoding the cue developed, the prior probability if of the A-cue was 0.81 (AX and AY trials comprised 81% of trials in prepotent sets). Baseline decoding (before cue onset) reflects the prior probability of the decoded task variable. Circles and triangles indicate significant differences in decoding strength between areas ($p < 0.05$, predrug > saline in gray circles, saline > predrug in blue circles, drug > saline in red triangles, saline > drug in blue triangles, permutation test, FDR corrected, Methods).

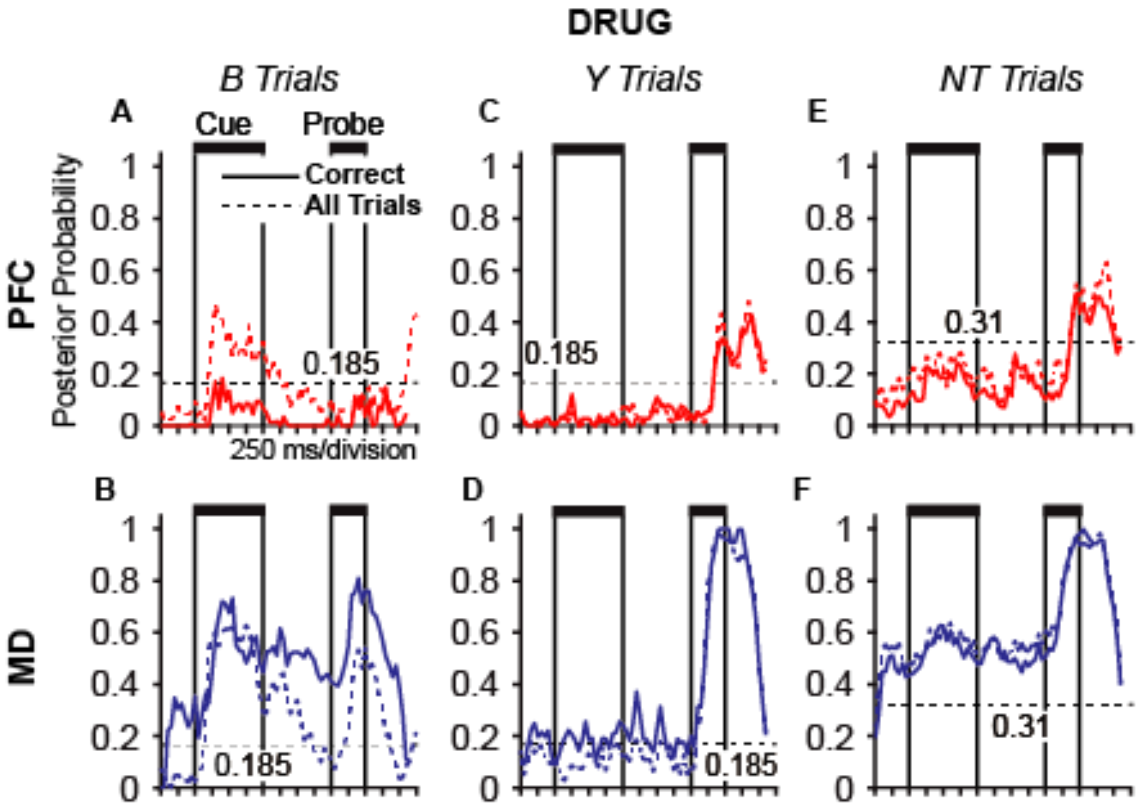

Figure 3.16. Time-resolved population decoding of invalid cue, probe and response variables on correct and error trials in MD and PFC neurons during NMDA receptor blockade. Functions plot the population average posterior probability associated with the neural representation of the B-cue (**A, B**), Y-probe (**C, D**), and NT-response (**E, F**) as a function of time in the trial, based on neural population activity of all significant neurons on correct trials (solid lines) and all trials (correct and error, dashed lines) in the PFC (**A, C, E**) and MD (**B, D, F**) in the drug condition.

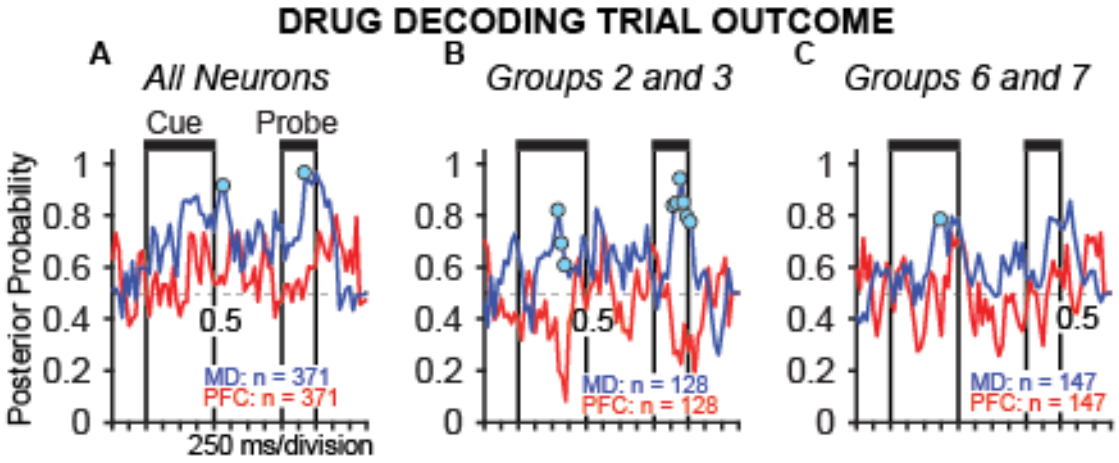

Figure 3.17. Time-resolved population decoding of trial outcome with MD and PFC neurons during NMDA receptor blockade. Functions plot the population average posterior probability associated with the neural representation of the trial outcome (correct or error) as a function of time in the trial, based on neural population activity of all significant neurons (**A**), neurons in groups 2 and 3 (**B**), and neurons in groups 6 and 7 (**C**). Neural data recorded on prepotent trial sets on BX trials only and equalized the number of trials for trial outcome (15 correct BX trials and 15 error BX trials). Circles indicate significant differences in decoding strength between areas ($p < 0.05$, MD > PFC in blue, permutation test, FDR corrected, Methods).

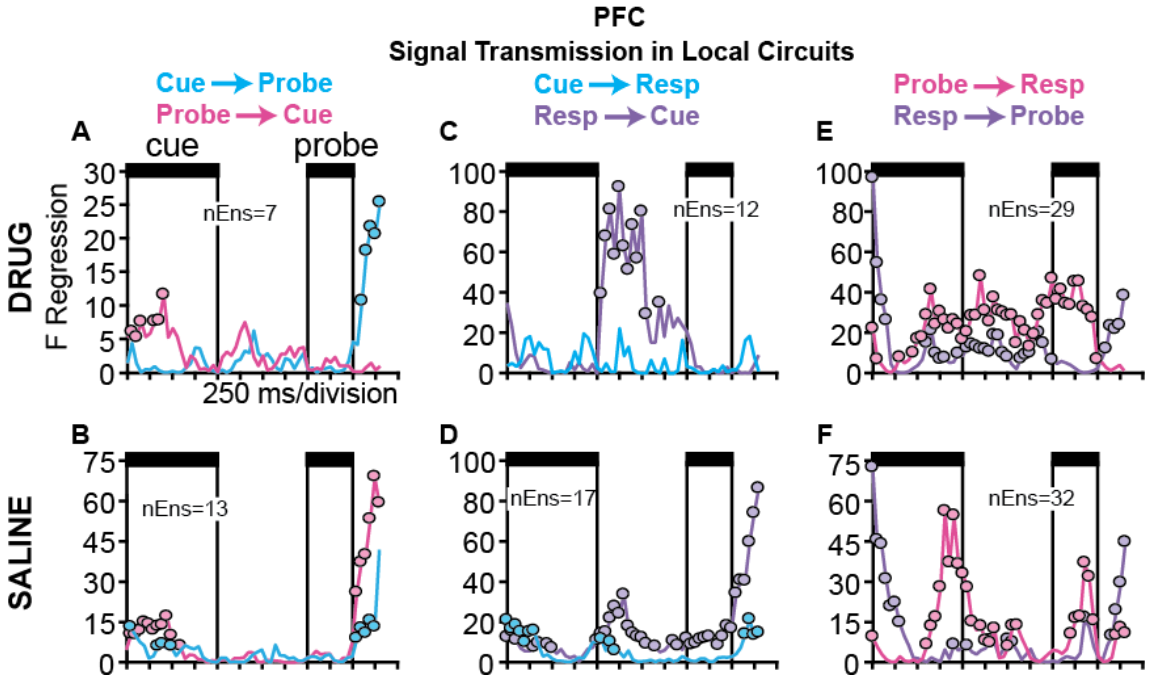

Figure 3.18. Task signal transmission between subsets of neurons within the PFC encoding the cue, probe and response in drug and saline conditions. Functions illustrate the time course of signal transmission between subsets of neurons located within the same brain area that encoded different task variables. The direction of signal transmission between neural subsets is indicated by color (see legend above each column). Circles indicate time points where the strength of transmission was significantly nonzero, defined as time points where the F-statistic exceeded the 95th percentile (FDR corrected) of a bootstrap distribution of F-statistics at that time point generated after shuffling trials of posterior probability time series to break the simultaneity of the underlying neural data and repeating the regression analysis and corrected for multiple comparisons. **A, C, E.** Transmission between subsets of neurons encoding the cue and probe (**A**), cue and response (**C**), and probe and response (**E**) following an injection of PCP. **B, D, F**. Corresponding data following a saline injection.

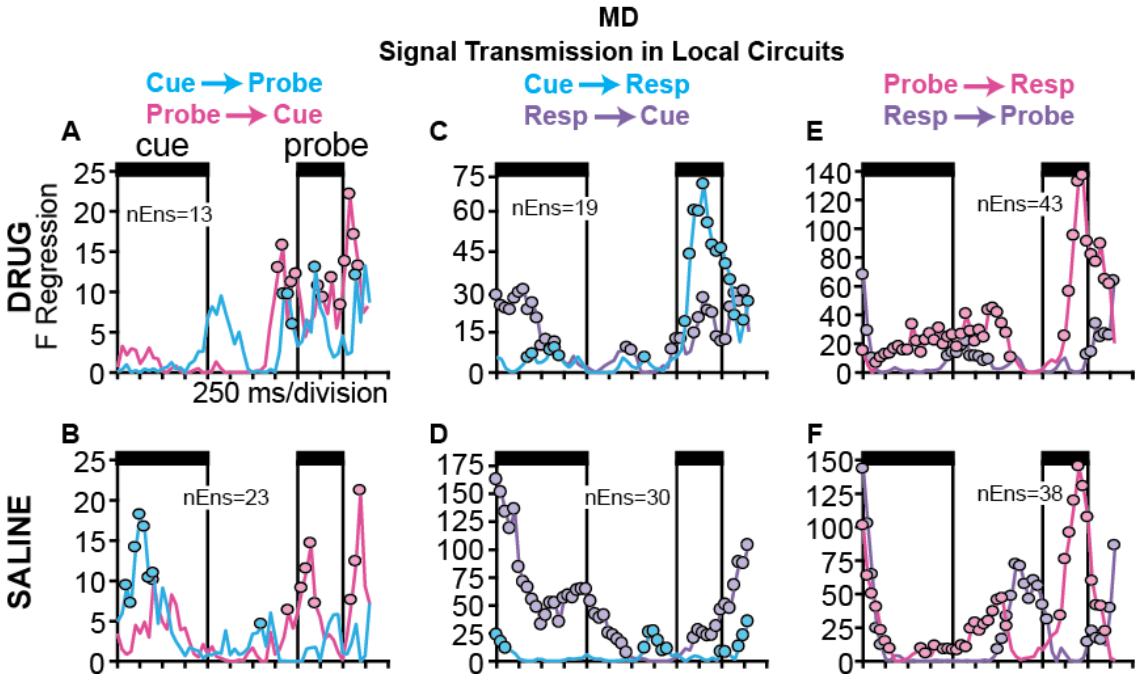

Figure 3.19. Task signal transmission between subsets of neurons within the MD encoding the cue, probe and response in drug and saline conditions. Functions illustrate the time course of signal transmission between subsets of neurons located within the same brain area that encoded different task variables. The direction of signal transmission between neural subsets is indicated by color (see legend above each column). Circles indicate time points where the strength of transmission was significantly nonzero, defined as time points where the F-statistic exceeded the 95th percentile (FDR corrected) of a bootstrap distribution of F-statistics at that time point generated after shuffling trials of posterior probability time series to break the simultaneity of the underlying neural data and repeating the regression analysis and corrected for multiple comparisons. **A, C, E.** Transmission between subsets of neurons encoding the cue and probe (**A**), cue and response (**C**), and probe and response (**E**) following an injection of PCP. **B, D, F**. Corresponding data following a saline injection.

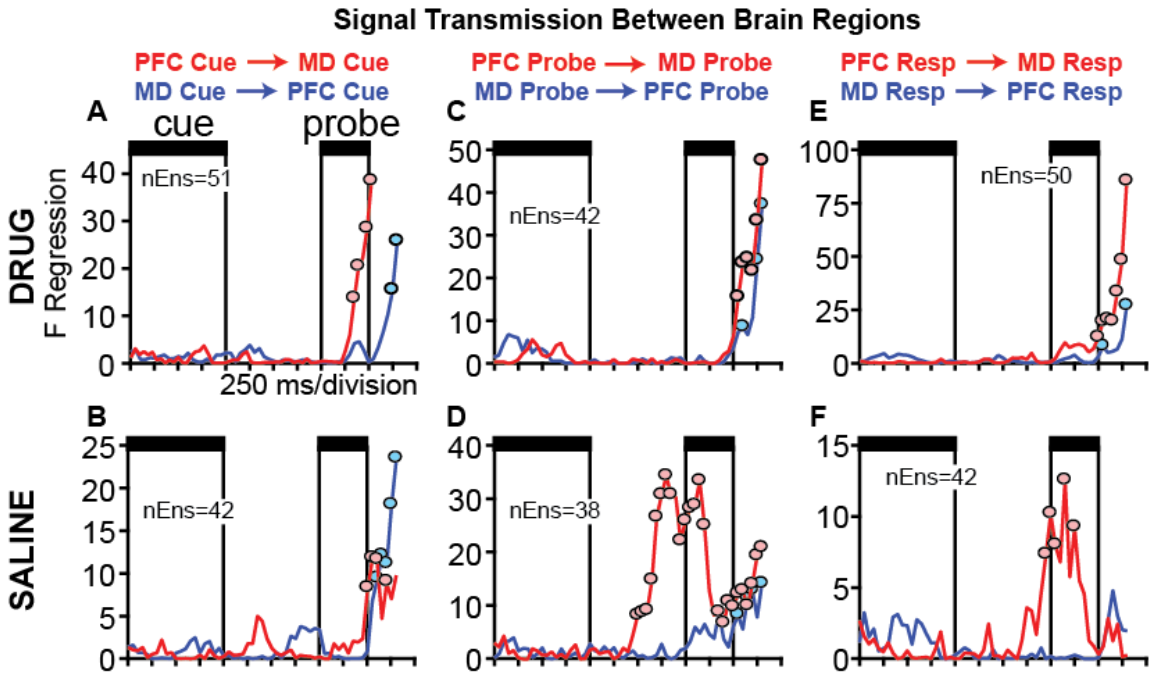

Figure 3.20. Signal transmission between PFC and MD neurons encoding the same task variable in the drug and saline injections. Functions plot is the time course of transmission of (**A, B**) cue, (**C, D**) probe, and (**E, F**) response signals between neurons in the MD and PFC. Top-down (PFC to MD) transmission in red and bottom-up (MD to PFC) in blue. Transmission between neurons recorded following an injection of drug (**A, C, E**) or saline (**B, D, F**). Signal transmission is indicated by circles, where regressions were significantly above the bootstrap regressions ($p < 0.05$; permutation test evaluating transmission in trial-shuffled data).

Chapter 4:

Conclusions

My dissertation work is the first characterization of the distributed processing underlying cognitive control of simultaneously recorded neural activity in the mediodorsal nucleus of the thalamus (MD) and prefrontal cortex (PFC), both in the healthy state and a Schizophrenia (SZ) -like state. The MD has been implicated as a partner of the PFC in cognitive control due to MD's reciprocal anatomical connections with the PFC, the findings that MD neurons exhibit similar activity patterns to their PFC counterparts during cognitive behaviors, and the fact that lesions of the MD nucleus or inhibition of MD neurons result in PFC-like deficits in cognition. Additionally, the MD and PFC have both been found to be dysfunctional in patients with SZ, including decreased functional connectivity between the two. In order to increase the translatability of my research in an animal model of the human disorder, I trained monkeys to perform the exact cognitive control task given to SZ patients, the dot pattern expectancy task (DPX). First, I characterized thalamocortical distributed processes and functional coupling arising from cellular activity of simultaneously recorded neurons in the MD and PFC in the healthy state. Then, I related underlying neural pathophysiology of the MD and PFC to the impaired performance on the DPX task caused by NMDA receptor (NMDAR) blockade. I provide the first evidence that neurons in the MD represent cognitive control state similar to PFC neurons and that neurons in the MD and PFC transmit this state information reciprocally during cognitive control performance. Further, I provide the first description that NMDAR blockade results in a differential loss of network level representation of

cognitive state in the MD and PFC and a loss of functional information transmission between the MD and PFC. These findings support the hypotheses that the neurons in the MD participate in cognitive control behaviors and that thalamocortical, specifically between the MD and the PFC, functional disconnection underlies cognitive deficits in patients with SZ.

Summary of findings

In Chapter 2, I describe distributed neural signals in the MD and PFC that underlie cognitive control as measured by the dot-pattern expectancy task (DPX). The DPX task requires a logical operation based on a cue stimulus that provides the context for the subsequent probe stimulus, which are separate by a delay. Once the probe is presented, a response must be made based on the combination of the cue and probe stimuli (i.e. if A-cue and X-probe, then target response). I report that the MD contained 'switch' neurons that encoded task state in a similar manner as PFC 'switch' neurons. These neurons are considered state neurons as they modulate their firing rate during scenarios when the counter-habitual response was required. Further, switch activity was augmented in MD and PFC neurons alike in response to scenarios of higher cognitive control demand. I also report that task state representation emerged earlier and stronger in the PFC at the beginning of the trial period and that task state representation in the MD was stronger at the end of the trial period during response selection. To this regard, the MD contained response-selective and probe-selective neurons for both valid and invalid variables compared to the PFC neurons, which were biased toward the invalid stimuli that signaled for the counter-habitual response. Lastly, I report that task state information was transmitted within each structure and between them. Top-down

information was transmitted from the PFC to the MD during the cue and response period and bottom-up transmission from the MD to the PFC largely occurred at during the cue period and delay periods. Taken together, these data indicate that cognitive control state information is distributed across the MD and PFC network and response selection occurs in the MD with support from PFC input about cognitive control state. Therefore, the MD may perform response selection by comparing information from the PFC about the probability of requiring a nontarget response and information from the basal ganglia about the habitual response. This largely fits with prior research on MD function during spatial working memory task that showed similar encoding of task variables (Watanabe and Funahashi, 2004b, a; Watanabe et al., 2009; Watanabe and Funahashi, 2018), more involvement of the MD in the motor response selection than the PFC (Watanabe and Funahashi, 2004a; Watanabe et al., 2009; Parnaudeau et al., 2013; Bolkan et al., 2017; Watanabe and Funahashi, 2018), and MD-PFC reciprocal functional connectivity during task performance (Parnaudeau et al., 2013; Bolkan et al., 2017; Schmitt et al., 2017). However, as none these prior studies have recorded single neurons in the MD and PFC simultaneously during performance of a cognitive control task, my work adds previously unknown insight into the role of thalamocortical networks during cognitive control.

In Chapter 3, I describe the effects of pharmacological NMDAR blockade on the distributed neural signals in the MD and PFC and relate them back to SZ-like cognitive control deficits. First, I report that following acute administration of PCP fewer single neurons exhibited task related activity and, although the basic activity patterns were largely intact in terms of the types of neural signals observed, the strength of activity modulation was weakened and delayed following PCP. Second, NMDAR blockade more

powerfully suppressed the neural representation of task variables at the population level in PFC than MD, as evidenced by more pronounced reduction in population decoding accuracy following drug. This suggests that MD and PFC circuits are differentially dependent on NMDAR synaptic function. Third, task-related information transmission, both in the top-down and bottom-up directions, was decreased following PCP exposure compared to saline conditions. All of these changes in neural dynamics were also present in the saline condition relative to the drug-naïve condition, albeit to a lesser degree than in the drug condition. These data suggest that periodic and repeated exposure to PCP may induce chronic changes in PFC thalamocortical dynamics, perhaps by reducing coincident spiking in this network, a mechanism proposed in our prior report (Zick et al., 2018). Taken together, these data indicate that ongoing computations performed by MD-PFC thalamocortical network dynamics are dependent on NMDAR synaptic integrity. In the DPX task, the core functional requirement is that state information (countermand probability) encoded in PFC networks must override a habitual response to a stimulus. From that perspective, the breakdown of state representation in the MD-PFC network may contribute to the higher rate of errors on BX trials reflecting a failure of the countermand operation. Following an injection of PCP, the PFC is less able to encode cognitive control state and communicate this information with the MD, potentially releasing the habitual target response that is strongly encoded by MD neurons. That could occur if basal ganglia input to the MD, presumably encoding the habitual response, was not counterbalanced by equally strong input from the PFC, encoding the state-dependent response. In some respects, many symptoms of SZ reflect aberrant cognitive and perceptual habits, patterns of thought or percepts that emerge and persist even though they are not contextually appropriate. This could reflect

a failure of PFC top-down control mechanisms involving the interplay between thalamic and cortical representations operating through the thalamus, consistent with some of the neural dynamics I have studied here. Our data fits with prior evidence in humans that activity in MD, and PFC, as well as functional connectivity between these areas is decreased in patients with SZ (Minzenberg et al., 2009; Welsh et al., 2010; Woodward et al., 2012; Anticevic et al., 2014b; Anticevic et al., 2014a; Tu et al., 2015). My data adds to our knowledge about the nature of MD-PFC network dysfunction at the level of spiking neurons as no prior studies have recorded neural activity in both areas simultaneously during performance of a cognitive control task following NMDAR blockade.

Limitations

There are a few limitations one should consider when assessing the results reported in my dissertation.

First, SZ is a markedly complicated disease that results from an array of genetic and environmental factors that align in such a way to trigger the appearance of the disorder. At this time, monkey models are not easily genetically manipulated to determine the effects of genetic risk mutations on primate behavior and neurophysiology. Therefore, rodent genetic models have better construct validity that the monkey drug model I have employed, because they incorporate genetic mutations known to cause risk of SZ in humans, making it possible to investigate how genetic factors influence neural information processing. However, the link between genes and SZ is anything but simple. Many mutations increase risk, studying one or a few may not capture the full range of manifestations in the disorder, or indicate where the many mutations functionally converge. In addition, anatomical and cognitive homology

between rodents and humans is limited, and it remains to be determined whether findings in rodents will ultimately succeed or fail to translate to humans. Nonhuman primate research, particularly of PFC mediated cognitive functions, is likely to remain an important stepping stone between rodent and human studies to understand how PFC malfunction could produce cognitive deficits in humans.

Second, the number of individual animals studied in any single primate experiment is a significant limitation for neuropsychiatric relevant research, as individual differences between patients strongly contributes to disease manifestation and course. However, my dissertation work was able to replicate the NMDAR induced BX error pattern reported in a prior study from our lab using different animals (Blackman et al., 2013), as well as several key aspects of neurophysiology, such as the presence of switch neurons coding cognitive state in prefrontal cortex (Blackman et al., 2016). Finally, there is evidence that altered NMDAR receptor function results from genetic mutations that increase SZ risk (Schizophrenia Working Group of the Psychiatric Genomics Consortium, 2014), therefore, though not as strong as rodent genetic models, the NMDAR antagonist model I employed nonetheless may operate through neural mechanisms like those driving the human disease, and therefore provide construct (neural mechanism) as well as face (behavior) validity.

Third, one of the main motivations for targeting the MD-PFC neural network in my dissertation was the fact that the two structures are anatomically connected. I therefore recorded in the MD and PFC simultaneously in order to be able to analyze their functional interaction and relate it to cognitive performance. However, although I could recover recording locations using structural imaging, I do not know if the neurons I recorded in the MD and PFC on any given day were anatomically connected. However,

functional connectivity results indicating that information in one region is transmitted to the other region (perhaps across polysynaptic pathways) may be enough to answer my questions of how MD and PFC work together to produce cognitive control and how functional disconnection in this network could contribute to cognitive control deficits.

Fourth, I was not able to record the same neural ensembles both before an injection of PCP and after, and I could only evaluate differences in neural activity at the population level and cannot make direct statements about how NMDAR blockade affected individual neurons.

Future directions

First, the data collected for my dissertation work can be explored further to develop more precise theories of thalamocortical network dynamics for both cognitive control and cognitive deficits in patients with SZ. Future experiments could explore the influence of NMDAR blockade on cell-level spike synchrony ('0-lag' spiking) within and between neurons in the MD and PFC further, using recent analytical techniques developed in our lab (Zick et al., 2018). If the activity-dependent disconnection hypothesis I proposed is true, then chronic effects on neuronal activity, communication and effective synaptic connectivity should be cumulative following repeated PCP exposure in the MD-PFC network. It will be important to determine the time course of chronic effects. Theories of prefrontal network failure have focused on changes in parvalbumin positive (PV) GABAergic interneurons with downstream dysregulation of neural synchrony in PFC networks (Lisman et al., 2008). Therefore, it may be information to differentiate pyramidal and interneurons based on the waveforms of their action potentials (Constantinidis and Goldman-Rakic, 2002), to determine if NMDAR

blockade has different effects on these two classes of neurons. My dissertation focused on analyzing neural spiking activity, however, I also recorded local field potentials (LFPs) in the MD and PFC throughout the experiment. Therefore, there is much information about the synchronicity within each structure and between them to be gleaned from future analyses of these data.

Second, the results of my dissertation work lead to new questions and provide a basis to design future experiments to address them. For one, recording neural activity simultaneously in the PFC, MD and the basal ganglia (specifically the substantia nigra or globus pallidus that provide input to the MD (Alexander et al., 1986; Haber and McFarland, 2001; Haber and Calzavara, 2009) could elucidate the mechanisms of neural competition involving all three structures between populations encoding the habitual and state-dependent behavioral responses that I have proposed. I have found that cognitive control state signals are weakened by NMDAR receptor blockade. Presumably this would make it more likely that neural populations coding the habitual response would win the neural competition, leading to BX errors. However, it remains to be determined whether competition between these two neural populations can explain BX errors on a trial-by-trial basis, or the extent to which MD mediates this competition between neural signals originating in PFC and basal ganglia.

Third, further understand of the pathophysiology underlying cognitive deficits could inform the development of future therapies targeting the MD-PFC network. This thalamocortical network may provide a useful inroad to modulating PFC function, since the MD is a relatively restricted structure where electrical stimulation, or genetic therapies, could have wide-ranging influence on prefrontal cortex. The efficacy of such an approach is supported by recent data indicating cognitive improvements were

correlated with increased thalamocortical functional connectivity in SZ patients (Ramsay et al., 2017). Developing better therapeutics for patients with SZ will require further exploration and understanding of the pathophysiology underlying the complex symptomology present in the population of patients with SZ.

REFERENCES

Abdul-Monim Z, Reynolds GP, Neill JC (2006) The effect of atypical and classical antipsychotics on sub-chronic PCP-induced cognitive deficits in a reversal-learning paradigm. Behav Brain Res 169:263-273.

Abramczyk RR, Jordan DE, Hegel M (1983) "Reverse" Stroop effect in the performance of schizophrenics. Percept Mot Skills 56:99-106.

Aggleton JP, Mishkin M (1983a) Memory impairments following restricted medial thalamic lesions in monkeys. Exp Brain Res 52:199-209.

Aggleton JP, Mishkin M (1983b) Visual recognition impairment following medial thalamic lesions in monkeys. Neuropsychologia 21:189-197.

Albus M, Hubmann W, Mohr F, Tiedemann TV, Pechler S, Drießlein D, Küchenhoff H (2019) Neurocognitive functioning in patients with first-episode schizophrenia: results of a prospective 15-year follow-up study. Eur Arch Psychiatry Clin Neurosci.

Alexander GE, Fuster JM (1973) Effects of cooling prefrontal cortex on cell firing in the nucleus medialis dorsalis. Brain Res 61:93-105.

Alexander GE, DeLong MR, Strick PL (1986) Parallel organization of functionally segregated circuits linking basal ganglia and cortex. Annu Rev Neurosci 9:357-381.

Anticevic A, Yang G, Savic A, Murray JD, Cole MW, Repovs G, Pearlson GD, Glahn DC (2014a) Mediodorsal and visual thalamic connectivity differ in schizophrenia and bipolar disorder with and without psychosis history. Schizophr Bull 40:1227-1243.

Anticevic A, Cole MW, Repovs G, Murray JD, Brumbaugh MS, Winkler AM, Savic A, Krystal JH, Pearlson GD, Glahn DC (2014b) Characterizing thalamo-cortical disturbances in schizophrenia and bipolar illness. Cereb Cortex 24:3116-3130.

Anticevic A, Corlett PR, Cole MW, Savic A, Gancsos M, Tang Y, Repovs G, Murray JD, Driesen NR, Morgan PT, Xu K, Wang F, Krystal JH (2015a) N-methyl-D-aspartate receptor antagonist effects on prefrontal cortical connectivity better model early than chronic schizophrenia. Biol Psychiatry 77:569-580.

Anticevic A et al. (2015b) Association of Thalamic Dysconnectivity and Conversion to Psychosis in Youth and Young Adults at Elevated Clinical Risk. JAMA Psychiatry 72:882-891.

Asaad WF, Rainer G, Miller EK (2000) Task-specific neural activity in the primate prefrontal cortex. J Neurophysiol 84:451-459. doi: 410.1152/jn.2000.1184.1151.1451.

Association AP (2013) Diagnostic and Statistical Manual of Mental Disorders (DSM-5 ®): American Psychiatric Pub. .

Averbeck BB, Chafee MV (2016) Using model systems to understand errant plasticity mechanisms in psychiatric disorders. Nat Neurosci 19:1418-1425.

Bachevalier J, Meunier M, Lu MX, Ungerleider LG (1997) Thalamic and temporal cortex input to medial prefrontal cortex in rhesus monkeys. Exp Brain Res 115:430-444.

Baddeley A, Della Sala S (1996) Working memory and executive control. Philos Trans R Soc Lond B Biol Sci 351:1397-1403; discussion 1403-1394.

Balu DT (2016) The NMDA Receptor and Schizophrenia: From Pathophysiology to Treatment. Adv Pharmacol 76:351-382.

Barbas H, Henion TH, Dermon CR (1991) Diverse thalamic projections to the prefrontal cortex in the rhesus monkey. J Comp Neurol 313:65-94.

Barch DM, Ceaser A (2012) Cognition in schizophrenia: core psychological and neural mechanisms. Trends Cogn Sci 16:27-34.

Barch DM, Carter CS, MacDonald AW, Braver TS, Cohen JD (2003) Context-processing deficits in schizophrenia: diagnostic specificity, 4-week course, and relationships to clinical symptoms. J Abnorm Psychol 112:132-143.

Barch DM, Mitropoulou V, Harvey PD, New AS, Silverman JM, Siever LJ (2004) Context-processing deficits in schizotypal personality disorder. J Abnorm Psychol 113:556-568.

Barch DM, Carter CS, Braver TS, Sabb FW, MacDonald A, Noll DC, Cohen JD (2001) Selective deficits in prefrontal cortex function in medication-naive patients with schizophrenia. Arch Gen Psychiatry 58:280-288.

Bartók E, Berecz R, Glaub T, Degrell I (2005) Cognitive functions in prepsychotic patients. Prog Neuropsychopharmacol Biol Psychiatry 29:621-625.

Berman KF, Zec RF, Weinberger DR (1986) Physiologic dysfunction of dorsolateral prefrontal cortex in schizophrenia. II. Role of neuroleptic treatment, attention, and mental effort. Arch Gen Psychiatry 43:126-135.

Blackman RK, Macdonald AW, Chafee MV (2013) Effects of ketamine on context-processing performance in monkeys: a new animal model of cognitive deficits in schizophrenia. Neuropsychopharmacology 38:2090-2100.

Blackman RK, Crowe DA, DeNicola AL, Sakellaridi S, MacDonald AW, 3rd, Chafee MV (2016) Monkey Prefrontal Neurons Reflect Logical Operations for Cognitive Control in a Variant of the AX Continuous Performance Task (AX-CPT). J Neurosci 36:4067-4079. doi: 4010.1523/JNEUROSCI.3578-4015.2016.

Block AE, Dhanji H, Thompson-Tardif SF, Floresco SB (2007) Thalamic-prefrontal cortical-ventral striatal circuitry mediates dissociable components of strategy set shifting. Cereb Cortex 17:1625-1636.

Bolkan SS, Stujenske JM, Parnaudeau S, Spellman TJ, Rauffenbart C, Abbas AI, Harris AZ, Gordon JA, Kellendonk C (2017) Thalamic projections sustain prefrontal activity during working memory maintenance. Nat Neurosci 20:987-996.

Bongard S, Nieder A (2010) Basic mathematical rules are encoded by primate prefrontal cortex neurons. Proc Natl Acad Sci U S A 107:2277-2282.

Boschin EA, Brkic MM, Simons JS, Buckley MJ (2017) Distinct Roles for the Anterior Cingulate and Dorsolateral Prefrontal Cortices During Conflict Between Abstract Rules. Cereb Cortex 27:34-45.

Brambilla P, Macdonald AW, Sassi RB, Johnson MK, Mallinger AG, Carter CS, Soares JC (2007) Context processing performance in bipolar disorder patients. Bipolar Disord 9:230-237.

Braver TS, Reynolds JR, Donaldson DI (2003) Neural mechanisms of transient and sustained cognitive control during task switching. Neuron 39:713-726.

Brincat SL, Miller EK (2016) Prefrontal Cortex Networks Shift from External to Internal Modes during Learning. J Neurosci 36:9739-9754.

Bunge SA, Hazeltine E, Scanlon MD, Rosen AC, Gabrieli JD (2002) Dissociable contributions of prefrontal and parietal cortices to response selection. Neuroimage 17:1562-1571.

Bunge SA, Kahn I, Wallis JD, Miller EK, Wagner AD (2003) Neural circuits subserving the retrieval and maintenance of abstract rules. J Neurophysiol 90:3419-3428.

Buschman TJ, Denovellis EL, Diogo C, Bullock D, Miller EK (2012) Synchronous oscillatory neural ensembles for rules in the prefrontal cortex. Neuron 76:838-846. doi: 810.1016/j.neuron.2012.1009.1029.

Cannon TD, Bearden CE, Hollister JM, Rosso IM, Sanchez LE, Hadley T (2000) Childhood cognitive functioning in schizophrenia patients and their unaffected siblings: a prospective cohort study. Schizophr Bull 26:379-393.

Carlén M (2017) What constitutes the prefrontal cortex? Science 358:478-482.

Celada P, Lladó-Pelfort L, Santana N, Kargieman L, Troyano-Rodriguez E, Riga MS, Artigas F (2013) Disruption of thalamocortical activity in schizophrenia models: relevance to antipsychotic drug action. Int J Neuropsychopharmacol 16:2145-2163.

Censits DM, Ragland JD, Gur RC, Gur RE (1997) Neuropsychological evidence supporting a neurodevelopmental model of schizophrenia: a longitudinal study. Schizophr Res 24:289-298.

Chafee MV, Goldman-Rakic PS (1998) Matching patterns of activity in primate prefrontal area 8a and parietal area 7ip neurons during a spatial working memory task. J Neurophysiol 79:2919-2940.

Chakraborty S, Kolling N, Walton ME, Mitchell AS (2016) Critical role for the mediodorsal thalamus in permitting rapid reward-guided updating in stochastic reward environments. Elife 5.

Cheng WJ, Chen CH, Chen CK, Huang MC, Pietrzak RH, Krystal JH, Xu K (2018) Similar psychotic and cognitive profile between ketamine dependence with persistent psychosis and schizophrenia. Schizophr Res 199:313-318.

Christoff K, Keramatian K, Gordon AM, Smith R, Mädler B (2009) Prefrontal organization of cognitive control according to levels of abstraction. Brain Res 1286:94-105.

Chudasama Y (2011) Animal models of prefrontal-executive function. Behav Neurosci 125:327-343.

Chudasama Y, Bussey TJ, Muir JL (2001) Effects of selective thalamic and prelimbic cortex lesions on two types of visual discrimination and reversal learning. Eur J Neurosci 14:1009-1020.

Chun CA, Ciceron L, Kwapil TR (2018) A meta-analysis of context integration deficits across the schizotypy spectrum using AX-CPT and DPX tasks. J Abnorm Psychol 127:789-806.

Cobia DJ, Smith MJ, Salinas I, Ng C, Gado M, Csernansky JG, Wang L (2017) Progressive deterioration of thalamic nuclei relates to cortical network decline in schizophrenia. Schizophr Res 180:21-27.

Cohen JD, Servan-Schreiber D (1992) Context, cortex, and dopamine: a connectionist approach to behavior and biology in schizophrenia. Psychol Rev 99:45-77.

Cohen JD, Barch DM, Carter C, Servan-Schreiber D (1999) Context-processing deficits in schizophrenia: converging evidence from three theoretically motivated cognitive tasks. J Abnorm Psychol 108:120-133.

Cohen MR, Maunsell JH (2009) Attention improves performance primarily by reducing interneuronal correlations. Nat Neurosci 12:1594-1600.

Consortium SWGotPG (2014) Biological insights from 108 schizophrenia-associated genetic loci. Nature 511:421-427.

Constantinidis C, Goldman-Rakic PS (2002) Correlated discharges among putative pyramidal neurons and interneurons in the primate prefrontal cortex. J Neurophysiol 88:3487-3497.

Crowe DA, Averbeck BB, Chafee MV (2010) Rapid sequences of population activity patterns dynamically encode task-critical spatial information in parietal cortex. J Neurosci 30:11640-11653.

Crowe DA, Zarco W, Bartolo R, Merchant H (2014) Dynamic representation of the temporal and sequential structure of rhythmic movements in the primate medial premotor cortex. J Neurosci 34:11972-11983.

Crowe DA, Goodwin SJ, Blackman RK, Sakellaridi S, Sponheim SR, MacDonald AW, 3rd, Chafee MV (2013a) Prefrontal neurons transmit signals to parietal neurons that reflect executive control of cognition. Nat Neurosci 16:1484-1491. doi: 1410.1038/nn.3509. Epub 2013 Sep 1481.

Crowe DA, Goodwin SJ, Blackman RK, Sakellaridi S, Sponheim SR, MacDonald AW, Chafee MV (2013b) Prefrontal neurons transmit signals to parietal neurons that reflect executive control of cognition. Nat Neurosci 16:1484-1491.

D'Esposito M, Postle BR, Rypma B (2000) Prefrontal cortical contributions to working memory: evidence from event-related fMRI studies. Exp Brain Res 133:3-11.

D'Esposito M, Postle BR, Ballard D, Lease J (1999) Maintenance versus manipulation of information held in working memory: an event-related fMRI study. Brain Cogn 41:66-86.

Dan Y, Poo MM (2004) Spike timing-dependent plasticity of neural circuits. Neuron 44:23-30.

de Zubicaray GI, McMahon K, Wilson SJ, Muthiah S (2001) Brain activity during the encoding, retention, and retrieval of stimulus representations. Learn Mem 8:243-251.

Dias EC, McGinnis T, Smiley JF, Foxe JJ, Schroeder CE, Javitt DC (2006) Changing plans: neural correlates of executive control in monkey and human frontal cortex. Exp Brain Res 174:279-291.

Didriksen M, Skarsfeldt T, Arnt J (2007) Reversal of PCP-induced learning and memory deficits in the Morris' water maze by sertindole and other antipsychotics. Psychopharmacology (Berl) 193:225-233.

Dorph-Petersen KA, Lewis DA (2017) Postmortem structural studies of the thalamus in schizophrenia. Schizophr Res 180:28-35.

Dove A, Pollmann S, Schubert T, Wiggins CJ, von Cramon DY (2000) Prefrontal cortex activation in task switching: an event-related fMRI study. Brain Res Cogn Brain Res 9:103-109.

Dreher JC, Berman KF (2002) Fractionating the neural substrate of cognitive control processes. Proc Natl Acad Sci U S A 99:14595-14600.

Eastvold AD, Heaton RK, Cadenhead KS (2007) Neurocognitive deficits in the (putative) prodrome and first episode of psychosis. Schizophr Res 93:266-277.

Egan MF, Goldberg TE, Gscheidle T, Weirich M, Rawlings R, Hyde TM, Bigelow L, Weinberger DR (2001) Relative risk for cognitive impairments in siblings of patients with schizophrenia. Biol Psychiatry 50:98-107.

Egner T, Hirsch J (2005) The neural correlates and functional integration of cognitive control in a Stroop task. Neuroimage 24:539-547.

Elliott R, Dolan RJ (1999) Differential neural responses during performance of matching and nonmatching to sample tasks at two delay intervals. J Neurosci 19:5066-5073.

Erickson SL, Lewis DA (2004) Cortical connections of the lateral mediodorsal thalamus in cynomolgus monkeys. J Comp Neurol 473:107-127.

Erickson SL, Melchitzky DS, Lewis DA (2004) Subcortical afferents to the lateral mediodorsal thalamus in cynomolgus monkeys. Neuroscience 129:675-690.

Faraone SV, Seidman LJ, Kremen WS, Pepple JR, Lyons MJ, Tsuang MT (1995) Neuropsychological functioning among the nonpsychotic relatives of schizophrenic patients: a diagnostic efficiency analysis. J Abnorm Psychol 104:286-304.

Feldman DE (2012) The spike-timing dependence of plasticity. Neuron 75:556-571.

Floresco SB, Braaksma DN, Phillips AG (1999) Thalamic-cortical-striatal circuitry subserves working memory during delayed responding on a radial arm maze. J Neurosci 19:11061-11071.

Fornito A, Zalesky A, Pantelis C, Bullmore ET (2012) Schizophrenia, neuroimaging and connectomics. Neuroimage 62:2296-2314.

Franke P, Maier W, Hardt J, Hain C (1993) Cognitive functioning and anhedonia in subjects at risk for schizophrenia. Schizophr Res 10:77-84.

Freedman DJ, Riesenhuber M, Poggio T, Miller EK (2001) Categorical representation of visual stimuli in the primate prefrontal cortex. Science 291:312-316.

Freedman DJ, Riesenhuber M, Poggio T, Miller EK (2003) A comparison of primate prefrontal and inferior temporal cortices during visual categorization. J Neurosci 23:5235-5246.

Friston KJ (1998) The disconnection hypothesis. Schizophr Res 30:115-125.

Frohlich J, Van Horn JD (2014) Reviewing the ketamine model for schizophrenia. J Psychopharmacol 28:287-302.

Funahashi S, Andreau JM (2013) Prefrontal cortex and neural mechanisms of executive function. J Physiol Paris 107:471-482.

Funahashi S, Inoue M, Kubota K (1993a) Delay-related activity in the primate prefrontal cortex during sequential reaching tasks with delay. Neurosci Res 18:171-175.

Funahashi S, Chafee MV, Goldman-Rakic PS (1993b) Prefrontal neuronal activity in rhesus monkeys performing a delayed anti-saccade task. Nature 365:753-756.

Funahashi S, Takeda K, Watanabe Y (2004) Neural mechanisms of spatial working memory: contributions of the dorsolateral prefrontal cortex and the thalamic mediodorsal nucleus. Cogn Affect Behav Neurosci 4:409-420.

Funk AJ, Rumbaugh G, Harotunian V, McCullumsmith RE, Meador-Woodruff JH (2009) Decreased expression of NMDA receptor-associated proteins in frontal cortex of elderly patients with schizophrenia. Neuroreport 20:1019-1022.

Furth KE, McCoy AJ, Dodge C, Walters JR, Buonanno A, Delaville C (2017) Neuronal correlates of ketamine and walking induced gamma oscillations in the medial prefrontal cortex and mediodorsal thalamus. PLoS One 12:e0186732.

Fuster JM (1990) Prefrontal cortex and the bridging of temporal gaps in the perception-action cycle. Ann N Y Acad Sci 608:318-329; discussion 330-316.

Fuster JM (2008) The Prefrontal Cortex 4th Edn. In. London: Academic Press.

Fuster JM, Alexander GE (1971) Neuron activity related to short-term memory. Science 173:652-654.

Fuster JM, Alexander GE (1973) Firing changes in cells of the nucleus medialis dorsalis associated with delayed response behavior. Brain Res 61:79-91.

Gaffan D, Murray EA (1990) Amygdalar interaction with the mediodorsal nucleus of the thalamus and the ventromedial prefrontal cortex in stimulus-reward associative learning in the monkey. J Neurosci 10:3479-3493.

Gaffan D, Watkins S (1991) Mediodorsal Thalamic Lesions Impair Long-Term Visual Associative Memory in Macaques. Eur J Neurosci 3:615-620.

Giguere M, Goldman-Rakic PS (1988) Mediodorsal nucleus: areal, laminar, and tangential distribution of afferents and efferents in the frontal lobe of rhesus monkeys. J Comp Neurol 277:195-213.

Giraldo-Chica M, Rogers BP, Damon SM, Landman BA, Woodward ND (2018) Prefrontal-Thalamic Anatomical Connectivity and Executive Cognitive Function in Schizophrenia. Biol Psychiatry 83:509-517.

Glahn DC, Ragland JD, Abramoff A, Barrett J, Laird AR, Bearden CE, Velligan DI (2005) Beyond hypofrontality: a quantitative meta-analysis of functional neuroimaging studies of working memory in schizophrenia. Hum Brain Mapp 25:60-69.

Glantz LA, Lewis DA (1997) Reduction of synaptophysin immunoreactivity in the prefrontal cortex of subjects with schizophrenia. Regional and diagnostic specificity. Arch Gen Psychiatry 54:660-669.

Glantz LA, Lewis DA (2000) Decreased dendritic spine density on prefrontal cortical pyramidal neurons in schizophrenia. Arch Gen Psychiatry 57:65-73.

Glausier JR, Lewis DA (2013) Dendritic spine pathology in schizophrenia. Neuroscience 251:90-107.

Gläscher J, Adolphs R, Damasio H, Bechara A, Rudrauf D, Calamia M, Paul LK, Tranel D (2012) Lesion mapping of cognitive control and value-based decision making in the prefrontal cortex. Proc Natl Acad Sci U S A 109:14681-14686.

Goff DC (2014) Bitopertin: the good news and bad news. JAMA Psychiatry 71:621-622.

Goldman-Rakic PS (1987) Motor control function of the prefrontal cortex. Ciba Found Symp 132:187-200.

Goldman-Rakic PS (1999) The "psychic" neuron of the cerebral cortex. Ann N Y Acad Sci 868:13-26.

Goldman-Rakic PS, Porrino LJ (1985) The primate mediodorsal (MD) nucleus and its projection to the frontal lobe. J Comp Neurol 242:535-560.

Goodwin SJ, Blackman RK, Sakellaridi S, Chafee MV (2012) Executive control over cognition: stronger and earlier rule-based modulation of spatial category signals in prefrontal cortex relative to parietal cortex. J Neurosci 32:3499-3515.

Green MF (2006) Cognitive impairment and functional outcome in schizophrenia and bipolar disorder. J Clin Psychiatry 67:e12.

Green MF, Kern RS, Heaton RK (2004) Longitudinal studies of cognition and functional outcome in schizophrenia: implications for MATRICS. Schizophr Res 72:41-51.

Green MF, Kern RS, Braff DL, Mintz J (2000) Neurocognitive deficits and functional outcome in schizophrenia: are we measuring the "right stuff"? Schizophr Bull 26:119-136.

Guillery RW, Sherman SM (2011) Branched thalamic afferents: what are the messages that they relay to the cortex? Brain Res Rev 66:205-219.

Haber S, McFarland NR (2001) The place of the thalamus in frontal cortical-basal ganglia circuits. Neuroscientist 7:315-324.

Haber SN, Calzavara R (2009) The cortico-basal ganglia integrative network: the role of the thalamus. Brain Res Bull 78:69-74.

Hajszan T, Leranth C, Roth RH (2006) Subchronic phencyclidine treatment decreases the number of dendritic spine synapses in the rat prefrontal cortex. Biol Psychiatry 60:639-644.

Harrison LM, Mair RG (1996) A comparison of the effects of frontal cortical and thalamic lesions on measures of spatial learning and memory in the rat. Behav Brain Res 75:195-206.

Hawkins KA, Addington J, Keefe RS, Christensen B, Perkins DO, Zipurksy R, Woods SW, Miller TJ, Marquez E, Breier A, McGlashan TH (2004) Neuropsychological status of subjects at high risk for a first episode of psychosis. Schizophr Res 67:115-122.

Heilbronner SR, Chafee MV (2019) Learning How Neurons Fail Inside of Networks: Nonhuman Primates Provide Critical Data for Psychiatry. Neuron 102:21-26.

Hoff AL, Riordan H, O'Donnell DW, Morris L, DeLisi LE (1992) Neuropsychological functioning of first-episode schizophreniform patients. Am J Psychiatry 149:898-903.

Holmes AJ, MacDonald A, Carter CS, Barch DM, Andrew Stenger V, Cohen JD (2005) Prefrontal functioning during context processing in schizophrenia and major depression: an event-related fMRI study. Schizophr Res 76:199-206.

Howes O, McCutcheon R, Stone J (2015) Glutamate and dopamine in schizophrenia: an update for the 21st century. J Psychopharmacol 29:97-115.

Humphries C, Mortimer A, Hirsch S, de Belleroche J (1996) NMDA receptor mRNA correlation with antemortem cognitive impairment in schizophrenia. Neuroreport 7:2051-2055.

Hunt PR, Aggleton JP (1998a) An examination of the spatial working memory deficit following neurotoxic medial dorsal thalamic lesions in rats. Behav Brain Res 97:129-141.

Hunt PR, Aggleton JP (1998b) Neurotoxic lesions of the dorsomedial thalamus impair the acquisition but not the performance of delayed matching to place by rats: a deficit in shifting response rules. J Neurosci 18:10045-10052.

Isseroff A, Rosvold HE, Galkin TW, Goldman-Rakic PS (1982) Spatial memory impairments following damage to the mediodorsal nucleus of the thalamus in rhesus monkeys. Brain Res 232:97-113.

Javitt DC (2007) Glutamate and schizophrenia: phencyclidine, N-methyl-D-aspartate receptors, and dopamine-glutamate interactions. Int Rev Neurobiol 78:69-108.

Jentsch JD, Tran A, Le D, Youngren KD, Roth RH (1997a) Subchronic phencyclidine administration reduces mesoprefrontal dopamine utilization and impairs prefrontal cortical-dependent cognition in the rat. Neuropsychopharmacology 17:92-99.

Jentsch JD, Dazzi L, Chhatwal JP, Verrico CD, Roth RH (1998) Reduced prefrontal cortical dopamine, but not acetylcholine, release in vivo after repeated, intermittent phencyclidine administration to rats. Neurosci Lett 258:175-178.

Jentsch JD, Redmond DE, Elsworth JD, Taylor JR, Youngren KD, Roth RH (1997b) Enduring cognitive deficits and cortical dopamine dysfunction in monkeys after long-term administration of phencyclidine. Science 277:953-955.

Johnson RA, Wichern DW (1998) Applied multivariate statistical analysis. In. Saddle River, NJ: Prentice Hall

Jones CA, Watson DJ, Fone KC (2011) Animal models of schizophrenia. Br J Pharmacol 164:1162-1194.

Jones EGe (1998) The Thalamus of Primates. In. Amsterdam: Elsevier.

Jones JA, Sponheim SR, MacDonald AW (2010) The dot pattern expectancy task: reliability and replication of deficits in schizophrenia. Psychol Assess 22:131-141.

Jones P, Rodgers B, Murray R, Marmot M (1994) Child development risk factors for adult schizophrenia in the British 1946 birth cohort. Lancet 344:1398-1402.

Keefe RS, Perkins DO, Gu H, Zipursky RB, Christensen BK, Lieberman JA (2006) A longitudinal study of neurocognitive function in individuals at-risk for psychosis. Schizophr Res 88:26-35.

Keefe RS, Silverman JM, Roitman SE, Harvey PD, Duncan MA, Alroy D, Siever LJ, Davis KL, Mohs RC (1994) Performance of nonpsychotic relatives of schizophrenic patients on cognitive tests. Psychiatry Res 53:1-12.

Kellendonk C, Simpson EH, Kandel ER (2009) Modeling cognitive endophenotypes of schizophrenia in mice. Trends Neurosci 32:347-358.

Kerns JG, Nuechterlein KH, Braver TS, Barch DM (2008) Executive functioning component mechanisms and schizophrenia. Biol Psychiatry 64:26-33.

Kerns JG, Cohen JD, MacDonald AW, Johnson MK, Stenger VA, Aizenstein H, Carter CS (2005) Decreased conflict- and error-related activity in the anterior cingulate cortex in subjects with schizophrenia. Am J Psychiatry 162:1833-1839.

Kiss T, Hoffmann WE, Scott L, Kawabe TT, Milici AJ, Nilsen EA, Hajós M (2011) Role of Thalamic Projection in NMDA Receptor-Induced Disruption of Cortical Slow Oscillation and Short-Term Plasticity. Front Psychiatry 2:14.

Klecka KR (1980) Discriminant Analysis. In. Newbury Park, CA: Sage Publications.

Kolluri N, Sun Z, Sampson AR, Lewis DA (2005) Lamina-specific reductions in dendritic spine density in the prefrontal cortex of subjects with schizophrenia. Am J Psychiatry 162:1200-1202.

Kravariti E, Morgan K, Fearon P, Zanelli JW, Lappin JM, Dazzan P, Morgan C, Doody GA, Harrison G, Jones PB, Murray RM, Reichenberg A (2009) Neuropsychological functioning in first-episode schizophrenia. Br J Psychiatry 195:336-345.

Krystal JH, Karper LP, Seibyl JP, Freeman GK, Delaney R, Bremner JD, Heninger GR, Bowers MB, Charney DS (1994) Subanesthetic effects of the noncompetitive NMDA antagonist, ketamine, in humans. Psychotomimetic, perceptual, cognitive, and neuroendocrine responses. Arch Gen Psychiatry 51:199-214.

Kuha A, Tuulio-Henriksson A, Eerola M, Perälä J, Suvisaari J, Partonen T, Lönnqvist J (2007) Impaired executive performance in healthy siblings of schizophrenia patients in a population-based study. Schizophr Res 92:142-150.

Kupferschmidt DA, Gordon JA (2018) The dynamics of disordered dialogue: Prefrontal, hippocampal and thalamic miscommunication underlying working memory deficits in schizophrenia. Brain Neurosci Adv 2.

Lencz T, Smith CW, McLaughlin D, Auther A, Nakayama E, Hovey L, Cornblatt BA (2006) Generalized and specific neurocognitive deficits in prodromal schizophrenia. Biol Psychiatry 59:863-871.

Lesh TA, Niendam TA, Minzenberg MJ, Carter CS (2011) Cognitive control deficits in schizophrenia: mechanisms and meaning. Neuropsychopharmacology 36:316-338.

Lesh TA, Westphal AJ, Niendam TA, Yoon JH, Minzenberg MJ, Ragland JD, Solomon M, Carter CS (2013) Proactive and reactive cognitive control and dorsolateral prefrontal cortex dysfunction in first episode schizophrenia. Neuroimage Clin 2:590-599.

Leung C, Jia Z (2016) Mouse Genetic Models of Human Brain Disorders. Front Genet 7:40.

Lewis DA, González-Burgos G (2008) Neuroplasticity of neocortical circuits in schizophrenia. Neuropsychopharmacology 33:141-165.

Lisman JE, Coyle JT, Green RW, Javitt DC, Benes FM, Heckers S, Grace AA (2008) Circuit-based framework for understanding neurotransmitter and risk gene interactions in schizophrenia. Trends Neurosci 31:234-242.

Liston C, Matalon S, Hare TA, Davidson MC, Casey BJ (2006) Anterior cingulate and posterior parietal cortices are sensitive to dissociable forms of conflict in a task-switching paradigm. Neuron 50:643-653.

Lodge D, Mercier MS (2015) Ketamine and phencyclidine: the good, the bad and the unexpected. Br J Pharmacol 172:4254-4276.

Lopez-Garcia P, Lesh TA, Salo T, Barch DM, MacDonald AW, Gold JM, Ragland JD, Strauss M, Silverstein SM, Carter CS (2016) The neural circuitry supporting goal maintenance during cognitive control: a comparison of expectancy AX-CPT and dot probe expectancy paradigms. Cogn Affect Behav Neurosci 16:164-175.

Luby ED, Cohen BD, Rosenbaum G, Gottlieb JS, Kelley R (1959) Study of a new schizophrenomimetic drug; sernyl. AMA Arch Neurol Psychiatry 81:363-369.

Ma L, Skoblenick K, Seamans JK, Everling S (2015) Ketamine-Induced Changes in the Signal and Noise of Rule Representation in Working Memory by Lateral Prefrontal Neurons. J Neurosci 35:11612-11622.

MacDonald AW (2008) Building a clinically relevant cognitive task: case study of the AX paradigm. Schizophr Bull 34:619-628.

MacDonald AW, Carter CS (2003) Event-related FMRI study of context processing in dorsolateral prefrontal cortex of patients with schizophrenia. J Abnorm Psychol 112:689-697.

MacDonald AW, Cohen JD, Stenger VA, Carter CS (2000) Dissociating the role of the dorsolateral prefrontal and anterior cingulate cortex in cognitive control. Science 288:1835-1838.

MacDonald AW, Pogue-Geile MF, Johnson MK, Carter CS (2003) A specific deficit in context processing in the unaffected siblings of patients with schizophrenia. Arch Gen Psychiatry 60:57-65.

MacDonald AW, Goghari VM, Hicks BM, Flory JD, Carter CS, Manuck SB (2005a) A convergent-divergent approach to context processing, general intellectual functioning, and the genetic liability to schizophrenia. Neuropsychology 19:814-821.

MacDonald AW, Carter CS, Kerns JG, Ursu S, Barch DM, Holmes AJ, Stenger VA, Cohen JD (2005b) Specificity of prefrontal dysfunction and context processing deficits to schizophrenia in never-medicated patients with first-episode psychosis. Am J Psychiatry 162:475-484.

Mante V, Sussillo D, Shenoy KV, Newsome WT (2013) Context-dependent computation by recurrent dynamics in prefrontal cortex. Nature 503:78-84.

McCleery A, Ventura J, Kern RS, Subotnik KL, Gretchen-Doorly D, Green MF, Hellemann GS, Nuechterlein KH (2014) Cognitive functioning in first-episode schizophrenia: MATRICS Consensus Cognitive Battery (MCCB) Profile of Impairment. Schizophr Res 157:33-39.

McFarland NR, Haber SN (2002) Thalamic relay nuclei of the basal ganglia form both reciprocal and nonreciprocal cortical connections, linking multiple frontal cortical areas. J Neurosci 22:8117-8132.

Menon V, Adleman NE, White CD, Glover GH, Reiss AL (2001) Error-related brain activation during a Go/NoGo response inhibition task. Hum Brain Mapp 12:131-143.

Miller EK (2000) The prefrontal cortex and cognitive control. Nat Rev Neurosci 1:59-65.

Miller EK, Cohen JD (2001) An integrative theory of prefrontal cortex function. Annu Rev Neurosci 24:167-202.:10.1146/annurev.neuro.1124.1141.1167.

Minzenberg MJ, Laird AR, Thelen S, Carter CS, Glahn DC (2009) Meta-analysis of 41 functional neuroimaging studies of executive function in schizophrenia. Arch Gen Psychiatry 66:811-822.

Miocinovic S, Noecker AM, Maks CB, Butson CR, McIntyre CC (2007) Cicerone: stereotactic neurophysiological recording and deep brain stimulation electrode placement software system. Acta Neurochir Suppl 97:561-567.

Mitchell AS (2015) The mediodorsal thalamus as a higher order thalamic relay nucleus important for learning and decision-making. Neurosci Biobehav Rev 54:76-88.

Mitchell AS, Dalrymple-Alford JC (2005) Dissociable memory effects after medial thalamus lesions in the rat. Eur J Neurosci 22:973-985.

Mitchell AS, Gaffan D (2008) The magnocellular mediodorsal thalamus is necessary for memory acquisition, but not retrieval. J Neurosci 28:258-263.

Mitchell AS, Chakraborty S (2013) What does the mediodorsal thalamus do? Front Syst Neurosci 7:37.

Mitchell AS, Baxter MG, Gaffan D (2007a) Dissociable performance on scene learning and strategy implementation after lesions to magnocellular mediodorsal thalamic nucleus. J Neurosci 27:11888-11895.

Mitchell AS, Browning PG, Baxter MG (2007b) Neurotoxic lesions of the medial mediodorsal nucleus of the thalamus disrupt reinforcer devaluation effects in rhesus monkeys. J Neurosci 27:11289-11295.

Mitchell AS, Sherman SM, Sommer MA, Mair RG, Vertes RP, Chudasama Y (2014) Advances in understanding mechanisms of thalamic relays in cognition and behavior. J Neurosci 34:15340-15346.

Mitchell AS, Thiele A, Petkov CI, Roberts A, Robbins TW, Schultz W, Lemon R (2018) Continued need for non-human primate neuroscience research. Curr Biol 28:R1186-R1187.

Mohamed S, Paulsen JS, O'Leary D, Arndt S, Andreasen N (1999) Generalized cognitive deficits in schizophrenia: a study of first-episode patients. Arch Gen Psychiatry 56:749-754.

Monchi O, Petrides M, Petre V, Worsley K, Dagher A (2001) Wisconsin Card Sorting revisited: distinct neural circuits participating in different stages of the task identified by event-related functional magnetic resonance imaging. J Neurosci 21:7733-7741.

Mortimer AM (1997) Cognitive function in schizophrenia--do neuroleptics make a difference? Pharmacol Biochem Behav 56:789-795.

Moskaleva M, Nieder A (2014) Stable numerosity representations irrespective of magnitude context in macaque prefrontal cortex. Eur J Neurosci 39:866-874.

Muhammad R, Wallis JD, Miller EK (2006) A comparison of abstract rules in the prefrontal cortex, premotor cortex, inferior temporal cortex, and striatum. J Cogn Neurosci 18:974-989.

Nieder A, Miller EK (2004) A parieto-frontal network for visual numerical information in the monkey. Proc Natl Acad Sci U S A 101:7457-7462.

Niendam TA, Bearden CE, Zinberg J, Johnson JK, O'Brien M, Cannon TD (2007) The course of neurocognition and social functioning in individuals at ultra high risk for psychosis. Schizophr Bull 33:772-781.

Niendam TA, Bearden CE, Rosso IM, Sanchez LE, Hadley T, Nuechterlein KH, Cannon TD (2003) A prospective study of childhood neurocognitive functioning in schizophrenic patients and their siblings. Am J Psychiatry 160:2060-2062.

Niendam TA, Bearden CE, Johnson JK, McKinley M, Loewy R, O'Brien M, Nuechterlein KH, Green MF, Cannon TD (2006) Neurocognitive performance and functional disability in the psychosis prodrome. Schizophr Res 84:100-111.

Nuechterlein KH, Dawson ME (1984) Information processing and attentional functioning in the developmental course of schizophrenic disorders. Schizophr Bull 10:160-203.

O'Tuathaigh CM, Moran PM, Waddington JL (2013) Genetic models of schizophrenia and related psychotic disorders: progress and pitfalls across the methodological "minefield". Cell Tissue Res 354:247-257.

Olejnik S, Algina J (2003) Generalized eta and omega squared statistics: measures of effect size for some common research designs. Psychol Methods 8:434-447.

Olney JW, Newcomer JW, Farber NB (1999) NMDA receptor hypofunction model of schizophrenia. J Psychiatr Res 33:523-533.

Ouhaz Z, Ba-M'hamed S, Mitchell AS, Elidrissi A, Bennis M (2015) Behavioral and cognitive changes after early postnatal lesions of the rat mediodorsal thalamus. Behav Brain Res 292:219-232.

Pachitariu M, Steinmetz NA, Caradini M, Harris KD (2016) Fast and accurate spike sorting of high channel count probes with kilosort. In, pp 4448 - 4456: Advances in Neural Information Processing Systems.

Pakkenberg B (1992) The volume of the mediodorsal thalamic nucleus in treated and untreated schizophrenics. Schizophr Res 7:95-100.

Parker A, Eacott MJ, Gaffan D (1997) The recognition memory deficit caused by mediodorsal thalamic lesion in non-human primates: a comparison with rhinal cortex lesion. Eur J Neurosci 9:2423-2431.

Parnaudeau S, Bolkan SS, Kellendonk C (2018) The Mediodorsal Thalamus: An Essential Partner of the Prefrontal Cortex for Cognition. Biol Psychiatry 83:648-656.

Parnaudeau S, Taylor K, Bolkan SS, Ward RD, Balsam PD, Kellendonk C (2015) Mediodorsal thalamus hypofunction impairs flexible goal-directed behavior. Biol Psychiatry 77:445-453.

Parnaudeau S, O'Neill PK, Bolkan SS, Ward RD, Abbas AI, Roth BL, Balsam PD, Gordon JA, Kellendonk C (2013) Inhibition of mediodorsal thalamus disrupts thalamofrontal connectivity and cognition. Neuron 77:1151-1162.

Perlstein WM, Dixit NK, Carter CS, Noll DC, Cohen JD (2003) Prefrontal cortex dysfunction mediates deficits in working memory and prepotent responding in schizophrenia. Biol Psychiatry 53:25-38.

Perner J, Lang B (1999) Development of theory of mind and executive control. Trends Cogn Sci 3:337-344.

Pineda DA (2000) [Executive function and its disorders]. Rev Neurol 30:764-768.

Popken GJ, Bunney WE, Potkin SG, Jones EG (2000) Subnucleus-specific loss of neurons in medial thalamus of schizophrenics. Proc Natl Acad Sci U S A 97:9276-9280.

Poppe AB, Barch DM, Carter CS, Gold JM, Ragland JD, Silverstein SM, MacDonald AW (2016) Reduced Frontoparietal Activity in Schizophrenia Is Linked to a Specific Deficit in Goal Maintenance: A Multisite Functional Imaging Study. Schizophr Bull 42:1149-1157.

Preuss TM (1995) Do rats have prefrontal cortex? The rose-woolsey-akert program reconsidered. J Cogn Neurosci 7:1-24.

Preuss TM, Goldman-Rakic PS (1987) Crossed corticothalamic and thalamocortical connections of macaque prefrontal cortex. J Comp Neurol 257:269-281.

Pukrop R, Ruhrmann S, Schultze-Lutter F, Bechdolf A, Brockhaus-Dumke A, Klosterkötter J (2007) Neurocognitive indicators for a conversion to psychosis: comparison of patients in a potentially initial prodromal state who did or did not convert to a psychosis. Schizophr Res 92:116-125.

Pukrop R, Schultze-Lutter F, Ruhrmann S, Brockhaus-Dumke A, Tendolkar I, Bechdolf A, Matuschek E, Klosterkötter J (2006) Neurocognitive functioning in subjects at risk for a first episode of psychosis compared with first- and multiple-episode schizophrenia. J Clin Exp Neuropsychol 28:1388-1407.

Ramsay IS, Nienow TM, MacDonald AW (2017) Increases in Intrinsic Thalamocortical Connectivity and Overall Cognition Following Cognitive Remediation in Chronic Schizophrenia. Biol Psychiatry Cogn Neurosci Neuroimaging 2:355-362.

Ray KL, Lesh TA, Howell AM, Salo TP, Ragland JD, MacDonald AW, Gold JM, Silverstein SM, Barch DM, Carter CS (2017) Functional network changes and cognitive control in schizophrenia. Neuroimage Clin 15:161-170.

Richard AE, Carter CS, Cohen JD, Cho RY (2013) Persistence, diagnostic specificity and genetic liability for context-processing deficits in schizophrenia. Schizophr Res 147:75-80.

Riley EM, McGovern D, Mockler D, Doku VC, OCeallaigh S, Fannon DG, Tennakoon L, Santamaria M, Soni W, Morris RG, Sharma T (2000) Neuropsychological functioning in first-episode psychosis--evidence of specific deficits. Schizophr Res 43:47-55.

Roberts BM, Seymour PA, Schmidt CJ, Williams GV, Castner SA (2010) Amelioration of ketamine-induced working memory deficits by dopamine D1 receptor agonists. Psychopharmacology (Berl) 210:407-418.

Rovó Z, Ulbert I, Acsády L (2012) Drivers of the primate thalamus. J Neurosci 32:17894-17908.

Rowe JB, Passingham RE (2001) Working memory for location and time: activity in prefrontal area 46 relates to selection rather than maintenance in memory. Neuroimage 14:77-86.

Rowe JB, Toni I, Josephs O, Frackowiak RS, Passingham RE (2000) The prefrontal cortex: response selection or maintenance within working memory? Science 288:1656-1660.

Roy JE, Riesenhuber M, Poggio T, Miller EK (2010) Prefrontal cortex activity during flexible categorization. J Neurosci 30:8519-8528.

Russchen FT, Amaral DG, Price JL (1987) The afferent input to the magnocellular division of the mediodorsal thalamic nucleus in the monkey, Macaca fascicularis. J Comp Neurol 256:175-210.

Saykin AJ, Shtasel DL, Gur RE, Kester DB, Mozley LH, Stafiniak P, Gur RC (1994) Neuropsychological deficits in neuroleptic naive patients with first-episode schizophrenia. Arch Gen Psychiatry 51:124-131.

Schiffer AM, Waszak F, Yeung N (2015) The role of prediction and outcomes in adaptive cognitive control. J Physiol Paris 109:38-52. doi: 10.1016/j.jphysparis.2015.1002.1001. Epub 2015 Feb 1017.

Schmitt LI, Wimmer RD, Nakajima M, Happ M, Mofakham S, Halassa MM (2017) Thalamic amplification of cortical connectivity sustains attentional control. Nature 545:219-223.

Schuepbach D, Keshavan MS, Kmiec JA, Sweeney JA (2002) Negative symptom resolution and improvements in specific cognitive deficits after acute treatment in first-episode schizophrenia. Schizophr Res 53:249-261.

Schulz CS, Green MF, Nelson KJ (2016) Schizophrenia and Psychotic Spectrum Disorders. In: Oxford University Press

Seidman LJ, Yurgelun-Todd D, Kremen WS, Woods BT, Goldstein JM, Faraone SV, Tsuang MT (1994) Relationship of prefrontal and temporal lobe MRI measures to neuropsychological performance in chronic schizophrenia. Biol Psychiatry 35:235-246.

Servan-Schreiber D, Cohen JD, Steingard S (1996) Schizophrenic deficits in the processing of context. A test of a theoretical model. Arch Gen Psychiatry 53:1105-1112.

Shallice T, Burgess PW (1991) Deficits in strategy application following frontal lobe damage in man. Brain 114 (Pt 2):727-741.

Sheffield JM, Barch DM (2016) Cognition and resting-state functional connectivity in schizophrenia. Neurosci Biobehav Rev 61:108-120.

Sherman SM (2012) Thalamocortical interactions. Curr Opin Neurobiol 22:575-579.
Sherman SM, Guillery RW (1996) Functional organization of thalamocortical relays. J Neurophysiol 76:1367-1395.

Sherman SM, Guillery RW (2002) The role of the thalamus in the flow of information to the cortex. Philos Trans R Soc Lond B Biol Sci 357:1695-1708.

Sherman SM, Guillery RW (2011) Distinct functions for direct and transthalamic corticocortical connections. J Neurophysiol 106:1068-1077.

Simon AE, Cattapan-Ludewig K, Zmilacher S, Arbach D, Gruber K, Dvorsky DN, Roth B, Isler E, Zimmer A, Umbricht D (2007) Cognitive functioning in the schizophrenia prodrome. Schizophr Bull 33:761-771.

Simpson EH, Kellendonk C (2017) Insights About Striatal Circuit Function and Schizophrenia From a Mouse Model of Dopamine D. Biol Psychiatry 81:21-30.

Skoblenick K, Everling S (2012) NMDA antagonist ketamine reduces task selectivity in macaque dorsolateral prefrontal neurons and impairs performance of randomly interleaved prosaccades and antisaccades. J Neurosci 32:12018-12027.

Skoblenick K, Everling S (2014) N-methyl-d-aspartate receptor antagonist ketamine impairs action-monitoring activity in the prefrontal cortex. J Cogn Neurosci 26:577-592.

Smith CW, Park S, Cornblatt B (2006) Spatial working memory deficits in adolescents at clinical high risk for schizophrenia. Schizophr Res 81:211-215.

Smith EE, Jonides J (1999) Storage and executive processes in the frontal lobes. Science 283:1657-1661.

Smith MJ, Wang L, Cronenwett W, Mamah D, Barch DM, Csernansky JG (2011) Thalamic morphology in schizophrenia and schizoaffective disorder. J Psychiatr Res 45:378-385.

Smucny J, Barch DM, Gold JM, Strauss ME, MacDonald AW, Boudewyn MA, Ragland JD, Silverstein SM, Carter CS (2019) Cross-diagnostic analysis of cognitive control in mental illness: Insights from the CNTRACS consortium. Schizophr Res 208:377-383.

Sohn MH, Ursu S, Anderson JR, Stenger VA, Carter CS (2000) The role of prefrontal cortex and posterior parietal cortex in task switching. Proc Natl Acad Sci U S A 97:13448-13453.

Sokolov BP (1998) Expression of NMDAR1, GluR1, GluR7, and KA1 glutamate receptor mRNAs is decreased in frontal cortex of "neuroleptic-free" schizophrenics:

evidence on reversible up-regulation by typical neuroleptics. J Neurochem 71:2454-2464.

Sommer MA, Wurtz RH (2004a) What the brain stem tells the frontal cortex. II. Role of the SC-MD-FEF pathway in corollary discharge. J Neurophysiol 91:1403-1423.

Sommer MA, Wurtz RH (2004b) What the brain stem tells the frontal cortex. I. Oculomotor signals sent from superior colliculus to frontal eye field via mediodorsal thalamus. J Neurophysiol 91:1381-1402.

Stephan KE, Baldeweg T, Friston KJ (2006) Synaptic plasticity and dysconnection in schizophrenia. Biol Psychiatry 59:929-939.

Stip E, Chouinard S, Boulay LJ (2005) On the trail of a cognitive enhancer for the treatment of schizophrenia. Prog Neuropsychopharmacol Biol Psychiatry 29:219-232.

Stone JM, Morrison PD, Pilowsky LS (2007) Glutamate and dopamine dysregulation in schizophrenia--a synthesis and selective review. J Psychopharmacol 21:440-452.

Strauss ME, McLouth CJ, Barch DM, Carter CS, Gold JM, Luck SJ, MacDonald AW, Ragland JD, Ranganath C, Keane BP, Silverstein SM (2014) Temporal stability and moderating effects of age and sex on CNTRaCS task performance. Schizophr Bull 40:835-844.

Sullivan EV, Mathalon DH, Zipursky RB, Kersteen-Tucker Z, Knight RT, Pfefferbaum A (1993) Factors of the Wisconsin Card Sorting Test as measures of frontal-lobe function in schizophrenia and in chronic alcoholism. Psychiatry Res 46:175-199.

Tandon R (2011) Antipsychotics in the treatment of schizophrenia: an overview. J Clin Psychiatry 72 Suppl 1:4-8.

Tanibuchi I, Goldman-Rakic PS (2003) Dissociation of spatial-, object-, and sound-coding neurons in the mediodorsal nucleus of the primate thalamus. J Neurophysiol 89:1067-1077.

Tanibuchi I, Kitano H, Jinnai K (2009a) Substantia nigra output to prefrontal cortex via thalamus in monkeys. I. Electrophysiological identification of thalamic relay neurons. J Neurophysiol 102:2933-2945.

Tanibuchi I, Kitano H, Jinnai K (2009b) Substantia nigra output to prefrontal cortex via thalamus in monkeys. II. Activity of thalamic relay neurons in delayed conditional go/no-go discrimination task. J Neurophysiol 102:2946-2954.

Thompson-Schill SL, Bedny M, Goldberg RF (2005) The frontal lobes and the regulation of mental activity. Curr Opin Neurobiol 15:219-224.

Thompson-Schill SL, Jonides J, Marshuetz C, Smith EE, D'Esposito M, Kan IP, Knight RT, Swick D (2002) Effects of frontal lobe damage on interference effects in working memory. Cogn Affect Behav Neurosci 2:109-120.

Townsend LA, Malla AK, Norman RM (2001) Cognitive functioning in stabilized first-episode psychosis patients. Psychiatry Res 104:119-131.

Tsai GE, Lin PY (2010) Strategies to enhance N-methyl-D-aspartate receptor-mediated neurotransmission in schizophrenia, a critical review and meta-analysis. Curr Pharm Des 16:522-537.

Tsukada H, Nishiyama S, Fukumoto D, Sato K, Kakiuchi T, Domino EF (2005) Chronic NMDA antagonism impairs working memory, decreases extracellular dopamine, and increases D1 receptor binding in prefrontal cortex of conscious monkeys. Neuropsychopharmacology 30:1861-1869.

Tu PC, Lee YC, Chen YS, Hsu JW, Li CT, Su TP (2015) Network-specific cortico-thalamic dysconnection in schizophrenia revealed by intrinsic functional connectivity analyses. Schizophr Res 166:137-143.

Umbricht D, Alberati D, Martin-Facklam M, Borroni E, Youssef EA, Ostland M, Wallace TL, Knoflach F, Dorflinger E, Wettstein JG, Bausch A, Garibaldi G, Santarelli L (2014) Effect of bitopertin, a glycine reuptake inhibitor, on negative symptoms of schizophrenia: a randomized, double-blind, proof-of-concept study. JAMA Psychiatry 71:637-646.

Uylings HB, Groenewegen HJ, Kolb B (2003) Do rats have a prefrontal cortex? Behav Brain Res 146:3-17.

Vallentin D, Bongard S, Nieder A (2012) Numerical rule coding in the prefrontal, premotor, and posterior parietal cortices of macaques. J Neurosci 32:6621-6630.

Van der Werf YD, Witter MP, Uylings HB, Jolles J (2000) Neuropsychology of infarctions in the thalamus: a review. Neuropsychologia 38:613-627.

Van der Werf YD, Scheltens P, Lindeboom J, Witter MP, Uylings HB, Jolles J (2003) Deficits of memory, executive functioning and attention following infarction in the thalamus; a study of 22 cases with localised lesions. Neuropsychologia 41:1330-1344.

Van L, Boot E, Bassett AS (2017) Update on the 22q11.2 deletion syndrome and its relevance to schizophrenia. Curr Opin Psychiatry 30:191-196.

Van Snellenberg JX, Torres IJ, Thornton AE (2006) Functional neuroimaging of working memory in schizophrenia: task performance as a moderating variable. Neuropsychology 20:497-510.

Van Snellenberg JX, Girgis RR, Horga G, van de Giessen E, Slifstein M, Ojeil N, Weinstein JJ, Moore H, Lieberman JA, Shohamy D, Smith EE, Abi-Dargham A (2016) Mechanisms of Working Memory Impairment in Schizophrenia. Biol Psychiatry 80:617-626.

Ventura J, Hellemann GS, Thames AD, Koellner V, Nuechterlein KH (2009) Symptoms as mediators of the relationship between neurocognition and functional outcome in schizophrenia: a meta-analysis. Schizophr Res 113:189-199.

Wallis JD, Anderson KC, Miller EK (2001a) Single neurons in prefrontal cortex encode abstract rules. Nature 411:953-956.

Wallis JD, Anderson KC, Miller EK (2001b) Single neurons in prefrontal cortex encode abstract rules. Nature 411:953-956. doi: 910.1038/35082081.

Wang M, Yang Y, Wang CJ, Gamo NJ, Jin LE, Mazer JA, Morrison JH, Wang XJ, Arnsten AF (2013) NMDA receptors subserve persistent neuronal firing during working memory in dorsolateral prefrontal cortex. Neuron 77:736-749.

Wang S, Eisenback MA, Bickford ME (2002) Relative distribution of synapses in the pulvinar nucleus of the cat: implications regarding the "driver/modulator" theory of thalamic function. J Comp Neurol 454:482-494.

Watanabe Y, Funahashi S (2004a) Neuronal activity throughout the primate mediodorsal nucleus of the thalamus during oculomotor delayed-responses. II. Activity encoding visual versus motor signal. J Neurophysiol 92:1756-1769.

Watanabe Y, Funahashi S (2004b) Neuronal activity throughout the primate mediodorsal nucleus of the thalamus during oculomotor delayed-responses. I. Cue-, delay-, and response-period activity. J Neurophysiol 92:1738-1755.

Watanabe Y, Funahashi S (2012) Thalamic mediodorsal nucleus and working memory. Neurosci Biobehav Rev 36:134-142.

Watanabe Y, Funahashi S (2018) Change of information represented by thalamic mediodorsal neurons during the delay period. Neuroreport 29:466-471.

Watanabe Y, Takeda K, Funahashi S (2009) Population vector analysis of primate mediodorsal thalamic activity during oculomotor delayed-response performance. Cereb Cortex 19:1313-1321.

Weickert TW, Terrazas A, Bigelow LB, Malley JD, Hyde T, Egan MF, Weinberger DR, Goldberg TE (2002) Habit and skill learning in schizophrenia: evidence of normal striatal processing with abnormal cortical input. Learn Mem 9:430-442.

Weinberger DR, Berman KF, Zec RF (1986) Physiologic dysfunction of dorsolateral prefrontal cortex in schizophrenia. I. Regional cerebral blood flow evidence. Arch Gen Psychiatry 43:114-124.

Weinberger DR, Berman KF, Suddath R, Torrey EF (1992) Evidence of dysfunction of a prefrontal-limbic network in schizophrenia: a magnetic resonance imaging and regional cerebral blood flow study of discordant monozygotic twins. Am J Psychiatry 149:890-897.

Weiser M, Heresco-Levy U, Davidson M, Javitt DC, Werbeloff N, Gershon AA, Abramovich Y, Amital D, Doron A, Konas S, Levkovitz Y, Liba D, Teitelbaum A, Mashiach M, Zimmerman Y (2012) A multicenter, add-on randomized controlled trial of low-dose d-serine for negative and cognitive symptoms of schizophrenia. J Clin Psychiatry 73:e728-734.

Welsh RC, Chen AC, Taylor SF (2010) Low-frequency BOLD fluctuations demonstrate altered thalamocortical connectivity in schizophrenia. Schizophr Bull 36:713-722.

Wood SJ, Pantelis C, Proffitt T, Phillips LJ, Stuart GW, Buchanan JA, Mahony K, Brewer W, Smith DJ, McGorry PD (2003) Spatial working memory ability is a marker of risk-for-psychosis. Psychol Med 33:1239-1247.

Woodward ND, Heckers S (2016) Mapping Thalamocortical Functional Connectivity in Chronic and Early Stages of Psychotic Disorders. Biol Psychiatry 79:1016-1025.

Woodward ND, Karbasforoushan H, Heckers S (2012) Thalamocortical dysconnectivity in schizophrenia. Am J Psychiatry 169:1092-1099.

Xiao D, Zikopoulos B, Barbas H (2009) Laminar and modular organization of prefrontal projections to multiple thalamic nuclei. Neuroscience 161:1067-1081.

Xu K, Krystal JH, Ning Y, Chen DC, He H, Wang D, Ke X, Zhang X, Ding Y, Liu Y, Gueorguieva R, Wang Z, Limoncelli D, Pietrzak RH, Petrakis IL, Fan N (2015) Preliminary analysis of positive and negative syndrome scale in ketamine-associated psychosis in comparison with schizophrenia. J Psychiatr Res 61:64-72.

Yeterian EH, Pandya DN (1994) Laminar origin of striatal and thalamic projections of the prefrontal cortex in rhesus monkeys. Exp Brain Res 99:383-398.

Yin HH, Knowlton BJ (2006) The role of the basal ganglia in habit formation. Nat Rev Neurosci 7:464-476.

Yoon JH, Minzenberg MJ, Ursu S, Ryan Walter BS, Walters R, Wendelken C, Ragland JD, Carter CS (2008) Association of dorsolateral prefrontal cortex dysfunction with disrupted coordinated brain activity in schizophrenia: relationship with impaired cognition, behavioral disorganization, and global function. Am J Psychiatry 165:1006-1014.

Young KA, Manaye KF, Liang C, Hicks PB, German DC (2000) Reduced number of mediodorsal and anterior thalamic neurons in schizophrenia. Biol Psychiatry 47:944-953.

Zick JL, Blackman RK, Crowe DA, Amirikian B, DeNicola AL, Netoff TI, Chafee MV (2018) Blocking NMDAR Disrupts Spike Timing and Decouples Monkey Prefrontal Circuits: Implications for Activity-Dependent Disconnection in Schizophrenia. Neuron 98:1243-1255.e1245. doi: 1210.1016/j.neuron.2018.1205.1010. Epub 2018 May 1231.

Zola-Morgan S, Squire LR (1985) Amnesia in monkeys after lesions of the mediodorsal nucleus of the thalamus. Ann Neurol 17:558-564.

Zoppelt D, Koch B, Schwarz M, Daum I (2003) Involvement of the mediodorsal thalamic nucleus in mediating recollection and familiarity. Neuropsychologia 41:1160-1170.